

**THERMAL AND MECHANICAL PROPERTIES OF POLYOLEFINS/WAX
PCM BLENDS PREPARED WITH AND WITHOUT EXPANDED
GRAPHITE**

by

MOKGAOTSA JONAS MOCHANE (M.Sc.)

Submitted in accordance with the requirements for the degree

Philosophiae Doctor (Ph.D.) in Polymer Science

Department of Chemistry

Faculty of Natural and Agricultural Sciences

at the

UNIVERSITY OF THE FREE STATE (QWAQWA CAMPUS)

SUPERVISOR: PROF AS LUYT

December 2014

DECLARATION

I, the undersigned, hereby declare that the research in this thesis is my own original work, which has not partly or fully been submitted to any other University in order to obtain a degree.

Mochane MJ (Mr)

DEDICATION

This work is dedicated to my late father (Samuel Mochane), my mother (Elizabeth Mochane) and the entire family of Mochane. Ho batjhana Nkamoheng Mochane, Buhle Mochane, Monki Mochane, Lehlohonolo Mochane, Bonolo Mochane, Malome o re thuto ke lefa bana baka , keo he ke e siya le lona. Ke kopa le futse Malome bana baka. Always remember to respect elders, out of nowhere God will put you somewhere. To my siblings Jappie Mochane, Molefe Mochane, Nthloro Mochane, Mohemi Mochane, Mokgethi Mochane, Monyatsi Mochane, and Ntswaki Mochane thank you very much for your support.

ABSTRACT

The study deals with the preparation of polyolefin/wax blends as form-stable, solid-liquid phase change materials (PCM) with the aim of enhancing both the thermal conductivity and flame resistance properties of the shape-stabilized PCMs. In such a composite, the wax serves as a latent heat storage material and the polyolefins (EVA and PP) act as supporting materials, preventing leakage of the molten wax and providing structural strength. To improve the thermal conductivity and flammability resistance of these blends, expanded graphite at loadings of 3, 6 and 9 wt% was added into the samples, whereas the polymer/wax blend was kept at a 1:1 weight ratio. To further improve the flammability resistance, combinations of EG with Cloisite 15A clay and diammonium phosphate (DAP) in EVA and an EVA/wax blend were investigated. Both the blends and composites were subjected to different characterization techniques in order to establish their morphology and thermal and mechanical properties. The techniques used were scanning electron microscopy (SEM), differential scanning calorimetry (DSC), thermal conductivity, thermogravimetric analysis (TGA), cone calorimetry, dynamic mechanical analysis (DMA), X-ray diffraction (XRD), tensile testing, and impact testing. It was generally observed that the EG particles agglomerated in the absence of wax, but dispersed much better in the blends when wax was present, probably because the wax penetrated in between the EG layers as a result of the better interaction between wax and EG, and separated the layers into smaller and better dispersed EG particles. This gave rise to better thermal conductivity and flame resistance. In the presence of EG+Cloisite 15A the material formed a dense and stable char layer (carbonized ceramic) which significantly improved the flame resistance of the materials. It was observed that the thermal degradation mechanisms of the polymers and blends did not change in the presence of EG, although the EG particles retarded the evolution of the volatile degradation products. There were no significant changes in the melting temperature of EVA in the EVA/EG composites, while the crystallinities of EVA were observably lower in the presence of EG. The EVA composites showed a decrease in impact strength with increasing EG and wax contents. The impact strength of the PP/wax/EG composites increased with increasing EG content in all the samples, but decreased with increasing wax content.

LIST OF ABBREVIATIONS AND SYMBOLS

APP	ammonium polyphosphate
ASEA	average specific extinction
BR	butadiene rubber
C=O	carboxylic
C15	chains containing 15 carbon atoms
C15A	Cloisite 15A
C78	chains containing 78 carbon atoms
CFA	char-foaming agent
C-H	carbon hydrogen bond
CNTs	carbon nanotubes
COP	carbon monoxide production
d	basal spacing
DAP	diammonium phosphate
DBP	dibenzoyl peroxide
DCP	dicumyl peroxide
DMA	dynamic mechanical analysis
DSC	differential scanning calorimetry
E	Young's modulus
EG	expanded graphite
EVA	ethylene vinyl acetate
ϵ_b	strain at break
FIGRA	fire growth index
FPI	fire performance index
FTIR	Fourier-transform infrared spectroscopy
HDPE	high-density polyethylene
HFFR	halogen-free flame retardants
HRR	heat release rate
HSO	hydroxyl silicone oil
IFR	intumescent flame retardant
i-MG	isocyanate modified graphite
LDPE	low-density polyethylene
LHS	latent heat storage

LHS	latent heat storage
LHTES	latent heat thermal energy storage
LLDPE	linear low-density polyethylene
M3 wax	medium-soft paraffin wax
MAPP	modified ammonium polyphosphate
MFI	melt flow index
MLR	mass loss rate
PA-6	nylon 6
PCM	phase-change material
PER	pentaerythritol
PHRR	peak heat release rate
PLA	polylactic acid
PP	polypropylene
PPS	polyphenylene sulfide
PTPA	poly[N ⁴ -biss(ethylenediamine)-phenyl phosphoric-N ² , and N ⁶ -bis(ethylenediamine)-1,3,5-triazine-N-phenyl phosphate]
SBR	styrene-butadiene rubber
SBS	styrene-butadiene-styrene
SEA	specific extinction area
SEM	scanning electron microscopy
SI	solution intercalation
SPR	smoke production rate
T _c	crystallization temperature
T _g	glass transition temperature
TGA	thermogravimetric Analysis
THR	total heat release rate
T _m	melting temperature
T _{o,m}	onset temperature of melting
T _{p,m}	peak temperature of melting
t _{PHRR}	time to peak heat release rate
TTI	time to ignition
UG	natural graphite
USA	United States of America
VA	vinyl acetate

vol.%	volume percentage
w	weight fraction
w/w	weight per weight
wt.%	weight percentage
XRD	X-ray diffraction
ZB	zinc borate
ΔH^{calc}	calculated enthalpy
ΔH_{m}	melting enthalpy
$\Delta H_{\text{m}}^{\text{norm}}$	normalised melting enthalpy
$\Delta H_{\text{m}}^{\text{obs}}$	observed melting enthalpy

TABLE OF CONTENTS

	Page
DECLARATION	i
DEDICATION	ii
ABSTRACT	iii
LIST OF ABBREVIATIONS	iv
TABLE OF CONTENTS	vii
LIST OF TABLES	xi
LIST OF FIGURES	xii
Chapter 1: General introduction and overview	1
1.1 General background	1
1.2 Overview	5
1.2.1 Morphology	5
1.2.2 Thermal properties	6
1.2.3 Thermal stability	7
1.2.4 Thermal conductivity	8
1.2.5 Mechanical properties	9
1.2.6 Thermomechanical properties	10
1.2.7 Flame resistance	10
1.3 Research objectives	11
1.4 Thesis organization	11
1.5 References	11
Chapter 2: The effect of expanded graphite on the thermal stability, latent heat and flammability properties of EVA/wax blends	19
2.1 Introduction	20

2.2	Materials and methods	21
2.2.1	Materials	21
2.2.2	Preparation of expanded graphite	22
2.2.3	Preparation of blend and composite samples	22
2.2.4	Sample analysis	22
2.3	Results and discussion	23
2.3.1	Microscopic analysis	23
2.3.2	Differential scanning calorimetry (DSC)	25
2.3.3	Thermogravimetric analysis (TGA)	27
2.3.4	Thermal conductivity	30
2.3.5	Cone calorimetry	31
2.4	Conclusions	36
2.5	References	37

Chapter 3: The effect of expanded graphite on the physical properties of conductive EVA/wax phase thermal energy storage 42

3.1	Introduction	43
3.2	Materials and methods	45
3.2.1	Materials	45
3.2.2	Preparation of expanded graphite	45
3.2.3	Preparation of blend and composite samples	45
3.2.4	Sample analysis	46
3.3	Results and discussion	47
3.3.1	Scanning electron microscopy (SEM)	47
3.3.2	Mechanical properties	48
3.3.3	Dynamic mechanical analysis (DMA)	53
3.4	Conclusions	57
3.5	References	57

Chapter 4: The effect of expanded graphite on the flammability and thermal conductivity properties phase change material based on PP/wax blends **64**

4.1	Introduction	65
4.2	Materials and methods	67
4.2.1	Materials	67
4.2.2	Preparation of expanded graphite	68
4.2.3	Preparation of PP/wax blends and PP/wax/EG composites	68
4.2.4	Sample analysis	68
4.3	Results and discussion	69
4.3.1	Fire-retardant properties	69
4.3.2	Thermogravimetric analysis (TGA)	74
4.3.3	Fourier-transform infrared (FTIR) analysis of volatiles from TGA analysis	77
4.3.4	Dynamic mechanical analysis (DMA)	80
4.3.5	Impact properties	82
4.3.6	Thermal conductivity	83
4.4	Conclusions	85
4.5	References	85

Chapter 5: Synergistic effect of expanded graphite, diammonium phosphate and Cloisite 15A flame retardant properties of EVA and EVA/wax blends **91**

5.1	Introduction	92
5.2	Materials and methods	93
5.2.1	Materials	93
5.2.2	Preparation of expanded graphite	94
5.2.3	Preparation of blend and composite samples	94
5.2.4	Sample analysis	95
5.3	Results and discussion	95
5.3.1	X-ray diffraction (XRD)	95
5.3.2	Thermal stability	100

5.3.3	Flammability	103
5.4	Conclusions	109
5.5	References	109
Chapter 6: Conclusions		115
Acknowledgements		117
Appendix		119

LIST OF TABLES

		Page
Table 1.1	Advantages and disadvantages of phase change materials	3
Table 2.1	Sample compositions used in this study	22
Table 2.2	Summary of melting temperatures and enthalpies for all the investigated samples	26
Table 2.3	TGA results for investigated samples	30
Table 2.4	Flammability data of an EVA/wax blend, as well as EVA/EG and EVA/wax/EG composites	33
Table 3.1	Sample compositions used in this study	46
Table 3.2	Tensile and impact properties of all the investigated samples	50
Table 4.1	Sample compositions used in this study	68
Table 4.2	Flammability data of PP, the PP/wax blend, and the PP/EG and PP/wax/EG composites	72
Table 4.3	Assignment of peaks for TGA-FTIR analysis results	80
Table 5.1	Sample compositions used in this study	94
Table 5.2	Basal spacings of the clay and EG in the samples	97
Table 5.3	Degradation temperatures at 10 and 70% mass for all the investigated samples	102
Table 5.4	Flammability data of the samples used in this study	106

LIST OF FIGURES

	Page	
Figure 1.1	Classification of phase change materials	2
Figure 2.1	SEM images of the (a) expandable graphite, b) expanded graphite, and (c) a wax/EG composite	24
Figure 2.2	Optical microscopy images of the (a) 94/6 w/w EVA/EG, and (b) 65.8/28.2/6 w/w EVA/wax/EG	24
Figure 2.3	DSC heating curves of EVA, wax, an EVA blend and some EVA/wax/EG composites	25
Figure 2.4	TGA curves of EVA, wax and EG	27
Figure 2.5	TGA curves of neat EVA and the EVA/EG composites	28
Figure 2.6	TGA curves of 70/30 w/w EVA/wax and EVA/wax/EG composites	29
Figure 2.7	Thermal conductivities of EVA and the EVA/wax blends with different amounts of expanded graphite	31
Figure 2.8	Heat release rate curves of an EVA/wax blend, as well as EVA/EG and EVA/wax/EG composites	32
Figure 2.9	MLR versus time graphs for an EVA/wax blend, as well as EVA/wax/EG and EVA/EG composites	34
Figure 2.10	Smoke production rate (SPR) plots of an EVA/wax blend, as well as EVA/EG and EVA/wax/EG composites	35
Figure 2.11	Carbon monoxide production (COP) plots of an EVA/wax blend, as well as EVA/EG and EVA/wax/EG composites at an external heat flux of 35 kW m^{-2}	36
Figure 3.1	SEM images of the (a) EVA/EG and (b) EVA/wax/EG composite	47
Figure 3.2	Impact strengths of EVA and EVA/wax blends containing different expanded graphite contents	48
Figure 3.3	Young's modulus of EVA and the EVA/wax blends as a function of expanded graphite content	51
Figure 3.4	Elongation at break of EVA and the EVA/wax blends as a function of	

	expanded graphite content	52
Figure 3.5	Stress at break of EVA and the EVA/wax blends as a function of expanded graphite content	53
Figure 3.6	Storage modulus as function of temperature for neat EVA, an EVA/wax blend, as well as EVA/EG and EVA/wax/EG composites	54
Figure 3.7	Loss modulus as function of temperature for neat EVA, an EVA/wax blend, as well as EVA/EG and EVA/wax/EG composites	55
Figure 3.8	Loss factor as function of temperature for neat EVA, an EVA/wax blend, as well as EVA/EG and EVA/wax/EG composites	56
Figure 4.1	Heat release rate curves for PP, the PP/wax blend, and the PP/EG and PP/wax/EG composites	70
Figure 4.2	Photos of the (a) PP/EG and (b) PP/wax/EG charred residues obtained at the end of the combustion process	73
Figure 4.3	a) Carbon monoxide and b) carbon dioxide production plots of PP, PP/wax blend, as well as PP/EG and PP/wax/EG composites	74
Figure 4.4	TGA curves of PP, wax and EG	75
Scheme 4.1	Degradation mechanism of polypropylene	75
Figure 4.5	TGA curves of neat PP and the PP/EG composites	76
Figure 4.6	TGA curves of PP/wax blend and PP/wax/EG composites	77
Figure 4.7	FTIR curves of a) wax and b) PP at different temperatures during the thermal degradation in a TGA at a heating rate of 10 °C min ⁻¹	78
Figure 4.8	FTIR curves of a) 70/30 w/w PP/wax and b) 65.8/28.2/6 w/w PP/wax/EG at different temperatures during the thermal degradation in a TGA at a heating rate of 10 °C min ⁻¹	78
Figure 4.9	FTIR curves of a) 70/30 w/w PP/wax and b) 65.8/28.2/6 w/w PP/wax/EG during the thermal degradation in a TGA at a heating rate of 10 °C min ⁻¹	79
Figure 4.10	FTIR curves of 94/6 w/w PP/EG at different temperatures during the thermal degradation in a TGA at a heating rate of 10 °C min ⁻¹	79
Figure 4.11	Storage modulus curves of PP, as well as the PP/EG and PP/wax/EG composites	80
Figure 4.12	Loss modulus curves of PP, as well as the PP/EG and PP/wax/EG	

	composites	81
Figure 4.13	Impact strengths of PP and PP/wax blends	83
Figure 4.14	Impact strengths of PP/wax blends containing different contents of expanded graphite	83
Figure 4.15	Thermal conductivities of PP and the PP/wax blends with different amounts of expanded graphite	84
Figure 5.1	X-ray diffractograms of EG and EVA	96
Figure 5.2	X-ray diffractograms of Cloisite 15A, EVA/(EG+Cloisite 15A) and EVA/wax/(EG+Cloisite 15A) at low diffraction angles	97
Figure 5.3	X-ray diffractograms showing the EG peak of EG and EG in the EVA/wax composites	99
Figure 5.4	X-ray diffractograms showing the EG peak of EG and EG in the EVA composites	99
Figure 5.5	TGA curves of EG, DAP and Cloisite 15A	100
Figure 5.6	TGA curves of neat EVA, EVA/EG as well as EVA/ (EG+Cloisite 15A) and EVA/ (EG+DAP) composites	101
Figure 5.7	TGA curves of 60/40 w/w EVA/wax, EVA/wax/EG as well as EVA/wax/ (EG+Cloisite 15A) and EVA/ wax/(EG+DAP) composites	103
Figure 5.8	Heat release rate curves for the EVA/wax blend, as well as the EVA/wax/EG, EVA/wax/(EG+Cloisite 15A) and EVA/wax/(EG+DAP) composites	104
Figure 5.9	SEM images of the a) EVA/wax/EG, b) EVA/wax/(EG+Cloisite 15A), and c) EVA/wax/(EG+DAP) composites	104
Figure 5.10	Heat release rate curves for EVA, as well as the EVA/EG, EVA/(EG+Cloisite 15A) and EVA/(EG+DAP) composites	107
Figure 5.11	SEM images of the char layers of a) 94/6 w/w EVA/EG,b) 94/6 w/w EVA/(EG+Cloisite 15A), and c) 94/6 w/w EVA/(EG+DAP) composites	107
Figure 5.12	a) Carbon monoxide and b) carbon dioxide production plots of EVA/wax blend, EVA/wax/EG, EVA/wax/(EG+Cloisite 15A) and EVA/wax/(EG+DAP) composites	108
Figure 5.13	a) Carbon monoxide and b) carbon dioxide production plots of EVA,	

Chapter 1

General introduction and overview

1.1 General background

The continuous increase in the level of greenhouse gas emissions and the climb in fuel prices are the main reasons for various sources of renewable energy to be effectively utilized [1]. In most parts of the world, direct solar radiation is considered to be one of the most prospective sources of energy. Another solution is to develop energy storage devices that are as important as new sources of energy [2]. These systems normally provide a valuable solution for the mismatch that is often found between supply and demand. Energy storage not only reduces the mismatch between supply and demand, but also improves the performance and reliability of energy systems. It further leads to the saving of premium fuels and making the systems more cost effective by reducing the wastage of energy and capital cost [3].

There are different forms in which energy can be stored i.e. mechanical, electrical and thermal energy. Thermal energy storage is, however, the most attractive because of the storing and releasing ability [4]. Thermal energy can be stored as sensible heat or latent heat through a change in the internal energy of a material, or thermochemical energy storage. Sensible heat storage is when heat is added to a material, increasing its temperature without changing its phase. Latent heat storage is the absorption or release of energy when a storage material undergoes a phase change. Thermochemical energy storage is when energy is absorbed and released by breaking and reforming of molecular bonds in a reversible chemical reaction [4-5].

Latent heat thermal energy storage is particularly attractive due to its ability to provide a high energy storage density, and it characteristically stores heat at a constant temperature corresponding to the phase transition temperature of the phase change material (PCM). Latent heat storage (LHS) can be accomplished through solid-liquid, liquid-gas, solid-gas and solid-solid transitions. The solid-liquid and solid-solid transitions are of more practical interest. The solid-gas and liquid-gas systems have limited utility because of large the volumes required for these systems. Of the two practical systems, the solid-liquid system is the most studied, and is

also commercially available. Solid-solid systems show a lot of promise, but have only recently been investigated.

One of the most prospective techniques of storing thermal energy is the application of phase change materials (PCMs). A large number of PCMs are available in different temperature ranges. Figure 1.1 shows the classification of PCMs, and Table 1.1 summarises the advantages and disadvantages of PCMs.

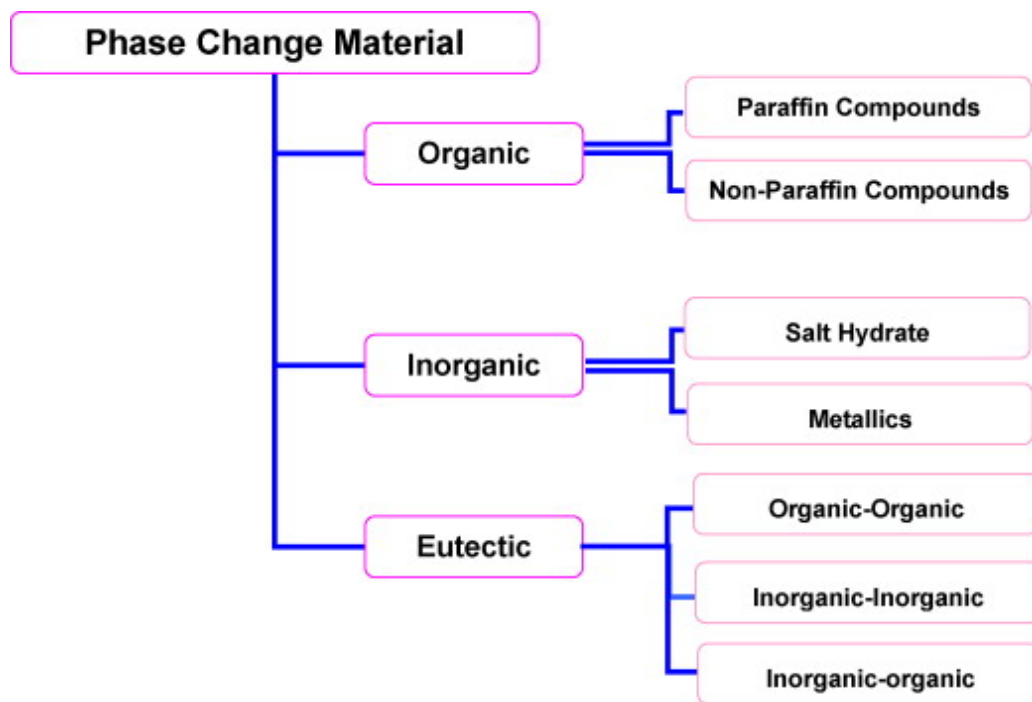


Figure 1.1 Classification of phase change materials [1]

Amongst the three classes of PCMs, organic compounds are the most broadly studied, and paraffin waxes in particular are of recent research interest due to their promising properties as phase change materials [6-7]. Paraffin waxes are saturated hydrocarbon mixtures that usually consist of a mixture of different alkanes. They are characterized by straight or branched carbon chains with generic formula C_nH_{2n+2} . They are used as phase change materials for thermal storage applications, because they have most of the required properties shown in Table 1. Their specific heat capacity is about $2.1 \text{ kJ kg}^{-1} \text{ K}^{-1}$, and their enthalpy lies between 180 and 230 kJ kg^{-1} , quite high for organic materials. The combination of these two values results in an excellent

energy storage density [6,8]. There is no single material that has all the required properties to be an ideal thermal storage medium, and one has to use the available materials and tries to make up for properties by an adequate system design. Paraffin waxes are conventional solid-liquid PCMs, and therefore are not convenient to use directly as phase change materials [9-11]. This means that paraffin waxes need to be encapsulated in order to prevent, for instance, leakage of molten paraffin wax during a phase transition. They have low thermal conductivity [12,13] and high flammability [14].

Table 1.1 Advantages and disadvantages of phase change materials

Organics	Inorganics	Eutectics
Advantages		
1. Availability over a large temperature range. 2. Freeze without much supercooling. 3. Ability to melt congruently. 4. Self-nucleating properties. 5. No segregation. 6. Chemically stable. 7. Large heat of fusion. 8. Safe and non-reactive. 9. Recyclable.	1. Large volumetric latent heat storage capacity. 2. Low cost and easy availability. 3. Sharp melting point. 4. High thermal conductivity. 5. Large latent of fusion. 6. Low volume change. 7. Non-flammable.	1. Volumetric storage density above organics. 2. Sharp melting point.
Disadvantages		
1. Low thermal conductivity in solid state. 2. High heat transfer rates required during freezing. 3. Volumetric latent storage capacity is low. 4. Flammable.	1. Change of volume is very high. 2. Supercooling is a major problem. 3. Nucleating agents are needed.	

A significant amount of research was done to solve the leakage problem and improve the thermal conductivity of paraffin [9,10,12]. There are different ways in which encapsulation of phase change materials can be achieved. The known methods of encapsulation are phase change materials in concrete or gypsum wallboards, in graphite or metal, and in polymers, with the last method being the most significantly researched [1,3,6]. It proved to be a very good encapsulation possibility for all kinds of PCMs, especially paraffin waxes. In this method, the paraffin is encapsulated in a three-dimensional net structure formed by the polymer, such as high density polyethylene (HDPE) and polypropylene [8]. The net structure of the form-stable (or shape-stabilized) material prevents the leakage of liquid to occur during the phase change of the paraffin. The increasing interest in this kind of encapsulation is primarily due to polymers having low densities, being non-corrosive and easy to manufacture, and less costly.

Good thermal conductivity is an important property for PCM composites in practical applications. A lot of work has been done to improve the thermal conductivity of the paraffin wax [10,12,15]. Metal foams, additives or fins were used by researchers to enhance the thermal conductivities of paraffin waxes [16]. However, these enhancers added significant weight and cost to the storage systems, and some of them were incompatible with the PCMs. Recently, carbon materials were used to enhance the heat transfer of PCMs, since they have good thermal conductivity, low bulk densities, and chemical inertness [17]. Moreover, these porous carbon materials have an open connected cell structure and the graphitic ligaments have good thermal conductivity values (bulk thermal conductivity of $(180 \text{ W m}^{-1} \text{ K}^{-1})$, which allow them to rapidly conduct heat through the PCM [18]. Expanded graphite (EG) is considered as one of the best heat transfer promoters, because of its desirable properties such as good thermal conductivity, good stability, compatibility with organic PCMs, and densities lower than those of metals, thus making the PCM composites lighter in weight compared to metal promoters [19].

Due to the chemical constitutions of the paraffin and supporting materials, shape-stabilized PCMs are easily flammable. Intumescent flame retardants can be applied in shape-stabilized PCM composites because of their advantages of good safety and relatively high flame retarding efficiency [20]. Traditionally, the halogenated flame retardants are popularly used within most engineering plastics due to their excellent retardant performance [18]. Taking into consideration the severe environmental impact of processing and combustion of various brominated flame

retardants, more and more halogen-free flame retardants have been explored and studied in the past couple of decades to replace brominated and chlorinated ones [21].

Materials which include metal hydroxides, expanded graphite, clay, phosphorus-nitrogen, and diammonium phosphate (DAP) were used as typical halogen-free flame retardants (HFFR). Clay, expanded graphite and diammonium phosphate are of interest in this study because of their extensive advantages. Expanded graphite is widely used to improve the flame resistance of various polymers because of its high flame retardant efficiency and low cost [20,22-23]. When exposed to heat, EG expands and generates voluminous insulating layers that reduce the flammability of the polymer. Nanoclay showed significant improvements in the physical and fire-retardant properties of polymers at very low loadings (2-10 wt.%) [24]. The presence of one kind of nanoparticle alone (in this case EG) is not sufficient to achieve an acceptable level of flame retardancy, and therefore synergistic agents were used to increase the strength and stability of char layer. In example investigations [20,25] the synergistic effect of phosphorus flame retardant (ammonium polyphosphate) and clay with EG was used to obtain an acceptable level of flame retardancy. For this reason we used a phosphorus flame retardant in the form of DAP in part of this study, because it is safe, inexpensive, and more efficient in improving the flammability resistance than other phosphorus compounds such as tributyl phosphate and triallyl phosphate [26].

1.2 Overview

1.2.1 Morphology

Paraffin waxes blended with polymers appear to be the best candidates for the preparation of smart polymeric phase change materials for different applications. A polymeric matrix fixes the phase change material in a compact form and suppresses leaking. A variety of polymer matrices, based on thermoplastic and thermosetting resins, are available with a large range of chemical and mechanical properties. Polyolefins seem to be the most frequently used polymer for blending with paraffin waxes to obtain PCMs. The morphology of polyolefin/paraffin wax blends were investigated by a large number of studies [1-3,6,8,27-36]. The results of these investigations showed that the paraffin was well dispersed into the net-like crystal structure of the polymer

matrix. This net-like crystal structure of polyolefins is said to be capable of preventing any leakage of molten paraffin during the heat storage process. It was further demonstrated from these studies that at 30% wax content and more a two- phase morphology was observed which implies the immiscibility of the polyolefins and wax.

During studies on conductive phase change materials [20,37-41] the authors found that the paraffin wax and conductive additives were uniformly dispersed in the network formed by the polymer matrix. The dispersion of the EG in polymer matrices was investigated in several studies [22-23,42-53]. Generally the authors observed clusters of graphite spread through the polymer matrix, especially as the filler content increases. The reason given was that the polymer melt cannot diffuse or intercalate into the pores of EG because of the high viscosities of the polymers. Graphene sheets always have the tendency to form agglomerates because of their large surface area, and therefore makes the penetration of the polymer chains into the inter-gallery very difficult. It was shown that solution mixing gave rise to better dispersion of the graphite nanoplatelets in the polymer than melt mixing, because the shear in melt mixing is not high enough to separate the firmly interlocked EG platelets. During solution mixing, sonication was found to be an effective way of ensuring the optimal dispersion of the graphite sheets in the polymer.

1.2.2 Thermal properties

A lot of work has been done on the thermal properties of polymer/wax blends [6,8,27-36], and a fair number of papers reported on the thermal properties of both conductive phase change materials [37-41] and polymer/EG composites [22,45-52]. It was generally observed that the total additive enthalpy of melting of the polymer and wax in the polymer/wax blends increased with an increase in wax content, which was due to the higher crystallinity of the wax. This increase was, however, in excellent agreement with the combined enthalpy of the polymer and wax calculated according to the additive rule. This was an important observation, since it confirmed that there was no leakage of paraffin wax from the blends during sample preparation. However, in one of the studies [8] the specific melting enthalpy values (evaluated separately as portions that belong to the individual peaks) were different from the theoretically expected ones when blending PP with soft and hard Fischer-Tropsch paraffin wax. This discrepancy was

attributed to the inhomogeneity of the samples, since the blends were significantly phase separated. It was demonstrated that the thermal properties of polymer/wax blends such as melting points (T_m), onset temperatures of melting ($T_{o,m}$), and melting enthalpies (ΔH_m) were strongly affected by cross-linking the blends. Dicumyl peroxide (DCP) and dibenzoyl peroxide (DBP) were used as crosslinking agents in these studies. Generally there was a decrease in melting temperatures and enthalpies with an increase in the content of both the crosslinking agents. It was suggested that the presence of crosslinking agents reduced the polyethylene (in this case LLDPE and LDPE) and wax crystallinities.

Various studies [37-41] showed that the presence of conductive filler did not significantly change the melting and crystallization temperatures of the polymer and wax in blends, irrespective of the type of filler used (EG, copper, aluminium nitride, etc). However, it was shown that the latent heat values of the conductive shape-stabilized PCMs were slightly lower than the theoretical values calculated by taking into account the mass percentage of paraffin in the blends. It was thought that these phenomena could possibly be correlated with the restricted thermal molecular movements of the PCM during the phase change, that were caused by the three-dimensional netted structure formed by the polymer matrix and the conductive filler. For polymer/graphite nanocomposites it was shown that all the graphite containing samples had a high level of crystallinity, which was linked to nucleation effects by the nanofiller. It was also shown that the addition of EG and natural graphite (UG) increased the crystallization temperature (T_c) of HDPE [46]. This increase was more significant in the case of the EG containing system. This was attributed to the fact that EG possesses a higher surface-to-volume ratio, giving rise to more nucleation sites.

1.2.3 Thermal stability

There are a fair number of studies on the thermal stabilities of polymer/wax blends [6,8,27-29,36]. The thermal stability of polyolefin/wax blends showed a large dependence on the wax content in the blends. Various researchers [27-28,30-31,33] demonstrated that an increase in wax mass fraction in the blends led to a decrease in the thermal stability of the blends. It did not matter which kind of wax or polymer matrix was used in the system. This was generally attributed to the low thermal stability of the waxes. The studies also demonstrated that in most

cases the blends were more thermally stable than the pure waxes due the presence of the thermally more stable polymer matrices.

The thermal stability of conductive shape-stabilized PCMs is important because it has to be taken into account when the material is used in the thermal management of electronic devices. It was found in several studies [37-41] that the most commonly used conductive fillers are inorganic materials that include graphite and metals and that, besides their good thermal conductivity, they are also thermally stable at higher temperatures. The presence of and increase in conductive filler content generally improved the thermal stability of the polymer/wax blends. This was attributed to the immobilization of the polymer and wax free radicals and volatile degradation products, which not only retarded the degradation process, but also gave rise to evolution of the degradation products at higher temperatures. Improvements in thermal stability of polymer/EG composites were reported by a number of studies [22,44-45,47-49]. Graphite as nanofiller has an excellent thermal stability and therefore has a strong influence on the thermal degradation mechanism of the polymer. The improvements in thermal stability were explained through the 2-dimensional planar structure of the EG in the matrix, which serves as a barrier preventing further degradation of the underlying matrix.

1.2.4 Thermal conductivity

The importance of thermal conductivity in polymer composites and conductive phase change materials is associated with the need for appreciable levels of thermal conductance in circuit boards, heat exchangers, appliances, and machinery. A number of studies reported on the thermal conductivity of polymer/EG composites [43-44,50,54], and a fair amount of work was devoted to improving the thermal conductive of polymer/wax blends [38,40-41,55]. For the improvement of the thermal conductivity of polymer/wax blends, conductive fillers such as metal foams and graphite received a great deal of attention because of their high thermal conductivities. EG is considered as an excellent promoter because it is inert to chemical reaction, compatible with PCMs, and has a lower density than metals, thus making the latent heat thermal energy storage (LHTES) system lighter than the same volume LHTES system with metal promoters. A general increase in the thermal conductivity of polymers and polymer/wax blends was observed with the addition of and with increasing in EG or metal filler content. However, the metal fillers generally

gave rise to better thermal conductivities than the expanded graphite because of their inherently higher thermal conductivity. The improvements in the case of the EG containing samples were attributed to the formation of thermal conductive networks in the composites. It was also pointed out that a well dispersed system provides higher thermal conductivities than an agglomerated one, which was attributed to a better dispersion of the smaller graphite particles, with smaller polymer/wax and polymer matrix areas between these particles, and more well-defined thermal conductive networks. It was also found that both polymer and polymer/PCM conductive composites prepared by solution mixing showed better thermal conductivities than those prepared through melt mixing. This was attributed to better intercalation of the EG in the samples prepared from solution and, as a result, more thermal conductive pathways that were formed at lower EG contents.

1.2.5 Mechanical properties

The mechanical properties of polyolefin/wax blends were reported in a number of papers [27,29,32-33]. It was generally found that the Young's moduli of the blends were dependent on the wax content, and normally increased with an increase in wax content in the blends. This was associated with the higher degree of crystallinity of the waxes compared to those of the different polyolefins. Elongation at yield and yield stress did not show similar trends, but varied according to the investigated polymer/wax system. It was also shown that the yield stress increased with increasing wax content in the blends. This behaviour was expected, since the wax increased the crystallinity of the blend, and yield stress depends on crystallinity. A reduction in elongation at yield was reported with an increase in wax content. This was attributed to the crystallization of the wax in the amorphous part of the polymer, restricting the polymer chain mobility and forming defect centres. Since wax molecules are too short to form tie chains, the number of chain ends, i.e. the number of dislocations, will increase with an increase in wax content. This will induce a decrease in the strain. In case of polymer/EG composites, various studies [43,49-51] showed that an improvement in Young's modulus with the addition of EG was related to the large strength and aspect ratio of the graphite nanoplatelets. These investigations also showed a reduction in mechanical properties, especially at higher EG content or when using natural graphite as a reinforcing filler. This was mainly attributed to filler agglomeration in the polymer

matrix. The presence of aggregates in the composite resulted in crazing in which the adhesion between the filler and matrix was destroyed, and this resulted in a reduction in the mechanical properties.

1.2.6 Thermomechanical properties

Different authors investigated and reported on the thermo-mechanical properties of polyolefin/wax blends [1,2,9,18] and polymer/EG composites [43,49-51]. Generally the storage modulus increased with increasing wax content below the melting point of wax, because wax acted as a highly crystalline filler that immobilized the polymer chains at the crystal surface, but decreased at temperatures above the melting point of wax, because of the plasticizing effect of the molten wax. In the case of conductive form-stable PCM composites (polymer/wax/conductive filler) [40-41], the DMA results confirmed the softening effect of the wax and the reinforcing effect of the conductive filler (copper, graphite, carbon fiber, etc.). The increase in storage and loss modulus of the polymer/EG composites was attributed to the restriction in chain mobility of the polymer matrix by the graphite platelets. It was further observed that the dynamic mechanical properties of the polymer/graphite composites that were prepared by solution intercalation (SI), showed larger storage modulus values than the composites prepared through melt mixing. The stiffening of the SI prepared samples was attributed to the better dispersion of EG in the polymer matrix which enhanced the surface-to-volume ratio of EG and the interfacial interactions.

1.2.7 Flame resistance

Polymer nanocomposites filled with nanosized carbonaceous fillers, such as carbon nanotubes (CNTs) and EG, were shown to exhibit a remarkable balance of performance in terms fire resistance and barrier properties [22]. Generally, the high cost of CNTs has limited their extensive use in industrial sectors, and other alternatives were considered. Graphite combines the lower price and the layered structure of clays with superior thermal stability and fire resistance [22]. A number of studies were carried out on the dispersion of graphite in polymer matrices [22-23,48,52], and its synergistic effect with other intumescent flame retardant (IFR) materials for

form-stable PCMs [20,37-39,42] were investigated to improve their heat resistance applications. It was found that the addition of graphite into different matrices, and its synergistic effect with other IFR materials for form-stable PCMs, decreased the maximum value of the heat release rate (HRR) peak, the total heat release rate (THR), and increased the time to ignition (TTI). The amount of char formed was also directly proportional to the percentage of graphite added. The improvement in flame resistance was attributed to delaying the polymer decomposition because of the formation of an efficient char layer.

1.3 Research objectives

The study deals with phase change materials based on polyolefins (EVA and PP) blended with wax and mixed with EG with the aim of enhancing both the thermal conductivity and flame resistance of the shape-stabilized PCMs. The blends and composites were prepared with expanded graphite loadings of 3, 6, and 9 wt.%, while the polymer: wax ratios were kept constant at 1:1. The synergistic effect of the expanded graphite, diammonium phosphate and clay on the flame resistance of the PCM blends was also investigated.

1.4. Thesis organization

This thesis contains six chapters. Between this chapter and the ‘Conclusions’ chapter there are four chapters in publication format, because this work has already been submitted for publication in international journals.

1.5 References

1. A. Sharma, V.V. Tyagi, C.R. Chen, D. Buddhi. Review on thermal energy storage with phase change materials and applications. *Renewable and Sustainable Energy Reviews* 2009; 13:318-345.
DOI: 10.1016/j.rser.2007.10.005
2. A. Pasupathy, R. Velraj, R.V. Seeniraj. Phase change material-based building architecture commercial establishments. *Renewable and Sustainable Energy Reviews* 2008; 12:39-64.

- DOI: 10.1016/j.rser.2006.05.010
3. A. Sari, K. Kaygusuz. Some fatty acids used for latent heat storage: Thermal stability and corrosion of metals with respect to thermal cycling. *Renewable Energy* 2003; 28:939-948.
DOI: 10.1016/S0960-1481(02)00110-6
 4. M.M. Farid, A.M. Khudhair, S.A.K. Razack, S. Al-Hallaj. A review on phase change energy storage: Materials and applications. *Energy Conversion and Management* 2004; 45:1597-1615.
DOI: 10.1016/j.enconman.2003.09.015
 5. S.M. Hasnain. Review on sustainable thermal energy storage technologies, Part 1: Heat storage materials and techniques. *Energy Conversion and Management* 1998; 39:1127-1138.
DOI: 10.1016/S0196-8904(98)00025-9
 6. I. Krupa, G. Miková, A.S. Luyt. Phase change materials based on low-density polyethylene/paraffin wax blends. *European Polymer Journal* 2007; 43:4695-4705.
DOI: 10.1016/j.eurpolymj.2007.08.022
 7. M. Akgün, O. Aydin, K. Kaygusuz. Experimental study on melting/solidification characteristics of a paraffin as PCM. *Energy Conversion and Management* 2007; 48:669-678.
DOI: 10.1016/j.enconman.2006.05.014
 8. I. Krupa, G. Miková, A.S. Luyt. Polypropylene as a potential matrix for the creation of shape stabilized phase change materials. *European Polymer Journal* 2007; 43:895-907.
DOI: 10.1016/j.eurpolymj.2006.12.019
 9. M. Xiao, B. Feng, K. Gong. Thermal performance of high conductive shape-stabilized thermal storage material. *Solar Energy Materials and Solar Cells* 2001; 69:293-296.
DOI: 10.1016/S0927-0248(01)00056-3
 10. L. Xing, L. Hongyan, W. Shujun, Z. Lu, C. Hua. Preparation and thermal properties of form-stable paraffin phase change material encapsulation. *Solar Energy* 2006; 80:1561-1567.
DOI: 10.1016/j.enconman.2005.10.031
 11. L. Xia, P. Zhang, R.Z. Wang. Preparation and thermal characterization of expanded graphite/paraffin composite phase change material. *Carbon* 2010; 48:2538-2548.

- DOI: 10.106/j.carbon.2010.03.030
12. A. Sari. Form-stable paraffin/high density polyethylene composites as solid-liquid phase change material for thermal energy storage: Preparation and thermal properties. *Energy Conversion and Management* 2004; 45:2033-2042.
DOI: 10.1016/j.enconman.2003.10.022
 13. M. Xiao, B. Feng, K. Gong. Preparation and performance of shape stabilized phase change thermal storage materials with high thermal conductivity. *Energy Conversion and Management* 2002; 43:103-108.
DOI: 10.1016/S0196-8904(01)00010-3
 14. A. Elgafy, K. Lafdi. Effect of carbon nanofiber additives on thermal behavior of phase change materials. *Carbon* 2005; 43:3067-3074.
DOI: 10.1016/j.carbon.2005.06.042
 15. L. Fan, J.M. Khodadadi. Thermal conductivity enhancement of phase change materials for thermal energy storage. A review. *Renewable and Sustainable Energy Reviews* 2011; 15:24-46.
DOI: 10.1016/j.rser.2010.08.007
 16. A. Mills, M. Farid, J.R. Selman, S. Al-Hallaj. Thermal conductivity enhancement of phase change materials using a graphite matrix. *Applied Thermal Engineering* 2006; 26:1652-1661.
DOI: 10.1016/j.applthermaleng.2005.11.022
 17. Z. Zhang, X. Fang. Study on paraffin/expanded graphite composite phase change thermal energy storage material. *Energy Conversion and Management* 2006; 47:303-310.
DOI: 10.1016/j.enconman.2005.03.004
 18. A. Karaipekli, A. Sari, K. Kaygusuz. Thermal conductivity improvement of a stearic acid using expanded graphite and carbon fiber for energy storage applications. *Renewable Energy* 2007; 32:2201-2210.
DOI: 10.1016/j.renene.2006.11.011
 19. L. Xia, P. Zhang, R.Z. Wang. Preparation and characterization of expanded graphite/paraffin composite phase change material. *Carbon* 2010; 48:2538-2548.
DOI: 10.1016/j.carbon.2010.03

20. P. Zhang, Y. Hu, L. Song, J. Ni, W. Xing, J. Wang. Effect of expanded graphite on properties of high-density polyethylene/paraffin composite with intumescent flame retardant as a shape-stabilized phase change material. *Solar Energy Materials and Solar Cells* 2010; 94:360-365.
DOI: 10.1016/j.solmat.2009.10.014
21. P. Rybiński, G. Janowska. Influence of synergistic effect of halloysite nanotubes and halogen-free flame retardants on properties nitrile rubber composites. *Thermochimica Acta* 2012; 557:24-30.
DOI: 10.1016/j.tca.2013.01.030
22. M. Murari, A.L. Dechief, L. Bonnaud, Y. Paint, A. Gallos, G. Fontaine, S. Bourbigot, P. Dubois. The production and properties of polylactide composites filled with expanded graphite. *Polymer Degradation and Stability* 2010; 2010:889-900.
DOI: 10.1016/j.polymdegradstab.2009.12.019
23. X. Wu, L. Wang, C. Wu, J. Yu, L. Xie, G. Wang, P. Jiang. Influence of char residues on flammability of EVA/EG, EVA/NG and EVA/GO composites. *Polymer Degradation and Stability* 2012; 97:54-63.
DOI: 10.01016/j.polydegradstab.2011.10.011
24. W. Yang, Y. Hu, Q. Tai, H. Lu, L. Song, R.K.K. Yuen. Fire and mechanical performance of nanoclay reinforced glass-fiber/PBT composites containing aluminium hypophosphite particles. *Composites: Part A* 2011; 42:794-800.
DOI: 10.1016/j.compositesa.2011.03.009
25. K. Fukushima, M. Murariu, G. Camino, P. Dubois. Effect of expanded graphite/layered-silicate clay on thermal, mechanical and fire retardant properties of poly(lactic acid). *Polymer Degradation and Stability* 2010; 95:1063-1076.
DOI: 10.1016/j.polymdegrastab.201.02.029
26. N.P.G. Suardana, M.S. Ku, J.K. Lim. Effects of diammonium phosphate on the flammability and mechanical properties of bio-composites. *Materials and Design* 2010; 32:1990-1999.
DOI: 10.1016/j.matdes.2010.11.069
27. I. Krupa, A.S. Luyt. Thermal and mechanical properties of extruded LLDPE/wax blends. *Polymer Degradation and Stability* 2001; 73:157-161.

- DOI: 10.1016/S0141-3910(01)00082-9
28. I. Krupa, A.S. Luyt. Thermal properties of uncross-linked and cross-linked LLDPE/wax blends. *Polymer Degradation and Stability* 2000; 70:111-117.
DOI: 10.1016/S0141-3910(00)00097-5
 29. I. Krupa, A.S. Luyt. Physical properties of blends of LLDPE and an oxidized paraffin wax. *Polymer* 2001; 42:7285-7289.
DOI: 10.1016/S0032-3861(01)00172-0
 30. I. Krupa, A.S. Luyt. Thermal properties of polypropylene/wax blends. *Thermochimica Acta* 2001; 372:137-141.
DOI: 10.1016/S0040-6031(01)00450-6
 31. T.N. Mtshali, I. Krupa, A.S. Luyt. The effect of cross-linking on the thermal properties of LDPE/wax blends. *Thermochimica Acta* 2001; 380:47-54.
DOI: 10.1016/S0040-6031(01)00636-0
 32. H.S. Mpanza, A.S. Luyt. Comparison of different waxes as processing agents for low-density polyethylene. *Polymer Testing* 2006; 25:436-442.
DOI: 10.1016/j.polymertesting.2006.01.008
 33. S.P. Hlangothi, I. Krupa, V. Djoković, A.S. Luyt. Thermal and mechanical properties of cross-linked and uncross-linked linear low-density polyethylene-wax blends. *Polymer Degradation and Stability* 2003; 79:53-59.
DOI: 10.1016/S0141-3910(02)00238-0
 34. Y. Hong, G. Xin-shi. Preparation of polyethylene-paraffin compound as a form-stable solid-liquid phase change material. *Solar Energy Materials and Solar Cells* 2000; 64:37-44.
DOI: 10.1016/S0927-0248(00)00041-6
 35. Y. Cai, Y. Hu, L. Song, Y. Tong, R. Yang, Y. Zhang, Z. Chen, W. Fang. Flammability and thermal properties of high density polyethylene as a form-stable phase change material. *Journal of Applied Polymer Science* 2006; 99:1320-1327.
DOI: 10.1002/app.22065
 36. M.J. Hato, A.S. Luyt. Thermal fractionation and properties of different polyethylene/wax blends. *Journal of Applied Polymer Science* 2007; 104:2225-2236.
DOI: 10.1002/app.25494

37. Y. Cai, Q. Qufu, F. Huang, S. Lin, F. Chen, W. Gao. Thermal stability, latent heat and flame retardant properties of the thermal energy storage phase change materials based on paraffin/high density polyethylene composites. *Renewable Energy* 2009; 34:2117-2123.
DOI: 10.1016/j.renene.2009.01.017
38. L. Zhang, J. Zhu, W. Zhou, J. Wang, Y. Wang. Thermal and electrical conductivity enhancement of graphite nanoplatelets on form-stable polyethylene glycol/polymethyl methacrylate composite phase change materials. *Energy* 2012; 39:294-302.
DOI: 10.1016/j.energy.2012.01.011
39. Y. Cai, Q. Wei, F. Huang, W. Gao. Preparation and properties studies of halogen-free flame retardant form-stable phase change materials based on paraffin/high density polyethylene composites. *Applied Energy* 2008; 85:765-775.
DOI: 10.1016/j.apenergy.2007.10.017
40. J.A. Molefi, A.S. Luyt, I. Krupa. Investigation of thermally conducting phase-change materials based on polyethylene/wax blends filled with copper particles. *Journal of Applied Polymer Science* 2010; 116:1766-1774.
DOI: 10.1002/app.31653
41. W. Mhike, W.W. Focke, J.P. Mofokeng, A.S. Luyt. Thermally conductive phase-change materials for energy storage based on low-density polyethylene, soft Fischer-Tropsch and graphite. *Thermochimica Acta* 2012; 527:75-82.
DOI: 10.1016/j.tca.2011.10.008
42. W. Zheng, S.C. Wong. Electrical conductivity and dielectric properties of PMMA/expanded graphite composites. *Composites Science and Technology* 2003; 63:225-235.
DOI: S0266-3538(02)00201-4
43. S. Ganguli, A.K. Roy, D.P. Anderson. Improved thermal conductivity for chemically functionalized exfoliated graphite/epoxy composites. *Carbon* 2008; 46:806-817.
DOI: 10.1016/j.carbon.2008.02.008
44. J.J. George, A.K. Bhowmick. Ethylene vinyl acetate/expanded graphite nanocomposites by solution intercalation: Preparation, characterization and properties. *Journal of Materials Science* 2008; 43:702-708.
DOI: 10.1007/s10853-007-2193-6

45. Y.F. Zhao, M. Xiao, S.J. Wang, X.C. Ge, Y.Z. Meng. Preparation and properties of electrically conductive PPS/expanded graphite nanocomposites. *Composites Science and Technology* 2007; 67:2528-2534.
DOI: 10.1016/j.compscitech.2006.12.009
46. W. Zheng, X. Lu, S.C. Wong. Electrical and mechanical properties of expanded graphite-reinforced high-density polyethylene. *Journal of Applied Polymer Science* 2004; 91:2781-2788.
DOI: 10.1002/app.13460
47. G. Hatui, P. Bhattacharya, S. Sahoo, S. Dhibar, C.K. Das. Combined effect of expanded and multiwall carbon nanotubes on the thermo mechanical, morphological as well as electrical conductivity of *in situ* bulk polymerized polystyrene composites. *Composites: Part A* 2014; 56:181-191.
DOI: 10.1016/j.compositesa.2013.10.007
48. W.W. Focke, H. Muiambo, W. Mhike, H.J. Kruger, O. Ofosu. Flexible PVC flame retarded with expandable graphite. *Polymer Degradation and Stability* 2014; 100:63-69.
DOI: 10.1016/j.polymdegrads.2013.12.013
49. M. Li, Y.G. Jeong. Poly(ethylene terephthalate)/exfoliated graphite nanocomposites with improved thermal stability, mechanical and electrical properties. *Composites: Part A* 2011; 42:560-566.
DOI: 10.1016/j.compositesa.2011.01.015
50. Q. Mu, S. Feng. Thermal conductivity of graphite/silicone rubber prepared by solution intercalation. *Thermochimica Acta* 2007; 462:70-75.
DOI: 10.1016/j.tca.2007.06.006
51. K. Sever, I.H. Tavman, Y. Seki, A. Turgut, M. Omastova, I. Ozdermir. Electrical and mechanical properties of expanded graphite/high density polyethylene nanocomposites. *Composites: Part B* 2013; 53:226-233.
DOI: 10.1016/j.compositesb.2013.04.069
52. F.M. Uhl, Q. Yao, H. Nakajima, E. Manias, C.A. Wilkie. Expandable graphite/polyamide-6. *Polymer Degradation and Stability* 2005; 89:70-84.
DOI: 10.1016/j.polymdegradstab.2005.01.004

53. Z. Li, B. Qu. Flammability characterization and synergistic effects of expandable graphite with magnesium hydroxide in halogen-free flame-retardant EVA blends. *Polymer Degradation and Stability* 2003; 81:401-408.
DOI: 10.1016/S0141-3910(03)00123-X
54. I. Krupa, I. Chodák. Physical properties of thermoplastic/graphite composites. *European Polymer Journal* 2001; 37:2159-2168.
DOI: S0014-3057(01)00115-X
55. J. Xiang, L.T. Drzal. Investigation of exfoliated graphite nanoplatelets (xGnP) in improving thermal conductivity of paraffin wax-based phase change material. *Solar Energy Materials and Solar Cells* 2011; 95:1811-1818.
DOI: 10.1016/j.solmat.2011.01.048

Chapter 2

The effect of expanded graphite on the thermal stability, latent heat and flammability properties of EVA/wax phase change blends

This chapter has been published online:

M.J. Mochane, A.S. Luyt. The effect of expanded graphite on the thermal stability, latent heat and flammability properties of EVA/wax phase change blends. Polymer Engineering and Science (DOI: 10.1002/pen.24063).

Abstract

This article reports on the morphology, melting and crystallization behavior, thermal stability, flammability and thermal conductivity of shape-stabilized phase-change materials (PCM) for thermal energy storage, based on a soft Fischer-Tropsch paraffin wax, the PCM, blended with ethylene vinyl acetate (EVA). These immiscible blends were melt-mixed with expanded graphite (EG) (up to 9 wt.%) to improve the thermal conductivity and flame resistance of the material. It was observed that the EG particles agglomerate in the absence of wax, but disperse much better in the EVA/wax blend, probably because the wax penetrates in between the EG layers (there seems to be a better interaction between wax and EG than between EVA and EG) and separates the layers, giving rise to smaller and better dispersed EG particles. This gives rise to better thermal conductivity and flame resistance. There were no significant changes in the melting temperature of EVA in the EVA/EG composites, while the crystallinities of EVA were observably lower in the presence of EG. The thermal stability and flammability results show an increase in thermal stability and flame resistance of EVA, which further improved in the presence of wax because of the smaller and better dispersed EG particles in these systems.

Keywords: Phase change material; wax; EVA; expanded graphite; flammability

2.1 Introduction

Phase change material (PCM) plays a significant role in thermal energy storage systems because of its large thermal energy storage capacity and isothermal behaviour when it changes phase [1-3]. Several types of PCM such as fatty acids and paraffin were studied recently for use as latent heat storage materials [4,5]. Among the investigated PCMs, paraffins exhibit desirable properties such little or no supercooling, self-nucleating behaviour, as well as thermal and chemical stability. Although paraffin wax has been found to display many desirable properties, drawbacks such as leakage, as well as low thermal conductivity and stability, restricted their extensive application [6].

In order to solve the leakage problem during a phase change, methods such as encapsulation and physical mixing were investigated [7-9]. The materials prepared by physical mixing are actually phase change composites. Paraffin wax was encapsulated in a three-dimensional network formed by polymers such as high density polyethylene (HDPE) and polypropylene (PP) [10-13]. The operating temperature of the paraffin wax should remain below the melting point of the supporting material, so that the shape stabilized PCM can keep its shape even when the paraffin changes from solid to liquid. The storage capacity of PCMs is dependent on the mass ratio of paraffin in the PCM blends and/or composites, and it is therefore necessary to introduce large amounts of paraffin to obtain PCMs with high energy storage. The energy storage capacity will still be lower than that of wax/EG composites, but the wax is not contained in the latter composites and can easily flow at temperatures above wax melting.

An increase in the number of different applications of PCMs demands the need for other potential polymers that can be used as shape stabilizing matrices for paraffin wax. There are some applications that require flexible thermal storage composite materials. Examples are diver wet suits, and metabolic heating/cooling blankets useful for treatment of patients. In this paper EVA has been chosen as the matrix, because it is a polymer that approaches elastomeric properties in terms of softness and flexibility, but it can still be processed like other thermoplastics. The melting point of the wax may be slightly too high for these applications, but our findings can easily be applied to similar composites containing lower melting point paraffins.

Thermal conductivity is important for the practical application of PCMs. To overcome the lower thermal conductivity of paraffin wax and the supporting polymer, metallic or non-metallic

materials with high thermal conductivities were introduced in PCMs, and PCMs were impregnated into high thermal conductivity materials with porous structures [14-16], such as carbon materials and metal foams. When compared with carbon materials, metal foams significantly increase the weight of the storage system and are also incompatible with PCMs [3]. Recently, expanded graphite was used to improve the heat transfer in the PCMs, due to its high thermal conductivity, good stability, good compatibility with organic PCMs, and lower density compared to metal promoters [17,18].

Although the preparation, leakage, thermal conductivity and thermal storage properties of PCMs were extensively studied [9-14], there are almost no reports on the flammability properties of the form-stable PCMs. Good flame resistance is important in a large number of applications, especially in the building industry [19]. Expanded graphite (EG) do not only act as a supporting material, but it can also improve the thermal conductivity and flame resistance of form-stable PCM composites. This paper deals with the preparation of shape-stabilized PCMs composed of paraffin wax, EVA and EG which should have excellent latent heat, thermal conductivity, and flame resistance, without liquid leakage during the phase-change process.

2.2 Materials and methods

2.2.1 Materials

Medium-soft Fischer-Tropsch paraffin wax (M3 wax) was supplied in powder form by Sasol Wax. It consists of approximately 99% of straight chain hydrocarbons, and it is primarily used in the candle-making industry. It has an average molar mass of 440 g mol⁻¹ and a carbon distribution between C15 and C78. Its density is 0.90 g cm⁻³ and it has a melting point range around 40-60 °C. EVA-460 was manufactured and supplied in granule form by DuPont Packaging & Industrial Polymers. EVA-460 contains 18% by weight of vinyl acetate (VA) with a BHT antioxidant thermal stabilizer. It has an MFI (190 °C / 2.16 kg) of 2.5 g/10 min (ASTM D1238-ISO 1133), T_m of 88 °C, and density of 0.941 g cm⁻³. Expandable graphite ES 250 B5 was supplied by Qingdao Kropfmuehl Graphite (Hauzenberg, Germany).

2.2.2 Preparation of expanded graphite

The expandable graphite was first dried in an oven at 60 °C for 10 h. The expandable graphite was then heated in a furnace to 600 °C using a glass beaker and maintained at that temperature for 15 min to form expanded graphite.

2.2.3 Preparation of blend and composite samples

All the samples (Table 2.1) were prepared by a melt mixing process using a Brabender Plastograph 50 mL internal mixer at 130 °C and 60 rpm for 20 min. For the blends, the dry components were physically premixed and then fed into the heated mixer, whereas for the composites, the EG was added into the Brabender mixing chamber within 5 minutes after adding the EVA or premixed EVA/wax blends. The samples were then melt-pressed at 130 °C for 5 min under 50 kPa pressure using a custom built 20 ton hydraulic melt press to form 15 x 15 cm² sheets.

Table 2.1 Sample compositions used in this study

EVA/EG (w/w)	EVA/wax/EG (w/w)	EVA/wax/EG (w/w)	EVA/wax/EG (w/w)
100/0	50/50/0	60/40/0	70/30/0
97/3	48.5/48.5/3	58.2/38.8/3	67.9/29.1/3
94/6	47/47/6	56.4/37.6/6	65.8/28.2/6
91/9	45.5/45.5/9	54.6/36.4/9	63.7/27.3/9

2.2.4 Sample analysis

To determine the morphology of the fracture surfaces, a TESCAN VEGA 3 scanning electron microscope was used and the analysis was done at room temperature. The samples were gold coated by sputtering to produce conductive coatings onto the samples.

The optical microscopy images were captured using a CETI (Belgium) optical microscope and the samples were cut using a microtome knife (Microtome American optical model 820).

The DSC analyses were done in a Perkin Elmer Pyris-1 differential scanning calorimeter under flowing nitrogen (flow rate 20 mL min⁻¹). Samples of mass 5-10 mg were sealed in aluminum pans and heated from -30 °C to 130 °C at a heating rate of 10 °C min⁻¹ and cooled under the same conditions. The peak temperature of crystallization and melting, as well as the crystallization and melting enthalpies, were determined from the cooling and second heating scans. The DSC measurements repeated on three different samples of the same composition. The temperatures and enthalpies are reported as average values with standard deviations.

The thermogravimetric (TGA) analyses were carried out in a Perkin Elmer Pyris-1 thermogravimetric analyzer. Samples ranging between 5 and 10 mg were heated from 30 to 650 °C at a heating rate of 10 °C min⁻¹ under nitrogen (flow rate 20 mL min⁻¹).

Thermal conductivity measurements were performed on discs 5 mm thick and 12 mm in a diameter using a ThermTest Inc. Hot Disk TPS 500 thermal constants analyzer. The instrument uses the transient plane source method. A 3.2 mm Kapton disk type sensor was selected for the analysis. The sensor was sandwiched between two sample discs. Three measurements were performed for each composition.

Cone calorimetry measurements were performed on a Dual Cone calorimeter using a cone shaped heater at an incident heat flux of 35 kW m⁻². The specimens, with dimensions of 6 x 100 mm x 100 mm³, were prepared by compression molding. The following quantities were measured using the cone calorimeter: Peak heat release rate, time to ignition, mass loss rate, as well as carbon monoxide and carbon dioxide yields.

2.3 Results and discussion

2.3.1 Microscopic analysis

Figure 2.1 shows the scanning electron microscopy (SEM) images of the expandable graphite, expanded graphite, as well as wax/expanded graphite composite. When intercalated (expandable) graphite is heated past a critical temperature, a large expansion (up to hundreds of times) of the graphite flakes occur along the c-axis (out of plane) direction, forming vermicular or worm-like structures with low density and multiple pores (Figure 2.1b). The open pores are interconnected with many surfaces, which allow them to be easily saturated with molten paraffin wax. The wax

in the composites strongly interacts with the EG and completely covers the EG surface, probably penetrating the pores. This is probably due to capillary and surface tension forces between the wax and the porous network of the EG. The porous network structure of EG provide a reasonable mechanical strength to the composites. Similar SEM images were obtained by other studies using different PCMs [15,17,20].

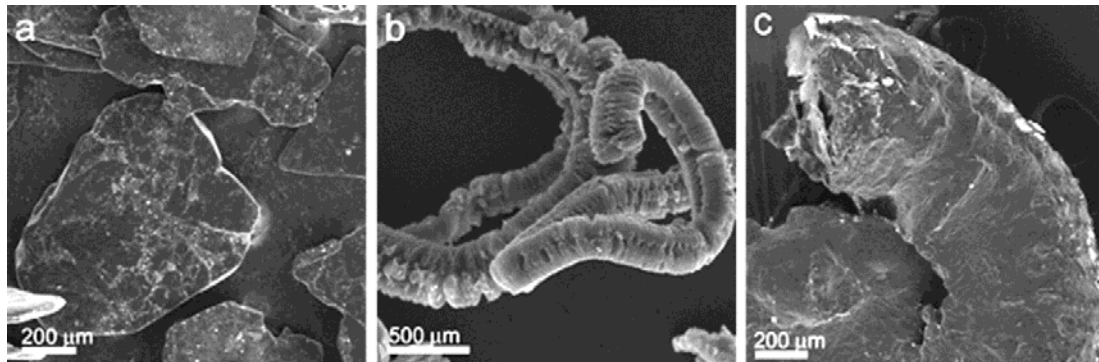


Figure 2.1 SEM images of the (a) expandable graphite, b) expanded graphite, and (c) a wax/EG composite

Figure 2.2 shows the optical microscopy images of some of the investigated samples. The image of the EVA/EG composite shows that the expanded graphite particles agglomerated in the absence of wax (arrow in Figure 2.2a), which probably results in the poorer thermal conductivity of these composites. The EVA/wax/EG composite, however, shows better dispersion of EG in the blend which should result in the formation of a thermally conductive network in the matrix and better thermal conductivity. The low molecular weight wax contributed to this improved dispersion by penetrating in between the EG layers and separating the layers, giving rise to smaller and better dispersed EG particles.

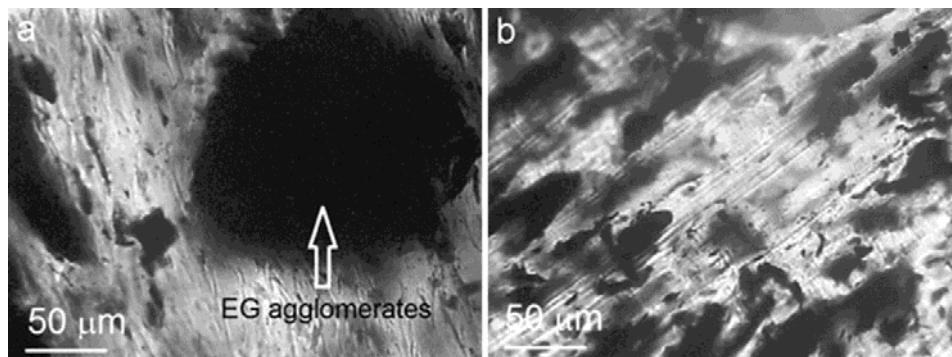


Figure 2.2 Optical microscopy images of the (a) 94/6 w/w EVA/EG, and (b) 65.8/28.2/6 w/w EVA/wax/EG

2.3.2 Differential scanning calorimetry (DSC)

The DSC results of the investigated samples are shown in Figure 2.3 and summarized in Table 2.2. The expected combined melting enthalpy of wax and EVA were calculated using Equation 1.

$$\Delta H^{\text{calc}} = (\Delta H_{m,\text{EVA}} \times w_{\text{EVA}}) + (\Delta H_{m,\text{wax}} \times w_{\text{wax}}) \quad (1)$$

where $\Delta H_{m,\text{EVA}}$ is the melting enthalpy and w_{EVA} the weight fraction of EVA, and $\Delta H_{m,\text{wax}}$ is melting enthalpy w_{wax} the weight fraction of wax, in the composites.

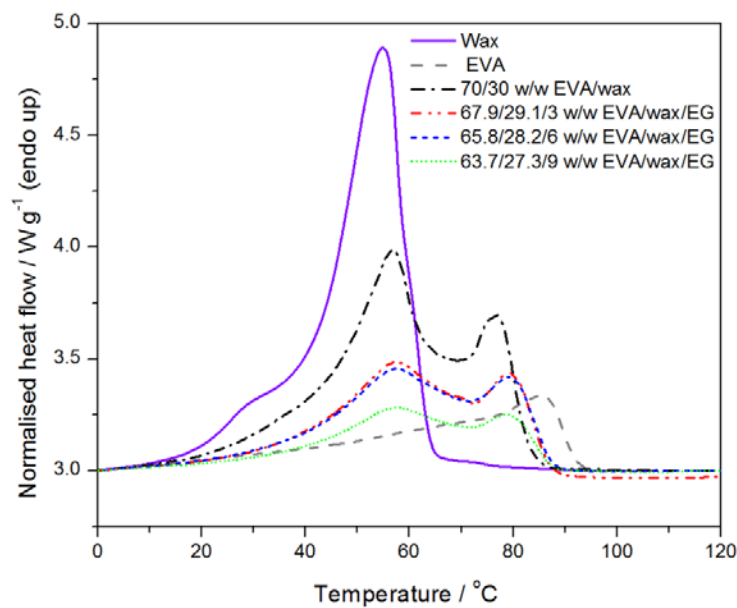


Figure 2.3 DSC heating curves of EVA, wax, an EVA blend and some EVA/wax/EG composites

The wax shows a melting peak at 57 °C, with a peak shoulder at 33 °C and a melting enthalpy of 205 J g⁻¹ (Figure 2.3). The peak shoulder relates to a solid-solid transition, and the main peak is associated with the melting of the crystallites [11]. This melting temperature makes the wax useful as phase-change material in buildings for heating and cooling applications, for under-floor heating systems, and for solar water heating. The application of shape-stabilized PCM plates for an under-floor electric heating system could shift half of the total electric heat energy from the peak to the off peak period, which would provide significant economic benefit. Similarly a lot of energy can be saved by developing a latent heat storage unit for evening and

morning hot water requirements, using a box type solar collector. The EVA melts at 86 °C and has a melting enthalpy of 86 J g⁻¹. The blend and composites show both these peaks, although strongly overlapped. The individual melting enthalpies of the wax and the EVA in the blend and composite samples could therefore not be determined with acceptable accuracy. The melting point of EVA in the blends and composites decreased with an increase in wax content, which indicated the plasticizing effect of the wax on the EVA.

Table 2.2 Summary of melting temperatures and enthalpies for all the investigated samples

Sample	T _{p,m} (EVA) / °C	T _{p,m} (wax) / °C	ΔH _m ^{obs} / J g ⁻¹	
EVA	86.2 ± 0.6		86.0 ± 0.7	
Wax		57.0 ± 0.9	205.2 ± 0.5	
EVA/EG (w/w)				ΔH_m^{norm} / J g⁻¹
97/3	87.5 ± 0.3		75.3 ± 2.2	77.6
94/6	87.6 ± 0.6		71.2 ± 5.1	75.7
91/9	87.6 ± 0.3		68.3 ± 3.0	75.1
EVA/wax (w/w)				ΔH_m^{calc} / J g⁻¹
70/30	85.2 ± 0.3	55.2 ± 0.4	120.0 ± 0.3	121.8
60/40	81.2 ± 1.7	55.3 ± 0.2	130.0 ± 1.2	133.7
50/50	77.7 ± 0.3	55.2 ± 0.4	141.0 ± 0.7	145.6
EVA/wax/EG (w/w)				
67.9/29.1/3	81.0 ± 0.4	56.2 ± 0.2	117.2 ± 0.8	118.1
65.8/28.2/6	81.5 ± 0.3	55.5 ± 0.2	112.9 ± 0.7	114.3
63.7/27.3/9	81.6 ± 0.8	55.2 ± 0.4	109.1 ± 0.9	110.8
58.2/38.8/3	79.9 ± 0.7	57.2 ± 0.5	127.4 ± 0.6	129.7
56.4/37.6/6	79.3 ± 0.2	55.8 ± 0.5	123.8 ± 0.9	125.7
54.6/36.4/9	78.8 ± 0.5	56.0 ± 1.0	118.1 ± 0.2	121.7
48.5/48.5/3	77.2 ± 0.4	55.4 ± 0.4	139.6 ± 0.2	141.2
47/47/6	76.9 ± 0.2	54.7 ± 0.5	133.2 ± 1.4	136.8
45.5/45.5/9	78.7 ± 1.1	54.9 ± 0.9	125.3 ± 0.5	132.5

T_{p,m}, ΔH_m^{obs}, ΔH_m^{norm}, and ΔH_m^{calc} are respectively the peak temperature of melting, the total enthalpy calculated from the overlapping wax and EVA melting peaks, the melting enthalpy normalised to the amount of EVA in the sample, and the expected melting enthalpy calculated from the melting enthalpies of pure wax and pure EVA and the respective mass ratios of EVA, wax and EG in the blend composites

There were no significant changes in the melting temperature of EVA in the EVA/EG composites. The melting enthalpies of EVA in the EVA/EG seem to decrease with increasing EG content. However, when normalised to the amount of EVA in the composites, the enthalpies are almost constant but significantly lower than that of pure EVA. When inorganic filler particles are very small, they normally act as nucleation sites for the crystallization of the polymer matrix. However, larger particles that are the result of agglomeration would rather restrict polymer chain mobility and reduce the extent of crystallization. This explains the reduced melting enthalpy in this case, because large agglomerated EG particles were observed in Figure 2.2.

2.3.3 Thermogravimetric analysis (TGA)

The TGA curves in Figure 2.4 show that EG is thermally stable up to temperatures much higher than the evaporation/decomposition temperature ranges for wax and EVA. Wax generally does not decompose, and in this case it evaporated at temperatures much lower than the decomposition temperatures of EVA. The EVA shows a two-step degradation related to deacetylation and main-chain decomposition [21].

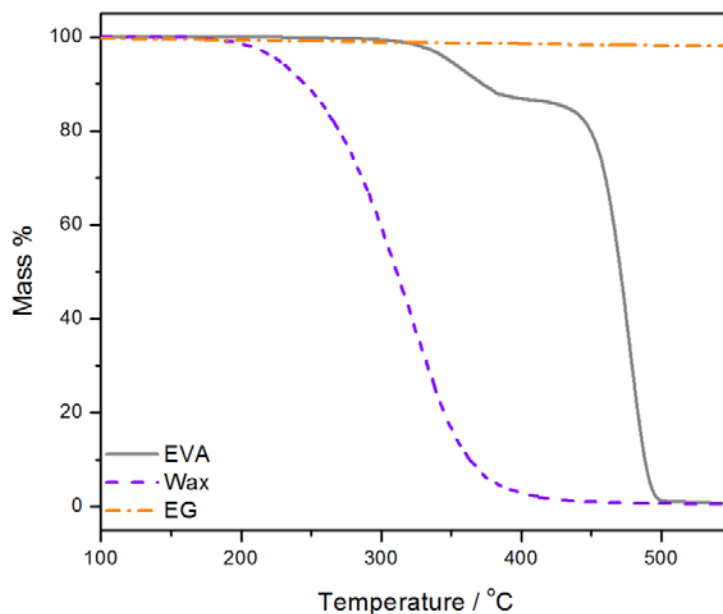


Figure 2.4 TGA curves of EVA, wax and EG

The presence of EG in EVA slightly improved the thermal stability of EVA (Figure 2.5 and Table 2.3). The reason for this is probably that the thermal energy is initially absorbed by the EG so that enough energy to initiate the EVA degradation only becomes available at slightly higher temperatures. It is also possible that the volatile decomposition products were adsorbed onto the EG surfaces, which retarded its diffusion out of the sample resulting in the onset of mass loss only being observed at slightly higher temperatures [22]. Murariu *et al.* [22] and Zhao *et al.* [23] studied the properties of PLA and PPS composites filled with EG and reported a delay in the thermo-degradation of these polymers. This was associated with the 2-dimensional planar structure of the well dispersed EG in the polymers, which served as a barrier preventing the further degradation of the polymers. Fawn *et al.* [24] reported that the temperature at maximum degradation rate of polyamide-6 in expandable graphite/polyamide-6 nanocomposites slightly increased at low graphite contents, but did not increase further with increasing graphite contents. They attributed this to the release of acid trapped between the graphite platelets when converting graphite into expanded graphite, which accelerated the degradation of the PA-6.

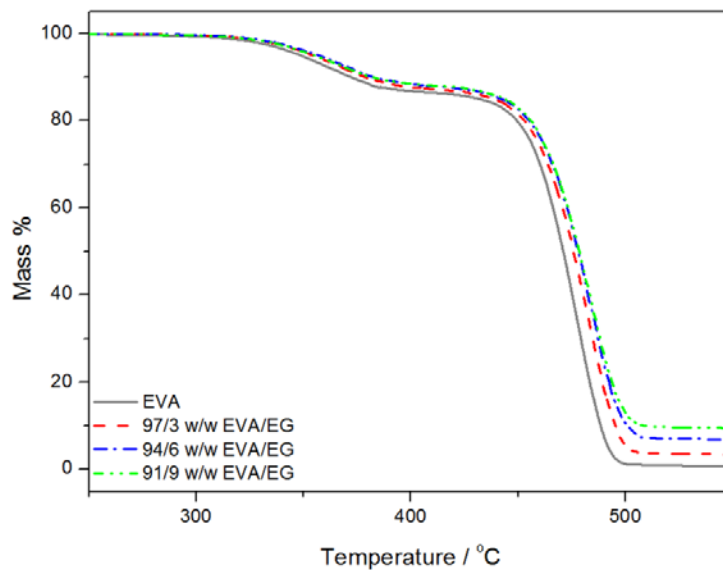


Figure 2.5 TGA curves of neat EVA and the EVA/EG composites

The EVA/wax blend and EVA/wax/EG blend composites (Figure 2.6) show two degradation steps; the first is attributed to the evaporation of wax immediately followed by deacetylation of EVA, with the second one due to the degradation of the EVA backbone. The presence of EG gives rise to mass loss starting at significantly higher temperatures (Table 2.3). The temperature at 10% mass loss, $T_{10\%}$, for the sample containing 3 wt% of expanded graphite is increased by 26 °C. However, the onset of degradation of the EVA main chains did not seem to change significantly (Figure 2.6). The EG, which interacted strongly with the wax, probably inhibited the diffusion of wax volatiles from the molten blend composite. However, after wax evaporation the EVA degradation seemed to have proceeded normally as in the case of the EVA/EG composites. For all the composites there is a good correlation between the % residue at 550 °C and the amount of graphite originally mixed into the composites, which indicates that the graphite was generally well dispersed in the EVA/wax blend.

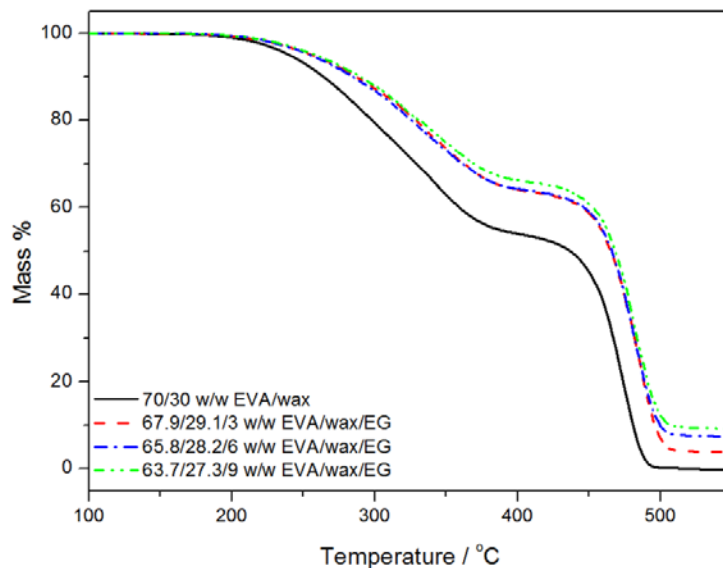


Figure 2.6 TGA curves of 70/30 w/w EVA/wax and EVA/wax/EG composites

Table 2.3 TGA results for investigated samples

Sample	T _{10%} / °C	T _{70%} / °C
EVA	373.7	479.0
EVA/wax (w/w)		
70/30	260.6	465.6
EVA/EG (w/w)		
97/3	375.6	482.7
94/6	380.5	485.6
91/9	381.0	487.3
EVA/wax/EG (w/w)		
67.9/29.1/3	286.9	481.7
65.8/28.2/6	287.0	480.6
63.7/27.3/9	288.1	484.9

T_{10%} and T_{70%} are degradation temperatures at 10% and 70% mass loss respectively

2.3.4 Thermal conductivity

The thermal conductivity values of all the investigated samples are shown Figure 2.7. The thermal conductivity of the samples increased (almost linearly) with increasing graphite content. Heat transport in graphite nanoplatelets occurs by phonons of varying frequencies. The high frequency phonons are the major heat energy carriers and low frequency phonon vibrations are available to carry a small amount of heat energy [25]. The thermal conductivity of EVA/EG increased slower with increasing EG content than that of EVA/wax/EG. The reason for this is probably the smaller and better dispersed EG particles in the EVA/wax blends. The smaller EG particles introduce more phonon scattering interfaces at the boundaries and facilitate phonon transport due to larger thermal contact areas. The distances between the larger number of smaller particles are also smaller, which will further improve the transport of thermal energy between the particles and through the samples. Because of the agglomeration of EG in the EVA matrix, a high thermal interface resistance exists between the boundaries and give rises to a reduction in heat transfer in the composites. In this case the phonons are transported over longer distances through the polymer (which has a low thermal conductivity) from one EG particle to another and

only low frequency phonon vibration modes are available to carry a small amount of energy. The thermal conductivity decreased with increasing wax content in the blends and composites. This may be ascribed to the lower thermal conductivity of $0.24 \text{ W m}^{-1} \text{ K}^{-1}$ for the wax compared to $0.37 \text{ W m}^{-1} \text{ K}^{-1}$ for EVA, as well as to the fact that the wax crystallizes mostly around the EG particles and ‘isolates’ them from the rest of the system.

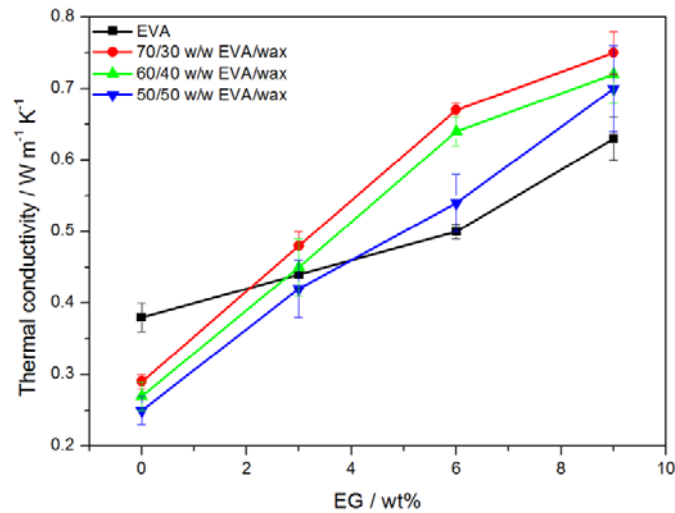


Figure 2.7 Thermal conductivities of EVA and the EVA/wax blends with different amounts of expanded graphite

One could expect further increases in thermal conductivity of the materials with increase in EG content, but larger amounts of inorganic filler will reduce the mechanical properties of the polymer and make it more brittle [6]. The improvement in thermal conductivity in the presence of EG means that heat may be transferred faster between the wax phase change material and the environment around the EVA/wax/EG composite.

2.3.5 Cone calorimetry

The cone calorimeter is one of the most effective bench scale methods for investigating the combustion properties of polymer composites. The cone calorimetry test is based on the oxygen consumption principle. The results correlate well with those obtained from large-scale fire tests and can be used to predict the combustion behaviour of materials in real fires. For instance, the peak HRR is a very important parameter, which can be used to express the intensity of fire [1,4].

The parameters available from the cone calorimeter are: heat release rate (HRR), and especially its peak value (PHRR), time to ignition, time to PHRR, and mass loss rate. Figure 2.8 shows the dynamic curves of HRR versus time for an EVA/wax blend, as well as EVA/EG and EVA/wax/EG composites. The first peak for the EVA/wax blend is attributed to the evaporation of wax. The second larger peak is caused by the heat release from the polymer. The wax releases heat before the polymer because of a lower pyrolysis temperature. The PHRR decreases with the addition of expanded graphite. A highly flame retardant system normally shows low HRR values [1,4,26]. The HRR is normally suppressed because of the efficiently protective char. The protective barrier limits the oxygen diffusion into the substrate and retards the volatilization of the flammable decomposition products. It is interesting to observe that the HRR of the EVA/wax/EG composite is lower than that of EVA/EG. The low PHRR values correlate with those of other well dispersed systems [24]. Sun *et al.* [27] reported that the HRR of HDPE/EVA/EG1 was lower than that of HDPE/EVA/EG2, where EG1 had smaller particles than EG2. This was attributed to the much more stable interfacial structure of the smaller particles, and to the better dispersion in the polymer matrix. The ideal situation would be one in which the time to ignition is increased while the PHRR is greatly reduced, indicating that not all the polymer burns.

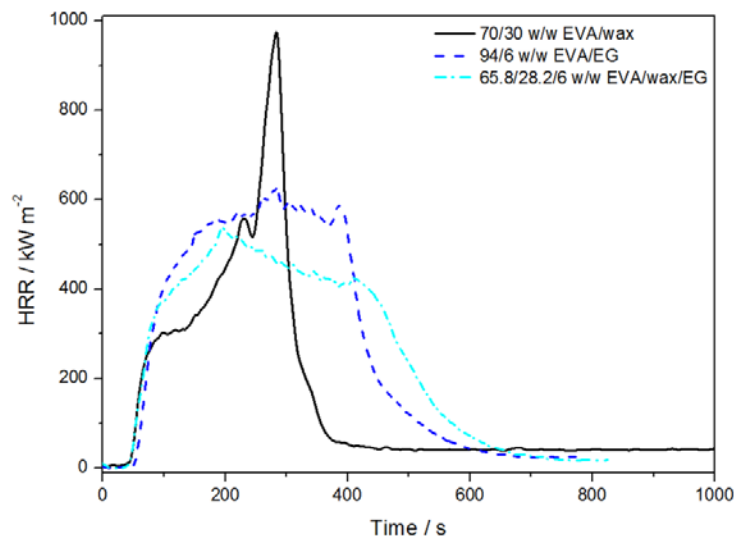


Figure 2.8 Heat release rate curves of an EVA/wax blend, as well as EVA/EG and EVA/wax/EG composites

The fire performance index (FPI), a parameter defined as the ratio of PHRR to time-to-ignition, is independent of the sample thickness and can be used to evaluate the fire resistance of a material. The lower the FPI value the more fire safe is a material. The fire growth index (FIGRA), used as the flame spread indicator parameter, is calculated as the ratio of PHRR to the time-to-PHRR. The lower the fire growth index the higher the fire safety of a given material. The FIGRA and FPI results in Table 2.4 show lower values for the EVA/EG and EVA/wax/EG composites than for the EVA/wax blend. The time to ignition of the EVA/EG and EVA/wax/EG composites is also longer than that of the EVA/wax blend. All these results confirm the flame retardant efficiency of the expanded graphite.

Table 2.4 Flammability data of an EVA/wax blend, as well as EVA/EG and EVA/wax/EG composites

Sample	PHRR / kW m ⁻²	TTI / s	t _{PHRR} / s	FPI / kW m ⁻² s ⁻¹	MLR* / g s ⁻¹	FIGRA / kW m ⁻² s ⁻¹	ASEA / m ² kg ⁻¹
70/30 w/w EVA/wax	851.8	43	268	19.8	0.86	3.2	119.2
65.8/28.2/6 w/w EVA/wax/EG	544.6	46	203	11.8	0.16	2.7	444.4
94/6 w/w EVA/EG	610.2	56	278	10.9	0.18	2.2	357.9

* Peak values from MLR curves in Figure 2.9

Another important parameter in the dynamic flammability characteristics of a material is the mass loss rate (MLR). Figure 2.9 shows the MLR curve versus time for the investigated samples. The MLR values of the EVA/EG and EVA/wax/EG samples are significantly lower than those of the EVA/wax blend (Table 2.4). The MLR data further supports the flame retardant efficiency of expanded graphite, which is very important for the practical usage of EG as a halogen-free flame retardant.

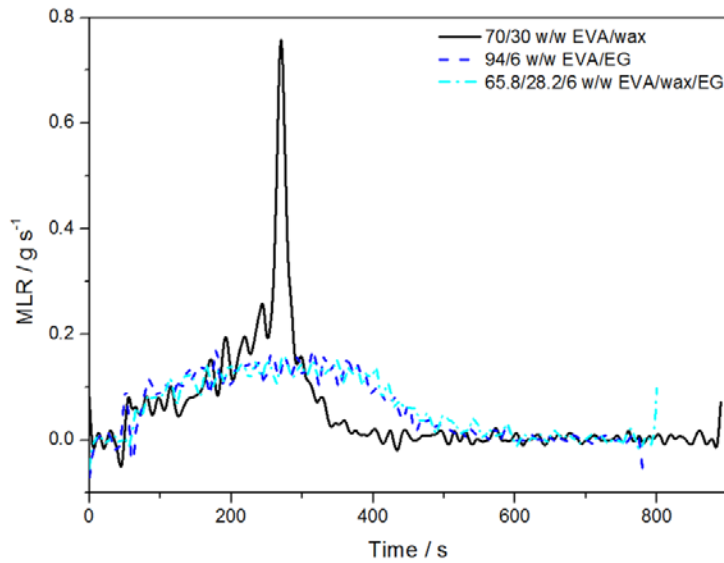


Figure 2.9 MLR versus time graphs for an EVA/wax blend, as well as EVA/wax/EG and EVA/EG composites

Generally, the smoke production rate (SPR) and HRR play a critical role in fire conditions. The SPR versus time curves of the EVA/wax blend and the EVA/EG and EVA/wax/EG composites are shown in Figure 2.10. Similar to the HRR curves, we can see that the maximum in the SPR plot of the EVA/wax/EG composite is lower than that of the EVA/wax blend and the EVA/EG composite. The SPR of EVA/wax slowly increases over time and reaches a single maximum value at approximately 280 s, after which it decreases rapidly until it reaches zero at about 360 s. EVA/EG, however, increases almost immediately until it reaches a maximum value which is almost the same as that of EVA/wax. It does, however, maintain this value over a much longer period of time. The reason for this is the presence of EG agglomerates in EVA, resulting in a longer period of time before an effective char layer is formed. The EVA/wax/EG shows a very similar trend, but in this case the maximum SPR is much lower than in the case of the other two samples. The well dispersed EG in the presence of wax forms a more effective char shield than the agglomerated EG in the EVA/EG composite, hence the lower SPR values because of the formation of an effective intumescent char shield, which is strong enough to resist heat from the cone calorimeter and prevent material from cracking and pursuing further degradation [28].

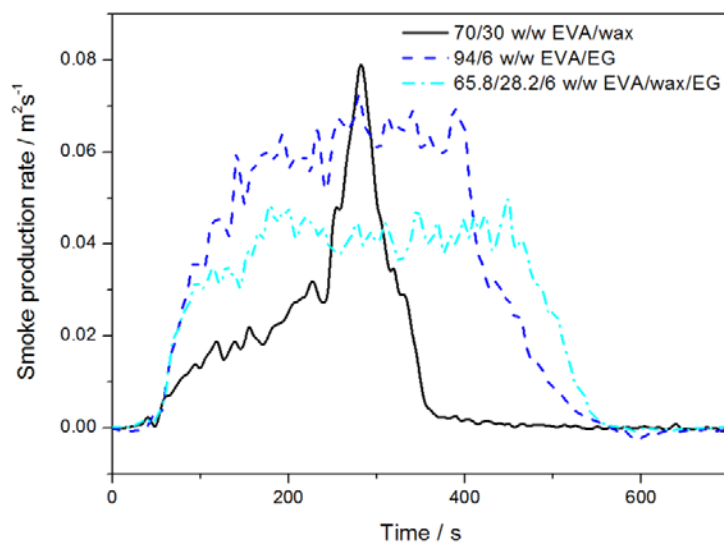
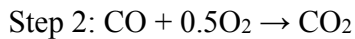
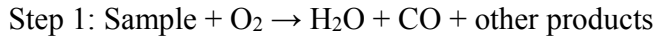


Figure 2.10 Smoke production rate (SPR) plots of an EVA/wax blend, as well as EVA/EG and EVA/wax/EG composites

The average specific extinction area (ASEA) is another parameter used to evaluate the smoke generation of samples during burning. The SEA is a measure of the instantaneous amount of smoke being produced per unit mass of specimen burnt. The SEA values for the EG containing samples are much higher than that for the EVA/wax blend (Table 2.4). The addition of EG (especially in the presence of wax) clearly reduces the rate of smoke production (Figure 2.10) because of the formation of char layer, but increases the total smoke production. This increased total smoke production is the result of the intumescent graphite layers, formed by the EG in the heat flux, inhibiting the penetration of air into the substrate and causing the incomplete combustion of the substance. Smoke from burning polymers is generally the result of incomplete combustion [29].

Carbon monoxide (CO) in fires is known as the dominant toxicant in fire deaths [30]. Generally, the formation of carbon monoxide in fire occurs at low temperatures in the early stages of fire development primarily attributed to incomplete combustion of the pyrolyzed polymer volatiles fuels [31]. When the fire develops, the temperature favours the formation of carbon dioxide, which is dependent on oxygen availability. Figure 2.11 shows that CO production is lower and spread over a much longer period of time for the expanded EG containing samples. There was a further reduction in CO production when wax was present. This could be attributed to the better dispersion of EG in the presence of wax. The second peak near

the end of the experiment is the result of the flame accelerating the oxidation reaction of CO, leading to a decrease in CO and an increase in CO₂. The production of CO and its reaction to form CO₂ can be expressed by the following two-step reaction:



According to this two-step reaction, a decrease in CO may be because the reaction rate of step 2 increases when flame is presented [30].

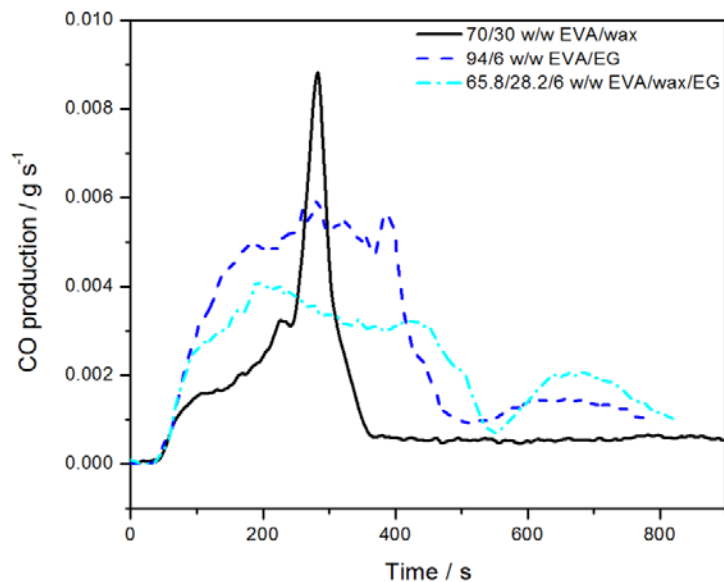


Figure 2.11 Carbon monoxide production (COP) plots of an EVA/wax blend, as well as EVA/EG and EVA/wax/EG composites at an external heat flux of 35 kW m⁻²

2.4 Conclusions

The thermal stability, flame resistance, melting enthalpy and thermal conductivity of EVA, EVA/wax blends, as well as EVA/EG and EVA/wax/EG composites were investigated. Significant improvements in the thermal stability, thermal conductivity, and flame resistance were observed for the EVA/EG composites, and these properties even further improved for the EVA/wax/EG composites. This was attributed to the smaller and better dispersed EG particles for the wax-containing systems. The crystallinity of EVA was smaller in the presence of EG

because of larger agglomerates that restricted the polymer chain mobility. The melting point of EVA in the blends and composites decreased with an increase in wax content as a result of the plasticizing effect of the wax on the EVA.

2.5 References

1. P. Zhang, L. Song, H. Lu, J. Wang, Y. Hu. The influence of expanded graphite on thermal properties for paraffin/high density polyethylene/chlorinated paraffin/antimony trioxide as a flame retardant phase change material. *Energy Conversion and Management* 2010; 51:2733-2737.
DOI: 10.1016/j.enconman.2010.06.009
2. J.A. Molefi, A.S. Luyt, I. Krupa. Investigation of thermally conducting phase change materials based on polyethylene/wax blends filled with copper particles. *Journal of Applied Polymer Science* 2010; 116:1766-1774.
DOI: 10.1002/app.31653
3. A. Sari, A. Karaipekli. Thermal conductivity and latent heat thermal energy storage characteristics of paraffin/expanded graphite composite as phase change material. *Applied Thermal Engineering* 2007; 27:1271-1277.
DOI: 10.1016/j.appltherleng.2006.11.004
4. P. Zhang, Y. Huang, L. Song, J. Ni, W. Xing, J. Wang. Effect of expanded graphite on properties of high-density polyethylene/paraffin composite with intumescent flame retardant as a shape-stabilized phase change material. *Solar Energy Materials and Solar Cells* 2009; 94:360-365.
DOI: 10.1016/j.solmat.2009.10.014
5. Y.J. Chen, D.D. Nguyen, M.Y. Shen, M.C. Yip, N.H. Tai. Thermal characterizations of the graphite nanosheets reinforced paraffin phase-change composites. *Composites Part A: Applied Science and Manufacturing* 2013; 44:40-46.
DOI: 10.1016/j.compositesa.2012.08.010
6. W. Mhike, W.W. Focke, J.P. Mofokeng, A.S. Luyt. Thermally conductive phase change materials for energy storage based on low-density polyethylene, soft Fischer-Tropsch wax and graphite. *Thermochimica Acta* 2012; 527:75-82.

- DOI: 10.1016/j.tca.2011.10.008
7. A. Sari. Form-stable paraffin/high density polyethylene composites as solid-liquid phase change material for thermal energy storage: Preparation and thermal properties. *Energy Conversion and Management* 2004; 45:2033-2042.
DOI: 10.1016/j.enconman.2003.10.022.
 8. Y. Cai, Q. Wei, F. Huang, S. Lin, F. Chen, W. Gao. Thermal stability, latent heat and flame retardant properties of the thermal energy storage phase change materials based on paraffin/high density polyethylene composites. *Renewable Energy* 2009; 34:2117-2123.
DOI: 10.1016/j.renene.2009.01.017
 9. M.K. Rathod, J. Banerjee. Thermal stability of phase change materials used in latent heat energy storage systems: A review. *Renewable and Sustainable Energy Reviews* 2013; 18:246-258.
DOI:10.1016/j.rser.2012.10.022
 10. W.L. Chen, R.M. Zhang, K. Xie, N. Liu, J. Wang. Heat conduction enhanced shape-stabilized paraffin/HDPE composite PCMs by graphite addition: Preparation and thermal properties. *Solar Energy Materials and Solar Cells* 2010; 94:1636-1642.
DOI: 10.1016/j.solmat.2010.05.020
 11. I. Krupa, G. Miková, A.S. Luyt. Phase change materials based on low-density polyethylene/paraffin wax blends. *European Polymer Journal* 2007; 43:4695-4705.
DOI:10.1016/j.europolymj.2007.08.022
 12. A.S. Luyt, I. Krupa. Thermal behaviour of low and high molecular weight paraffin waxes used for designing phase change materials. *Thermochimica Acta* 2008; 467:117-120.
DOI: 10.1016/j.tca.2007.11.001
 13. C. Alkan, K. Kaya, A. Sari. Preparation, thermal properties and thermal reliability of form-stable paraffin/polypropylene composite for thermal energy storage. *Journal of Polymers and the Environment* 2009; 17:254-258.
DOI: 10.1007/s10924-009-0146-7
 14. L. Fan, J.M. Khodadadi. Thermal conductivity enhancement of phase change materials for thermal energy storage: A review. *Renewable and Sustainable Energy Reviews* 2011; 15:24-46.
DOI: 10.1016/j.rser.2010.08.007

15. A. Mills, M. Farid, J.R. Selman, S. Al-Hallaj. Thermal conductivity enhancement of phase change materials using a graphite matrix. *Applied Thermal Engineering* 2006; 26:1652-1661.
DOI: 10.1016/j.applthermaleng.2005.11.022
16. Y. Zhang, J. Ding, X. Wang, R. Yang, K. Lin. Influence of additives on thermal conductivity of shape-stabilized phase change material. *Solar Energy Materials and Solar Cells* 2006; 90:1692-1702.
DOI: 10.1016/j.solmat.2005.09.007
17. Z. Zhang, X. Fang. Study on paraffin/expanded graphite composite phase change thermal energy storage material. *Energy Conversion and Management* 2006; 47:303-310.
DOI: 10.1016/j.enconman.2005.03.004
18. A. Karaipekli, A. Sari, K. Kaygusuz. Thermal conductivity improvement of stearic acid using expanded graphite and carbon fiber for energy storage applications. *Renewable Energy* 2007; 32:2201-2210.
DOI: 10.1016/j.renene.2006.11.011
19. Y. Wang, T.D. Xia, H. Zheng, H.X. Feng. Stearic acid/silica fume composite as form-stable phase change material for thermal energy storage. *Energy and Buildings* 2011; 43:2365-2370.
DOI: 10.1016/j.enbuild.2011.05.019
20. L. Xia, P. Zhang, R.Z. Wang. Preparation and characterization of expanded graphite/paraffin composite phase change material. *Carbon* 2010; 48:2538-2548.
DOI:10.1016/j.carbon.2010.03
21. J.J. George, A.K. Bhowmick. Ethylene vinyl acetate/expanded graphite nanocomposites by solution intercalation: Preparation, characterization and properties. *Journal of Materials Science* 2008; 43:702-708.
DOI: 10.1007/s 10853-007-2193-6
22. M. Murariu, A.L. Dechief, L. Bonnaud, Y. Paint, A. Gallos, G. Fontaine, S. Bourigot, P. Dubois. The production and properties of polylactide composites filled with expanded graphite. *Polymer Degradation and Stability* 2010; 95:889-900.
DOI:10.1016/j.polymdegradstab.2009.12.019

23. Y.F. Zhao, M. Xiao, S.J. Wang, X.C. Ge, Y.Z. Meng. Preparation and properties of electrically conductive PPS/expanded graphite nanocomposites. *Composites Science and Technology* 2007; 67:2528-2534.
DOI: 10.1016/j.compscitech.2006.12.009
24. U.M. Fawn, Q. Yao, H. Nakajima, E. Manias, C.A. Wilkie. Expandable graphite/polyamide-6 nanocomposites. *Polymer Degradation and Stability* 2005; 89:70-84.
DOI: 10.1016/j.polymdegradstab.2005.01.004
25. J. Xiang, L.T. Drzal. Investigation of exfoliated graphite nanoplatelets (χ GnP) in improving thermal conductivity of paraffin wax-based phase change material. *Solar Energy Materials and Solar Cells* 2011; 95:1811-1818.
DOI: 10.1016/j.solmat.2011.01.048
26. L. Ye, B. Qu. Flammability characteristics and flame retardant mechanism of phosphate-intercalated hydrotalcite in halogen-free flame retardant EVA blends. *Polymer Degradation and Stability* 2008; 93:918-924.
DOI: 10.1016/j.polymdegradstab.2008.02.002
27. Z. Sun, Y. Ma, Y. Xu, X. Chen, M. Chen, J. Yu, S. Hu, Z. Zhang. Effect of the particle size of expandable graphite on the thermal stability, flammability, and mechanical properties of high-density polyethylene/ethylene vinyl-acetate/expandable graphite composites. *Polymer Engineering and Science* 2014; 54:1162-1169.
DOI: 10.1002/pen.23659
28. Z.Z. Xu, J.Q. Huang, M.J. Chen, Y. Tan, Y.Z. Wang. Flame retardant mechanism of an efficient flame-retardant polymeric synergistic with ammonium polyphosphate for polypropylene. *Polymer Degradation and Stability* 2013; 98:2011-2020.
DOI: 10.1016/j.polymdegradstab.2013.07.001
29. A.R. Horrocks, D. Price. *Fire Retardant Materials*. Woodhead Publishing Limited, Cambridge (2001).
30. L. Shi, M.Y.L. Chew. Experimental study of carbon monoxide for woods under spontaneous ignition condition. *Fuel* 2012; 102:709-715.
DOI: 10.1016/j.fuel.2012.06.053

31. Y.W. Yan, L. Chen, R.K. Jian, S. Kong, Y.Z. Wang. Intumescence: An effect way to flame retardance and smoke suppression for polystyrene. *Polymer Degradation and Stability* 2012; 97:1423-1431.

DOI: 10.1016/j.polyimdegrastab.2012.05.013

Chapter 3

The effect of expanded graphite on the physical properties of conductive EVA/wax phase change blends for thermal energy storage

This chapter has been submitted as a publication:

M.J. Mochane, A.S. Luyt. The effect of expanded graphite on the physical properties of conductive EVA/wax phase change blends for thermal energy storage. Polymer Composites.

Abstract

A study of the morphology, dynamic mechanical, impact and tensile properties of ethylene vinyl acetate copolymer (EVA)/expanded graphite (EG) and EVA/wax/EG composites is presented. The composites were prepared by melt blending. The EVA/EG composites showed ductile behaviour, while brittle behaviour was observed in the presence of wax. A finer dispersion of EG was observed in the matrix when wax was present. The storage modulus of the EVA/wax/EG composite was higher than that of the EVA/EG composite, which is ascribed to a better interaction between the EVA and the wax-covered EG that significantly reduced the EVA chain mobility. The composites showed a decrease in impact strength with increasing EG and wax contents. There was a significant difference in the elongation at break between the EVA/EG and EVA/wax/EG composites, and little change in Young's modulus of EVA in the presence of EG and with increasing EG content. However, the Young's modulus of the EVA/wax blends increased in the presence of and with increasing EG content. In all the investigated samples containing EVA and wax, irrespective of the EG content, the stress at break decreased with an increase in wax content.

Keywords: phase-change material; expanded graphite; mechanical properties; paraffin wax; EVA

3.1 Introduction

Latent heat thermal energy storage (LHTES) techniques can reduce the imbalance between thermal energy supply and demand by using phase change materials (PCM) to store and release thermal energy. LHTES has wide applications in many fields, such as solar energy utilization, industrial waste heat recovering, and active and passive cooling of electronic devices. PCMs can be classified into two major categories: inorganic compounds and organic compounds. Inorganic PCMs include salt hydrates, metals and alloys, while organic PCMs are comprised of paraffins, fatty acids and glycols. Paraffins are some of the most promising phase change materials because they possess desirable properties such as high latent heat, chemical inertness and commercial availability [1-5].

A number of papers reported on the preparation, thermal energy storage and thermal conductivity properties of the PCMs based on paraffins [6-10]. Several thermoplastic matrices such as polyolefins were blended with various grades of wax. Polyethylenes and polypropylene (PP) belong to the most studied matrices [11-18]. The dispersed wax phase in the continuous polymer phase served as PCM. It was generally found that there was no leakage of molten PCMs from the blends during the melting of the PCM. This was due to the ability of the polymers, with higher melting temperatures, to contain the PCMs and keep the form/shape of the blends and/or composites intact. The blends and/or composites were therefore termed form-stable or shape-stabilized PCMs [6-8]. However, an increase in a number of different applications of PCMs still demands the need for other potential polymers that could be used as shape stabilizing matrices for paraffin wax. There are some applications that require flexible thermal storage composite material when the PCM undergoes heating/cooling cycles. Examples are diver wet suits, ski boot liners, metabolic heating/cooling blankets useful for treating hypothermia or fever patients in a medical setting, and therapeutic heating/cooling orthopedic joint supports. A composite material having a flexible matrix containing a phase change material is suitable for the above mentioned applications. EVA has been chosen as a matrix in this case because it is a polymer that approaches elastomeric properties in terms of softness and flexibility [19,20], but can still be processed like other thermoplastics. Currently little has been published on phase change materials based on EVA/wax blends.

There were a number of studies on the improvement of the thermal conductivity of form-stable PCMs. For example, Sari [9] has found that the thermal conductivity of form-stable HDPE/paraffin composites increased with 14-24% after addition of as little as 3 wt% expanded graphite. The thermal conductivity of shape-stabilized PCMs was also improved by adding some solid powders with high thermal conductivity, such as diatomite, wollastonite and organic bentonite [10]. Zhang and Fang studied the effect of EG on the thermal properties of paraffin (with a melting range of 48-50 °C)/EG composites prepared as form-stable PCMs, and they concluded that the latent heat capacity of the PCM decreased with an increase in mass fraction of graphite [21].

A fair amount of research work has been done on the mechanical properties of phase change materials based on tensile testing, but not much has been done on the improvement of their mechanical properties. A few authors, Krupa *et al.* [22], Beginn [23] and Meingjin *et al.* [24] reported on the tensile properties of these materials. It was found that the mechanical properties were significantly affected by the amount of wax. Paraffin wax has short and linear chains which induced an increase in blend crystallization. As a result, parameters like Young's modulus and yield stress of the blends increased with an increase in wax content. However, when blending low density polyethylene (LDPE) with soft paraffin wax, Krupa *et al.* [22] found that an increase in wax content led to a decrease in the ultimate strength and tensile elongation. The storage capacity of PCMs is dependent on the mass ratio of paraffin in the PCM blends and/or composites, and it is necessary to have high wax contents to obtain PCMs with high energy storage. A possible solution to the problem of reduced mechanical properties with increasing paraffin wax content is to introduce reinforcing filler to improve these properties. It is well known that natural graphite as such is not reinforcing in nature. However, when modified to expanded graphite by high temperature heat treatment, it could reinforce various polymers, in addition to improving the thermal conductivity [20].

Although a lot has been published on the preparation, thermal energy storage and thermal conductivity properties of polymer/wax blends, there are few reports regarding the effect of expanded graphite on the mechanical, thermomechanical and impact properties of these blends. In this paper we report on these properties of EVA, EVA/wax blends as well as EVA/EG and EVA/wax/EG composites prepared through melt blending.

3.2 Materials and methods

3.2.1 Materials

Medium-soft Fischer-Tropsch paraffin wax (M3 wax) was supplied in powder form by Sasol Wax (Sasolburg, South Africa). It is a Fischer-Tropsch paraffin wax consisting of approximately 99% of straight chain hydrocarbons and few branched chains, and it is primarily used in the candle-making industry. It has an average molar mass of 440 g mol^{-1} and a carbon distribution between C15 and C78. Its density is 0.90 g cm^{-3} and it has a melting point range around 40-60 °C. EVA-460 was manufactured and supplied in granule form by Du Pont Packaging & Industrial Polymers. It contains 18% by weight of VA with a BHT antioxidant thermal stabilizer. It has an MFI (190 °C / 2.16 kg) of 2.5 g/10 min (ASTM D1238-ISO 1133), T_m of 88 °C, and a density of 0.941 g cm^{-3} . Expandable graphite ES 250 B5 was supplied by Qingdao Kropfmuehl Graphite (Hauzenberg, Germany).

3.2.2 Preparation of expanded graphite

The expandable graphite was first dried in an oven at 60 °C for 10 h. It was then heated in a furnace to 600 °C using a glass beaker and maintained at this temperature for 15 min to form expanded graphite.

3.2.3 Preparation of EVA/wax blends and EVA/wax/EG composites

All the samples (Table 3.1) were prepared through melt mixing using a Brabender Plastograph 50 mL internal mixer at 130 °C and 60 rpm for 20 min. For the blends, the dry components were physically premixed and then fed into the heated mixer, whereas for the composites, the EG was added into the Brabender mixing chamber 5 minutes after adding the EVA or premixed EVA/wax blends. The samples were then melt-pressed at 130 °C for 5 min under 50 kPa pressure using a hydraulic melt press to form $15 \times 15 \text{ cm}^2$ sheets.

Table 3.1 Sample compositions used in this study

EVA/EG (w/w)	EVA/wax (w/w)	EVA/wax/EG (w/w)	EVA/wax/EG (w/w)	EVA/wax/EG (w/w)
100/0	100/0	50/50	60/40	70/30
97/3	70/30	48.5/48.5/3	58.2/38.8/3	67.9/29.1/3
94/6	60/40	47/47/6	56.4/37.6/6	65.8/28.2/6
91/9	50/50	45.5/45.5/9	54.6/36.4/9	63.7/27.3/9

3.2.4 Sample analysis

To determine the morphology of the fracture surfaces, a TESCAN VEGA 3 scanning electron microscope was used and the analysis was done at room temperature. The samples were gold coated by sputtering to produce conductive coatings onto the samples.

A Ceast Impactor II was used to investigate the impact properties of the blends and composites, in order to establish whether EG gives rise to improved impact properties. The samples were rectangular with a width of 10 mm, a thickness of 3 mm and length of 83 mm, and were V- notched (2 mm deep) edgewise. The pendulum hammer was situated at an angle of 50° from the release spot and the samples were tested at an ambient temperature of 24 °C. Five samples of each composition were tested and the average and standard deviation values are presented.

The tensile analysis of the samples was performed by a Hounsfield H5KS universal testing machine. The dumbbell shaped samples had a Gauge length of 20 mm, a thickness of 2 mm and a width of 5 mm. The cross-head speed was 10 mm min⁻¹, and the samples were tested at a controlled ambient temperature of 24 °C. Five samples of each composition were tested and average values with standard deviations are presented.

Dynamic mechanical analysis was performed from -90 to 90 °C in bending (dual cantilever) mode at a heating rate of 3 °C min⁻¹ and a frequency of 1 Hz.

3.3 Results and discussion

3.3.1 Scanning electron microscopy (SEM)

When intercalated (expandable) graphite is heated past a critical temperature, a large expansion (up to hundreds of times) of graphite flakes occur along the c-axis, forming a worm-like structure with low density and with multiple pores (see Figure 2.1). This puffed-up product is known as exfoliated or expanded graphite (EG). The open pores are interconnected with many surfaces, which allow them to be easily saturated with molten paraffin wax. Similar SEM images were obtained by other studies using different PCMs [21,25,26]. As shown in Figure 2.1c, the paraffin wax in the composites was embedded and dispersed in the porous network of the EG. This may be due to the capillary and surface tension forces between the paraffin wax and the porous network of the EG.

The EVA is very ductile, but the ductility decreased with the incorporation of EG, and even further decreased with the incorporation of wax (Figure 3.1). The rigid EG particles increase the stiffness of the composite, and form defect centres for the initiation of brittle fracture, and the highly crystalline wax further increases the stiffness and brittleness of the composites. No EG aggregates are visible in the SEM picture of the EVA/wax/EG composite (Figure 3.1b), probably because of the finer dispersion of EG when wax is present and of the coverage of the EG particles by the wax.

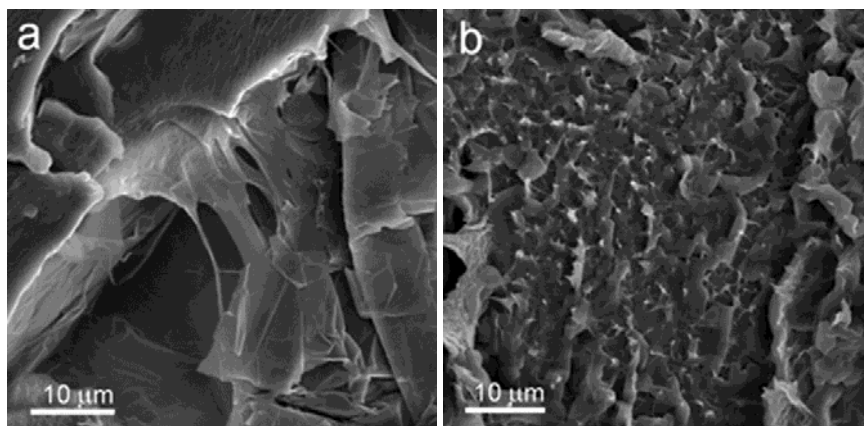


Figure 3.1 SEM images of the (a) EVA/EG and (b) EVA/wax/EG composite

3.3.2 Mechanical properties

The impact strength of the EVA/wax/EG composites decreased with increasing wax and graphite contents (Figure 3.2). Different factors may have contributed to this observation, like the elasticity of the composites, particle size, filler aspect ratio, rigidity and concentration, the interaction between the filler and the matrix, and nucleation. In this case the addition of rigid EG decreases the impact strength of the EVA/wax blends, because the EG particles act as stress concentrators for the development of cracks. The incorporation of fillers into a polymer matrix generally decreases the impact strength [27]. It is interesting to observe that at high wax contents the amount of graphite has little influence on the impact strength of the composites. This may be attributed to two factors: the low molecular weight wax crystals may act as internal flaws with high stress concentrations, and therefore as defects points for the initiation and propagation of stress cracking, and the increasing content of brittle wax and decreasing content of high impact strength EVA. It is known that brittle materials or particles cannot effectively stop/stabilize crack propagation [28], and therefore the presence of solid graphite particles has little influence on the already low impact strength of these EVA/wax blends.

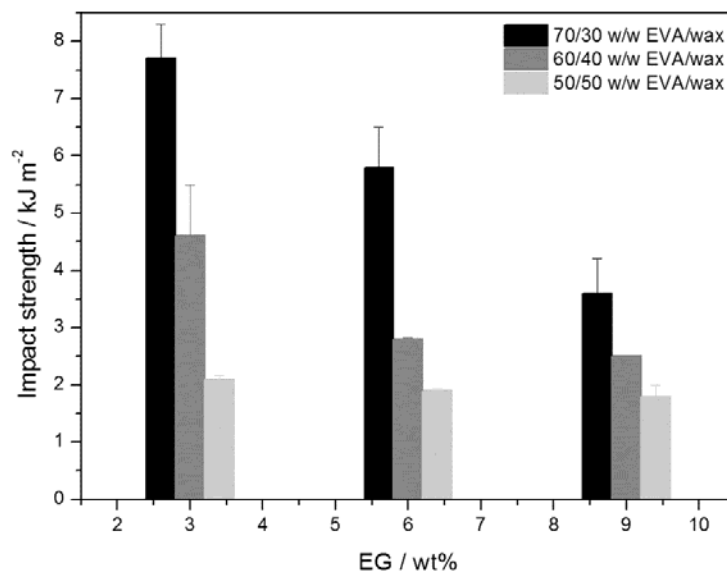


Figure 3.2 Impact strengths of EVA and EVA/wax blends containing different expanded graphite contents

The tensile modulus, as well as the elongation and stress at break of the blends and composites, were determined from stress-strain curves (Appendix B) and are presented in Figures 3.3 to 3.5 and Table 3.2. Generally, the addition of fillers into a polymer is expected to result in improved tensile strength and modulus. The Young's modulus of the EVA/wax blends is higher than that of EVA (Figure 3.3). This is associated with the overall higher crystallinity of the blend due to the presence of the highly crystalline wax [29-31]. There was little change in the Young's modulus of EVA in the presence of EG and with increasing EG content. This is probably because of the weak interaction between the EVA and the EG particles, giving rise to the filler having very little influence on the chain mobility of the polymer. The Young's modulus of the EVA/wax blends increased in the presence of and with increasing EG content. This is the result of the smaller and more well dispersed EG particles in the EVA/wax blends. Murariu *et al* [32] studied the production and properties of polylactide composites filled with expanded graphite, and reported an increase in modulus with increasing EG content. This was associated with the high modulus of EG (1 TPa), which led to a significant reinforcing effect and an increase in the rigidity of PLA. In our case the significantly higher values for the EVA/wax/EG composites can be attributed to the high strength and aspect ratio of the graphite nanoplatelets that were smaller and better dispersed after being covered with wax. The wax on the EG surface also improved the interaction with the EVA matrix, giving rise to a good dispersion and effective stress transfer as well as to the uniform distribution and good interfacial adhesion between the platelets and the matrix. The well dispersed EG in the EVA/wax/EG composites are more efficient in transferring applied load than the aggregated EG in EVA. It is well known that an improvement in elastic modulus can be attributed to a good dispersion of nanosized particles and to good interfacial adhesion between the particles and the matrix so that the mobility of the polymer chains is restricted under loading [32-34].

Table 3.2 Tensile and impact properties of all the investigated samples

Sample	σ_b / MPa	E / MPa	ε_b / %	Impact strength / kJ m ⁻²
EVA	14.9 ± 3.0	18.2 ± 1.3	1005 ± 125	
EVA/EG (w/w)				
97/3	9.0 ± 0.3	23.5 ± 1.2	687 ± 53	
94/6	7.1 ± 0.2	20.5 ± 3.0	601 ± 44	
91/9	5.7 ± 1.2	25.7 ± 3.7	411 ± 60	
EVA/wax (w/w)				
70/30	7.8 ± 2.0	92.3 ± 20.5	114 ± 20	
60/40	4.3 ± 1.4	66.6 ± 6.5	46.0 ± 9.9	
50/50	6.7 ± 0.3	72.1 ± 14.3	37.7 ± 13.6	
EVA/wax/EG (w/w)				
67.9/29.1/3	5.3 ± 0.7	117 ± 9	3.6 ± 0.3	7.7 ± 0.6
65.8/28.2/6	4.7 ± 0.3	127 ± 9	2.5 ± 0.2	5.8 ± 0.7
63.7/27.3/9	6.8 ± 2.3	233 ± 6	2.0 ± 0.2	3.6 ± 0.6
58.2/38.8/3	4.5 ± 0.1	187 ± 21	6.9 ± 1.6	4.6 ± 0.9
56.4/37.6/6	4.5 ± 0.5	186 ± 16	6.3 ± 0.4	2.8 ± 0.0
54.6/36.4/9	4.6 ± 0.3	210 ± 21	5.6 ± 0.4	2.5 ± 0.0
48.5/48.5/3	3.4 ± 0.3	165 ± 11	4.4 ± 0.3	2.1 ± 0.1
47/47/6	3.8 ± 0.7	175 ± 11	4.8 ± 0.4	1.9 ± 0.1
45.5/45.5/9	4.4 ± 0.5	214 ± 5	4.4 ± 0.7	1.8 ± 0.2

ε_b , σ_b and E are elongation at break, stress at break, and Young's modulus of elasticity

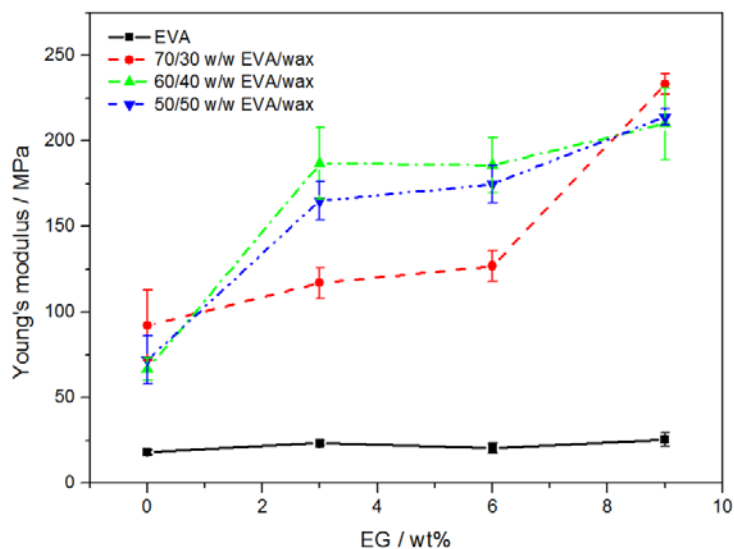


Figure 3.3 Young's modulus of EVA and the EVA/wax blends as a function of expanded graphite content

The elongation at break of EVA observably decreased with the incorporation of EG, and it further decreased with increasing filler content (Figure 3.4). This is to be expected, since the EG is significantly agglomerated and does not have a very good interaction with EVA. They therefore form defect centres from where cracks can initiate and propagate. The presence of wax in EVA significantly reduces the elongation at break, because wax is very brittle and EVA/wax blends can easily fracture because of the large concentrations of brittle wax crystals dispersed in the EVA matrix. There is a significant difference in the elongation at break between the EVA/EG composites and the comparable EVA/wax/EG composites. The reason is probably that the highly crystalline, brittle wax covers the EG particles, which contributes to the easier formation and propagation of cracks under tensile forces. Better interaction between the EVA and wax-covered EG may also significantly reduce the EVA chain mobility. It has been reported in the literature that weaker filler-polymer interphase interaction and poor filler dispersion result in higher values of elongation at break [35]. Similar results were obtained by Gogoi *et al.* [36] who investigated jatropha curcas oil based alkyd/epoxy resin/expanded graphite reinforced bio-composites. They observed that the composite reinforced with 5 wt% EG platelets showed about 60% decrease in elongation at break when compared with the alkyd/epoxy resin blend. This was attributed to a

large aspect ratio and the interaction between the filler and polymer, which reduced the polymer chain mobility.

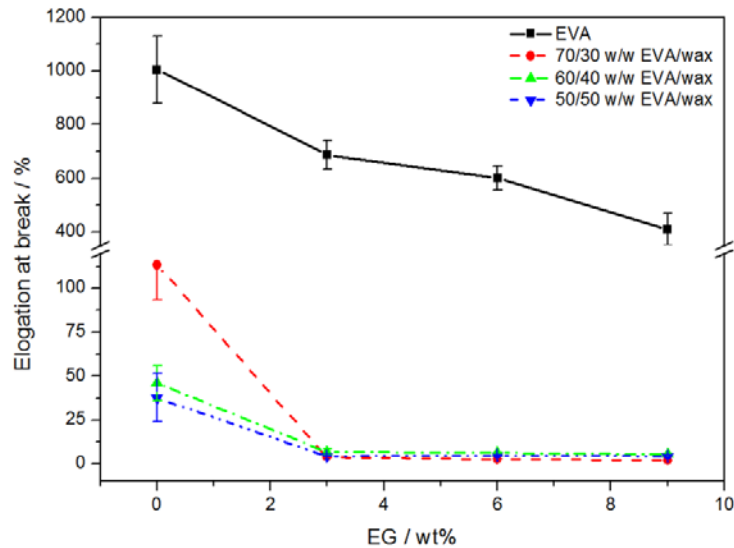


Figure 3.4 Elongation at break of EVA and the EVA/wax blends as a function of expanded graphite content

The stress at break of EVA decreased with incorporation of the EG, and it further decreased with increasing filler content (Figure 3.5). This can be explained by the weak interfacial interaction between EVA and EG, where the agglomerated EG particles act as defect points for the initiation and propagation of stress cracking. It has been established previously that if the interfacial interaction between the polymer and filler is weak, the stress at break of the composites decreases when increasing the filler content, but if the interfacial interaction is sufficient, the stress at break increases [37]. In all the investigated samples containing EVA and wax, irrespective of the EG content, the stress at break decreased with an increase in wax content (Figure 3.5). The main reason for this decrease is the increased amount of low molecular weight, highly crystalline wax, which deteriorates the tensile strength of the composites. Wax itself has very poor tensile properties and the wax-covered EG crystals in the amorphous phase of the EVA act as defects points for the initiation and propagation of stress cracking.

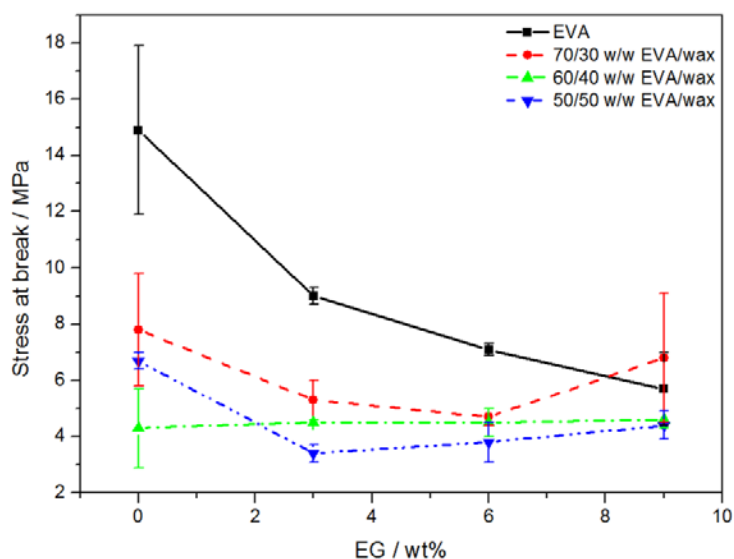


Figure 3.5 Stress at break of EVA and the EVA/wax blends as a function of expanded graphite content

3.3.3 Dynamic mechanical analysis (DMA)

The DMA storage modulus curves in Figure 3.6 show an observable increase in storage modulus of the EVA/wax blend, and the EVA/EG and EVA/wax/EG composites, compared to that of pure EVA. This increase is the result of the highly crystalline wax which crystallizes in the amorphous phase of the EVA and which increases the total stiffness of the blend. The presence of EG also increases the storage modulus of the composites, which is the result of the inherently higher storage modulus of EG and some immobilization of the EVA chains by the EG. It is interesting to observe that the storage modulus of the EVA/wax/EG composite is higher than that of the EVA/EG composite. This may be attributed to a better interaction between the EVA and the wax-covered EG, which may significantly reduce the EVA chain mobility. The finely dispersed multilayer graphene sheets penetrate into the inter gallery of the polymer chains, and therefore a good dispersion of the EG particles in the polymer matrix could enhance the filler aspect ratio and interfacial dimensions, which would as a whole contribute to the stiffening effect of the composite [38]. Similar trends were reported by Malas *et al.* [39], who investigated the effect of EG and isocyanate modified graphite (i-MG) on the dynamic mechanical properties of SBR and SBR/BR blends. The authors observed higher storage modulus values for the SBR/BR

composites, which was due to the homogenous mixing of SBR with BR and to the well dispersed nanofillers in the rubber blend.

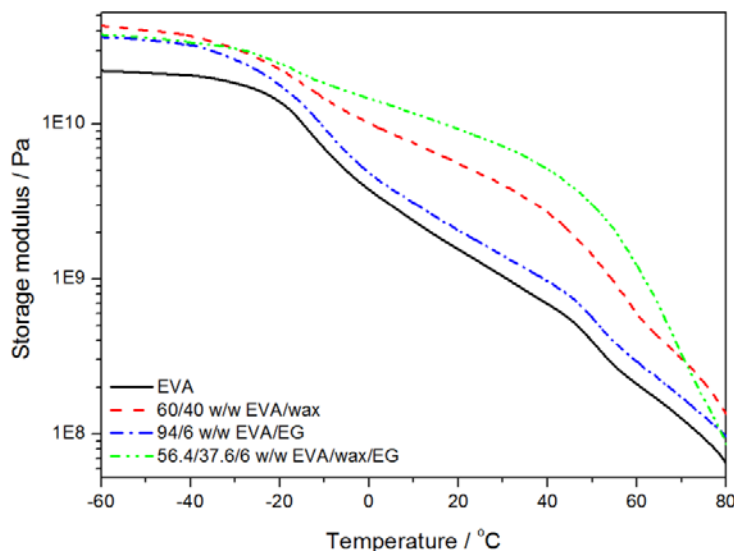


Figure 3.6 Storage modulus as function of temperature for neat EVA, an EVA/wax blend, as well as EVA/EG and EVA/wax/EG composites

Three transitions are observable from the loss modulus and loss factor curves in Figures 3.7 and 3.8. Neat EVA and its composites with EG show a β -relaxation between -40 and 0 °C and an α -relaxation at 28 °C. The β -relaxation is attributed to the motion of the amorphous region side chains from the polymer backbone [40], and is known as the glass transition (T_g). Below T_g the molecular chain segments are frozen in, the damping is low and little energy is stored for elastic deformations. In the rubbery region, the damping is high compared to the glassy state, because the molecular segments are free to move causing a decrease in stiffness, and excess energy is dissipated as heat. However, in the transition region, damping is high due to initiation of micro-Brownian motion of the molecular chain segments and their relaxation [41]. The α -relaxation-is related to the motion of amorphous regions in the vicinity of the crystalline lamellae and that of the crystal defects [42]. The α -transition can also reflect the relaxation of flexible chains of the vinyl acetate (VA) groups present in the EVA copolymer chains. The transition between 40 and 60 °C in the curves of the EVA/wax blend and EVA/wax/EG composite is the result of the melting of the wax in the blend and composite.

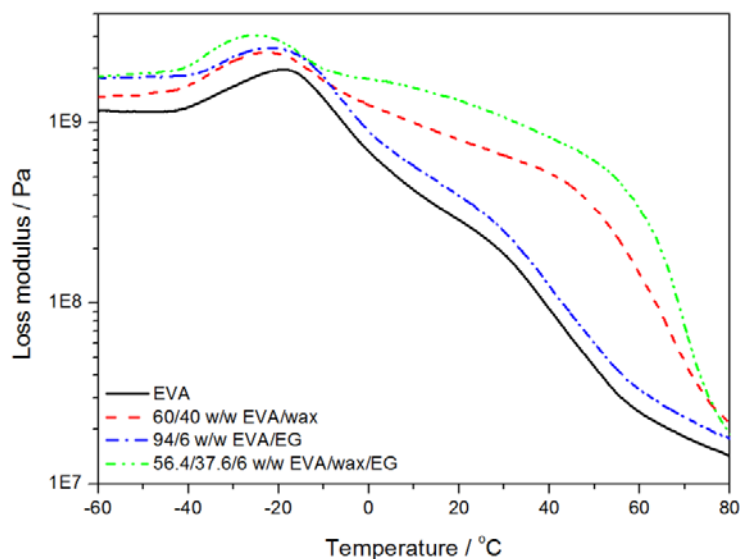


Figure 3.7 Loss modulus as function of temperature for neat EVA, an EVA/wax blend, as well as EVA/EG and EVA/wax/EG composites

It is clear from the loss factor curves (Figure 3.8) that the melting temperature of the wax in the EVA/wax/EG composite is higher than that of the EVA/wax blend. This may be attributed to the strong interaction between the wax and EG, which gave rise to restricted motion of the wax chains. There is an obvious decrease in the intensities of the α - and β -transition peaks in the loss factor curves of the EVA/wax blend and the EVA/wax/EG composite compared to those of EVA and the EVA/EG composite. Since these peaks are related to the EVA component in the blend, their intensities are expected to decrease because of the smaller amount of EVA in a 60/40 w/w EVA/wax blend.

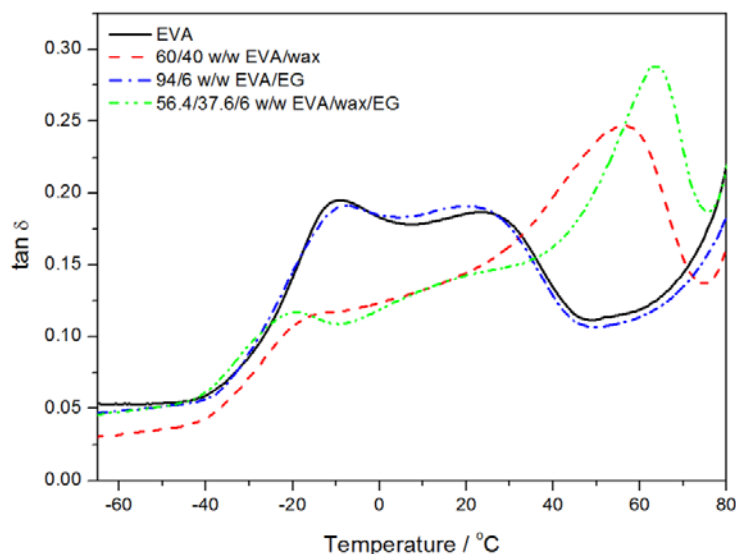


Figure 3.8 Loss factor as function of temperature for neat EVA, an EVA/wax blend, as well as EVA/EG and EVA/wax/EG composites

In both the loss modulus and $\tan \delta$ curves the glass transition of EVA in the EVA/wax blend and the EVA/wax/EG composite shifts to lower temperatures compared to that of neat EVA. This may be attributed to an increase in the mobility of the EVA chains in the presence of wax, with the wax acting as a plasticizer. It has previously been stated that wax, both in its solid and liquid states, softens the polymer matrix [43]. There is slight shift in the glass transition temperature of EVA towards higher temperatures in the EVA/EG composite, and this is more obvious in the $\tan \delta$ curves (Figure 3.8). There are several factors that can affect the glass transition temperature of polymers in composites, which include the degree of particle dispersion, homogeneity, degree of crosslinking, molecular motion, orientation and spacing between particles [33,44]. In this case it is most likely that the graphite platelets restricted the molecular motions and also reduced the free volume, thereby restricting the motion of the EVA chains. There was an equal decrease in the α -transition temperature, which may be related to the graphite particles acting as nucleation centres and in some way influencing the crystalline morphology of the EVA and the related segmental motions.

3.4 Conclusions

The effect of expanded graphite on the morphology, thermomechanical behaviour, as well as impact and tensile properties of EVA and EVA/wax composites was investigated. The SEM pictures showed no visible EG agglomerates in the EVA/wax/EG composite, because of the finer dispersion of EG when wax was present, and the coverage of the EG by the wax. The storage modulus results confirmed the reinforcing effect of the graphite and the immobilization of the EVA chains by the highly crystalline wax in the different investigated samples. The impact strength of the EVA/wax/EG composites decreased with increasing wax and graphite contents because of the rigidity of EG and the brittleness of the wax. At high wax contents the effect on the impact strength of the samples was so strong that the presence of EG made little difference. The tensile modulus of the EVA/wax/EG composites was higher than that of the EVA/EG composites because of the smaller and more well dispersed EG when wax was present in the blends, and because of the more rigid wax crystals. However, the elongation at break for the EVA/wax/EG composites was lower than that of the EVA/EG composites, which was attributed to better interaction between the EVA and the wax-covered EG which reduced the EVA chain mobility.

3.5 References

1. N. Sarier, E. Onder. The manufacture of microencapsulated phase change materials suitable for design of thermally enhanced fabrics. *Thermochimica Acta* 2007; 452:149-160.
DOI: 10.1016/j.tca.2006.08.002
2. L. Sánchez-Silva, J.F. Rodríguez, A. Romero, A.M. Borreguero, M. Carmona, P. Sánchez. Microencapsulation of PCMs with a styrene-methyl methacrylate copolymer shell by suspension-like polymerisation. *Chemical Engineering Journal* 2010; 157:216-222.
DOI: 10.1016/j.cej.2009.12.013

3. A. Sharma, V.V. Tyagi, C.R. Chen, D. Buddhi. Review on thermal energy storage with phase change materials and applications. *Renewable and Sustainable Energy Reviews* 2009; 13:318-345.
DOI: 10.1016/j.rser.2007.10.005
4. M.M. Farid, A.M. Khudhair, S.A.K. Razack, S. Al-Hallaj. A review on phase change energy storage: Materials and applications. *Energy Conversion and Management* 2004; 45:1597-1615.
DOI: 10.1016/j.enconman.2003.09.015
5. Y. Zhang, Q. Guo, S. Li, J. Shi, L. Liu. Heat transfer enhancement of paraffin wax using graphite foam for thermal energy storage. *Solar Energy Materials and Solar Cells* 2010; 94:1011-1014.
DOI: 10.1016/j.solmat.2010.02.004
6. I. Krupa, G. Miková, A.S. Luyt. Polypropylene as a potential matrix for the creation of shape stabilized phase change materials. *European Polymer Journal* 2007; 43:895-907.
DOI: 10.1016/j.eurpolymj.2006.12.019
7. M. Xiao, B. Feng, K. Gong. Preparation and performance of shape stabilized phase change thermal storage materials with high thermal conductivity. *Energy Conversion and Management* 2002; 43:103-108.
DOI: 10.1016/S0196-8904(01)00010-3
8. H. Inaba, P. Tu. Evaluation of thermophysical characteristics on shape-stabilized paraffin as a solid-liquid phase change material. *Heat and Mass Transfer* 1997; 32:307-312.
DOI: 10.1007/s002310050126
9. A. Sari. Form-stable paraffin/high density polyethylene composites as solid-liquid phase change material for thermal energy storage: Preparation and thermal properties. *Energy Conversion and Management* 2004; 45:2033-2042.
DOI: 10.1016/j.enconman.2003.10.022
10. Y.P. Zhang, J.H. Ding, X. Wang, R. Yang, K.P. Lin. Influence of additives on thermal conductivity of shaped-stabilized phase change material. *Solar Energy Materials and Solar Cells* 2006; 90:1692-1702.
DOI: 10.1016/j.solmat.2005.09.007

11. I. Krupa, A.S. Luyt. Mechanical properties of uncrosslinked and crosslinked linear low-density polyethylene/wax blends. *Journal of Applied Polymer Science* 2001; 81:973-980.
DOI: 10.1002/app.1519
12. I. Krupa, A.S. Luyt. Thermal properties of polypropylene/wax blends. *Thermochimica Acta* 2001; 372:137-141.
DOI: 10.1016/S0040-6031(01)00450-56
13. I. Krupa, A.S. Luyt. Thermal and mechanical properties of extruded LLDPE/wax blends. *Polymer Degradation and Stability* 2001; 73:157-161.
DOI: 10.1016/S0141-3910(01)00082-9
14. I. Krupa, A.S. Luyt. Physical properties of blends of LLDPE and an oxidized paraffin wax. *Polymer* 2001; 42:7285-7289.
DOI: 10.1016/S0032-3861(01)00172-0
15. M.J. Hato, A.S. Luyt. Thermal fractionation and properties of different polyethylene/wax blends. *Journal of Applied Polymer Science* 2007; 104:2225-2236.
DOI: 10.1002/aapp.25494
16. I. Krupa, A.S. Luyt. Thermal properties of uncross-linked and cross-linked LLDPE/wax blends. *Polymer Degradation and Stability* 2000; 70:111-117.
DOI: 10.1016/S0141-3910(00)00097-5
17. T.N. Mtshali, I. Krupa, A.S. Luyt. The effect of cross-linking on the thermal properties of LDPE/wax blends. *Thermochimica Acta* 2001; 380:47-54
DOI: 10.1016/S0040-6031(01)00636-0
18. S.P. Hlangothi, I. Krupa, V. Djoković, A.S. Luyt. Thermal and mechanical properties of cross-linked and uncross-linked linear low-density polyethylene-wax blends. *Polymer Degradation and Stability* 2003; 79:53-59.
DOI: 10.1016/S0141-3910(02)00238-0
19. D. Kakkar, S.N. Maiti. Effect of flexibility of ethylene vinyl acetate and crystallization of polypropylene on the mechanical properties of i-PP/EVA blends. *Journal of Applied Polymer Science* 2012; 123:1905-1912.
DOI: 10.1002/app.34680

20. J.J. George, A.K. Bhowmick. Ethylene vinyl acetate/expanded graphite nanocomposites by solution intercalation: Preparation, characterization and properties. *Journal of Materials Science* 2008; 43:702-708.
DOI: 10.1007/s10853-007-2193-6
21. Z.G. Zhang, X.M. Fang. Study on paraffin/expanded graphite composite phase change thermal energy storage material. *Energy Conversion and Management* 2006; 47:303-310.
DOI: 10.1016/j.enconman.2005.03.004
22. I. Krupa, G. Miková, A.S. Luyt. Phase change materials based on low-density polyethylene/paraffin wax blends. *European Polymer Journal* 2007; 43:4695-4705.
DOI: 10.1016/j.eurpolymj.2007.08.022
23. U. Beginn. Applicability of frozen gels from ultra-high molecular weight solid/liquid phase change materials. *Macromolecular Materials and Engineering* 2003; 288:245-251.
DOI: 10.1002/mame.200390021
24. J. Mengjin, S. Xiaoqing, X. Jianjun, Y. Guangdou. Preparation of a new thermal regulating fibre based on PVA and paraffin. *Solar Energy Materials and Solar Cells* 2008; 92:1657-1660.
DOI: 10.1016/j.solmat.2008.07.018
25. A. Mills, M. Farid, J.R. Selman, S. Al-Hallaj. Thermal conductivity enhancement of phase change materials using a graphite matrix. *Applied Thermal Engineering* 2006; 26:1652-1661.
DOI: 10.1016/j.applthermaleng.2005.11.022
26. L. Xia, P. Zhang, R.Z. Wang. Preparation and characterization of expanded graphite/paraffin composite phase change material. *Carbon* 2010; 48:2538-2548.
DOI: 10.1016/j.carbon.2010.03
27. I. Švab, V. Musil, I. Šmit, M. Makarovič. Mechanical properties of wollastonite-reinforced polypropylene composites modified with SEBS and SEBS-g-MA elastomers. *Polymer Engineering and Science* 2007; 47:1873-1880.
DOI: 10.1002/pen.20897
28. A. Lazzeri, S.M. Zebarjad, M. Pracella, K. Cavalier, R. Rosa. Filler toughening of plastics. Part 1 - The effect of surface interactions on physico-mechanical properties and

- rheological behaviour of ultrafine CaCO₃/HDPE nanocomposites. *Polymer* 2004; 46:827-844.
DOI: 10.1016/j.polymer.2004.11.111
29. J.A. Molefi, A.S. Luyt, I. Krupa. Comparison of LDPE, LLDPE and HDPE as matrices for phase change materials based on a soft Fischer-Tropsch paraffin wax. *Thermochimica Acta* 2010; 500:88-92.
DOI: 10.1016/j.tca.2010.01.002
30. H.S. Mpanza, A.S. Luyt. Comparison of different waxes as processing agents for low-density polyethylene. *Polymer Testing* 2006; 25:436-442.
DOI: 10.1016/j.polymertesting.2006.0.008
31. A.S. Luyt, V.G. Geethamma. Effect of oxidized paraffin wax on the thermal and mechanical properties of linear low-density-layered silicate nanocomposites. *Polymer Testing* 2007; 26:461-470.
DOI: 10.1016/j.polymertesting.2006.12.015
32. M. Murariu, A.L. Dechief, L. Bonnaud, Y. Paint, A. Gallos, G. Fontaine, S. Bourigot, P. Dubois. The production and properties of polylactide composites filled with expanded graphite. *Polymer Degradation and Stability* 2010; 95:889-900.
DOI: 10.1016/j.polymdegradstab.2009.12.019
33. A. Yasmin, I.M. Daniel. Mechanical and thermal properties of graphite platelet/epoxy composites. *Polymer* 2004; 45:8211-8219.
DOI: 10.1016/j.polymer.2004.09.054
34. W. Zheng, X. Lu, S.C. Wong. Electrical and mechanical properties of expanded graphite-reinforced high-density polyethylene. *Journal of Applied Polymer Science* 2004; 91:2781-2788.
DOI: 10.1002/app.13460
35. B.T. Poh, H. Ismail, K.S. Tan. Effect of filler loading on tensile and tear properties of SMR L/ENR 25 and SMR L/SBR blends cured via semi-efficient vulcanization system. *Polymer Testing* 2002; 21:801-806.
DOI: 10.1016/S0142-9418(02)00014-4
36. P. Gogoi, M. Boruah, C. Bora, S.K. Dolui. Jatropha curcas oil alkyd/epoxy resin/expanded graphite (EG) reinforced bio-composite: Evaluation of the thermal,

- mechanical and flame retardancy properties. *Progress in Organic Coatings* 2014; 77:87-93.
DOI: 10.1016/j.porgcoat.2013.08.006
37. V. Cecean, A. Boudenne, L. Ibos, I. Novák, Z. Nógellová, J. Prokeš, I. Krupa. Electrical, mechanical and adhesive properties of ethylene-vinylacetate copolymer (EVA) filled with wollastonite fibers coated by silver. *European Polymer Journal* 2008; 44:3827-3834.
DOI: 10.1016/j.eurpolymj.2008.07.053
38. G. Hatui, P. Bhattacharya, S. Sahoo, S. Dhibar, C.K. Das. Combined effect of expanded graphite and multiwall carbon nanotubes on thermo mechanical, morphological as well as electrical conductivity of *in situ* bulk polymerized polystyrene composites. *Composites: Part A* 2014; 56:181-191.
DOI: 10.1016/j.compositesa.2013.10.007
39. A. Malas, C.K. Das, A. Das, G. Heinrich. Development of expanded graphite filled natural rubber vulcanizates in presence and absence of carbon black: Mechanical, thermal and morphological properties. *Materials and Design* 2012; 39:410-417.
DOI: 10.1016/j.matdes.2012.03.007
40. O. Grigoryeva, A. Fainleib, O. Starostenko, A. Tolstov, W. Brostow. Thermoplastic elastomers from rubber and recycled polyethylene: Chemical reactions at interphases for property enhancement. *Polymer International* 2004; 53:1693-1703.
DOI: 10.1002/pi.1530
41. N. Hameed, P.A. Sreekumar, B. Francis, W. Yang, S. Thomas. Morphology, dynamic mechanical and thermal studies on poly(styrene-co-acrylonitrile) modified epoxy resin/glass fibre composites. *Composites Part A* 2007; 38:2422-2432.
DOI: 10.1016/j.compositesa.2007.08.009
42. B. John, K.T. Varughese, Z. Oommen, P. Pötschke, S. Thomas. Dynamic mechanical behaviour of high-density polyethylene/ethylene vinyl acetate copolymer blends: The effects of the blend ratio, reactive compatibilization, and dynamic vulcanization. *Journal of Applied Polymer Science* 2003; 87:2083-2099.
DOI: 10.1002/app.11458

43. W. Mhike, W.W. Focke, J.P. Mofokeng, A.S. Luyt. Thermally conductive phase-change materials for energy storage based on low-density polyethylene, soft Fischer-Tropsch wax and graphite. *Thermochimica Acta* 2012; 527:75-82.
DOI: 10.1016/j.tca.2011.10.008
44. S. Ganguli, A.K. Roy, D.P. Anderson. Improved thermal conductivity for chemically functionalized exfoliated graphite/epoxy composites. *Carbon* 2008; 46:806-817.
DOI: 10.1016/j.carbon.2008.02.008

Chapter 4

The effect of expanded graphite on the flammability and thermal conductivity properties of phase change material based on PP/wax blends

This chapter has been submitted as a publication:

M.J. Mochane, A.S. Luyt. The effect of expanded graphite on the flammability and thermal conductivity properties of phase change material based on PP/wax blends. Polymer Bulletin.

Abstract

The study reports on the flammability, thermal stability, impact properties and thermal conductivity of shape-stabilized phase change materials based on a soft Fischer-Tropsch paraffin wax blended with polypropylene (PP). The blends were melt-mixed with expanded graphite (EG) up to 9 wt.% to improve the thermal conductivity and flammability resistance of the material. The thermal stability and flammability results show an increase in thermal stability and flame resistance of PP in the presence of EG, with the flammability further increasing in the presence of wax, probably because of the smaller and better dispersed EG particles in the PP/wax/EG composite that gave rise to a more compact char layer. Although the thermal degradation mechanism did not change in the presence of EG, the EG particles retarded the evolution of the volatile degradation products. The storage modulus of the PP/wax/EG composite was lower than those of PP and PP/EG, and decreased with increasing wax content because of the plasticizing effect of the wax. The impact strength of the PP/wax/EG composites increased with increasing EG content in all the samples, but decreased with increasing wax content.

Keywords: Polypropylene; wax; expanded graphite; flammability; thermal stability; mechanical properties

4.1 Introduction

The cost of energy resources have become the main reason for the development of phase change materials [1-3]. By implementing proper energy storage methods, the discrepancy between the energy supply and demand can be overcome. Energy storage methods are generally classified as sensible storage or latent heat storage, or a combination of the two. Latent heat storage is based on the absorption or release of energy when a storage material undergoes a phase change. Sensible heat storage happens when energy is added to the material, thus increasing the temperature of the material without changing its phase [4-5]. The advantages of latent heat storage (LHS) in comparison to sensible heat storage are high heat storage densities, small system sizes, and a narrow temperature changes during charging and discharging processes.

Phase change materials are latent heat storage materials. Thermal energy transfer occurs when a material undergoes solid-liquid, or liquid-solid phase changes [6]. In recent years a new type of PCM, called a shaped-stabilized PCM, was developed. Shape-stabilized PCMs are composites consisting of paraffin wax encapsulated in a three-dimensional net structure formed by polymers, such as high-density polyethylene [7] or styrene-butadiene-styrene (SBS) copolymers [8]. The net structure of the shape-stabilized PCM composites prevents the leakage of liquid during the phase change of the paraffin. As long as the operating temperature is below the melting point of the supporting material, the shape-stabilized PCM can keep its shape even when the paraffin changes from solid to liquid.

Despite the many desirable properties of PCMs, their low thermal conductivity (generally below $0.3 \text{ W m}^{-1}\text{K}^{-1}$) is a major drawback which leads to low heat storage/retrieval rates and which in turn limits its widespread utilization as an energy storage material. Many studies [9-13] have therefore been carried out with the aim of enhancing the thermal conductivity in PCM. Methods for the improvement of the thermal conductivity of PCMs involve the dispersion of metallic or nonmetallic materials with high thermal conductivity into the PCM. Carbon nanoparticles and nanofibers in particular attracted more interest because of their higher thermal conductivities. Another method used to improve the thermal conductivity is the impregnation of the PCM into a high thermal conductivity material with a porous structure, such as expanded graphite (EG) and carbon fiber brushes. For an example, Fukai and co-workers [14] inserted 2 vol.% carbon fiber brushes into PCM, and reported a six-fold increase in thermal conductivity of

the composites compared to that of the pure PCMs. Zhang and Fang [15] prepared EG/paraffin PCM composites with 15wt.% EG. When this system was used in latent heat thermal energy storage (LHTES) system, the durations for heat storage and retrieval were reduced by 27.4% and 56.4% respectively, compared with those of paraffin.

In the current study of a form-stable PCM, the polypropylene (PP) has excellent mechanical and physiochemical properties and is used in a wide variety of applications, such as the automobile industry, electricity, engineering, housing materials, and transportation [16-18]. However, its inherent combustibility limits the range of applications. Intumescent flame retardants can be introduced into polyolefins because of the advantages of good safety and relatively high flame retarding efficiency [19]. According to literature the following three components are incorporated into formulations to obtain intumescent flame retardancy: acid-source, char-forming agent and blowing agent [20].

Halogenated flame retardants are generally used in most engineering plastics because of their excellent retardant performance [21]. However, the severe environmental impact of the processing and combustion of various brominated flame retardants motivated the investigation into halogen-free flame retardants to replace brominated and chlorinated ones [22]. Graphite and metallic hydroxide flame retardants are the most interesting and promising of the halogen-free flame retardants [23]. Expanded graphite is widely used to increase char yield and promote the thermal stability of intumescent flame retardants (IFR) because of their low cost and simple preparation with most polymers [24].

Chlorinated paraffins, ammonium polyphosphate (APP) and pentaerythritol (PER) were used as flame retardants for PP [16-17, 25-26]. Shao and co-workers [17] reported that the PP/ethylene diamine modified ammonium polyphosphate (MAPP) systems showed more effective flame retardancy than the PP/ unmodified ammonium polyphosphate (APP) systems. This was attributed to the formation of a stable char layer and the prevention of the flammable volatiles going into the flame zone, which leads to the formation of the intumescent, compact and stable char layers, consequently leading to the better flame retardant performance of MAPP. Chen *et al.* [25] studied flame retardant polypropylene composites prepared by melt-mixing APP, PER and hydroxyl silicone oil (HSO) with the polymer. Cone calorimetry results showed that a synergistic effect occurred when HSO and an intumescent flame retardant (IFR) are both present in polypropylene composites. HSO reacts with APP to form a silicon-phosphate and ceramic-like

structure, which increases the efficiency of the intumescent char shield. Apparently solid acids formed through the reaction of APP and SiO₂ on the surface of the burning composite, and their chemical catalytic action further reduced the HRR of the composite.

A fair amount of studies investigated the flammability of shape-stabilized PCMs [19,27-28]. In these studies, the shape-stabilized PCMs were mostly based on paraffin, HDPE, expanded graphite and an intumescent flame retardant. Zhang *et al.* [19] showed an improvement in the flame retardancy of paraffin/HDPE/IFR (APP and PER) with the addition of EG. Intumescent char layers were formed in the case of IFR (APP and PER), but with the addition of EG into the IFR system the strength and stability of the intumescent char layer further increased. Better flammability properties were also found for a paraffin/HDPE/zinc borate + EG system compared to a paraffin/HDPE/APP/EG system [27]. No reports were found on the flammability of PP/wax/EG systems.

Based on the above literature studies, EG was added as flame retardant to the PP/paraffin wax blends in order to decrease the flammability of the form-stable PCM. Expanded graphite was also added to improve the thermal conductivity of the blends since both polypropylene (PP) and paraffin wax have low thermal conductivities. The prepared form-stable PCM blends, with and without a flame retardants, were studied by means of cone calorimetry, impact testing, thermogravimetric analysis (TGA), and dynamic mechanical analysis (DMA).

4.2 Materials and methods

4.2.1 Materials

Medium-soft Fischer-Tropsch paraffin wax (M3 wax) was supplied in powder form by Sasol Wax, South Africa. It is a paraffin wax consisting of approximately 99% of straight chain hydrocarbons and few branched chains, and it is primarily used in the candle industry. It has an average molar mass of 440 g mol⁻¹ and a carbon distribution of C15-C78. Its density is 0.90 g cm⁻³ and it has a melting point of around 40-60 °C. Isotactic polypropylene was supplied as pellets by Sasol Polymers, South Africa. It has an MFI of 10 g min⁻¹, specific enthalpy of melting of 90 J g⁻¹, melting temperature of 163-165 °C, and a density of 0.901 g cm⁻³. Expandable graphite ES 250 B5 was supplied by Qingdao Kropfmuehl Graphite (Hauzenberg, Germany).

4.2.2 Preparation of expanded graphite

The expandable graphite was first dried in an oven at 60 °C for 10 h. The expandable graphite was then heated in a furnace to 600 °C using a glass beaker and maintained at that temperature for 15 min to form expanded graphite.

4.2.3 Preparation of PP/wax blends and PP/wax/EG composites

All the samples (Table 1) were prepared by a melt mixing process using a Brabender Plastograph 50 mL internal mixer at 180 °C and 60 rpm for 20 min. For the blends, the components were physically premixed and then fed into the heated mixer, whereas for the composites, the EG was added into the Brabender mixing chamber within 5 min after adding the PP or premixed PP/wax blends. The samples were then melt-pressed at 180 °C for 5 min under 50 kPa pressure using a hydraulic melt press to form 15 x 15 x 2 cm³ sheets.

Table 4.1 Sample compositions used in this study

PP/EG (w/w)	PP/wax (w/w)	PP/wax/EG (w/w)	PP/wax/EG (w/w)	PP/wax/EG (w/w)
100/0	100/0	50/50	60/40	70/30
97/3	70/30	48.5/48.5/3	58.2/38.8/3	67.9/29.1/3
94/6	60/40	47/47/6	56.4/37.6/6	65.8/28.2/6
91/9	50/50	45.5/45.5/9	54.6/36.4/9	63.7/27.3/9

4.2.4 Sample analysis

A Ceast Impactor II was used to investigate the impact properties of the blends and composites in order to establish whether EG gives rise to improved impact properties. The samples were rectangular with a width of 10 mm, a thickness of 3 mm and length of 83 mm, and were V-notched (2 mm deep) edgewise. The pendulum hammer was situated at an angle of 50° from the release spot and the samples were tested at an ambient temperature of 24 °C. Five samples of each composition were tested and the average and standard deviation values are presented.

Dynamic mechanical analysis was performed from -90 to 90 °C in bending (dual cantilever) mode at a heating rate of 3 °C min⁻¹ and a frequency of 1 Hz.

Cone calorimetry measurements were performed on an FTT dual analysis cone calorimeter using a cone shaped heater at an incident heat flux of 35 kW m⁻². The specimens, with dimensions of 6 x 100 mm x 100 mm³, were prepared by compression molding. The following quantities were measured using the cone calorimeter: Peak heat release rate, time to ignition, mass loss rate, and carbon monoxide and carbon dioxide yields.

The thermogravimetric (TGA) analyses were carried out in a Perkin Elmer Pyris-1 thermogravimetric analyzer. Samples ranging between 5 and 10 mg were heated from 30 to 650 °C at a heating rate of 10 °C min⁻¹ under nitrogen flow (20 mL min⁻¹). The TGA-Fourier-transform infrared (TGA-FTIR) analyses were performed in a Perkin Elmer STA6000 simultaneous thermal analyser from Waltham, Massachusetts, U.S.A. The analyses were done under flowing nitrogen at a constant flow rate of 20 mL min⁻¹. Samples (20-25 mg) were heated from 30 to 650 °C at 10° C min⁻¹ and held for 4 min at 650 °C. The furnace was linked to the FTIR (Perkin Elmer Spectrum 100, Massachusetts, U.S.A.) with a gas transfer line. The volatiles were scanned over a 4000-400 cm⁻¹ wavenumber range at a resolution of 4 cm⁻¹. The FTIR spectra were recorded in the transmittance mode at different temperatures during the thermal degradation process.

Thermal conductivity measurements were performed on circular discs 5 mm thick and 12 mm in diameter using a ThermTest Inc. Hot Disk TPS 500 thermal constants analyzer. The instrument uses the transient plane source method. A 3.2 mm Kapton disk type sensor was selected for the analysis. The sensor was sandwiched between two sample discs. Three measurements were performed for each composition.

4.3 Results and discussion

4.3.1 Fire-retardant properties

Nanofillers (CNTs and graphite) have recently received much attention and are considered as potential additives for their positive impact on principal thermo-mechanical properties and on flame retardancy. Generally these nanofillers lead to the formation of a protective thermally

stable surface layer, which limits the heat transfer from the flame to the substrate and mass transfer from the substrate to the flame. The overall rate of flame feeding by combustible products from polymer pyrolysis and thermo-oxidation is therefore decreased. The heat release rate (HRR) is a very important parameter, and can be used to express the intensity of fire [29]. A highly flame retardant system normally shows a low HRR peak. The HRR plots for the PP, PP/wax blend and their EG composites are shown Figure 4.1. When EG is introduced into the neat PP and PP/wax blend systems, the peak HRRs are dramatically reduced. HRR is a function of heat generation rate and heat transfer, and the heat generation rate is related to oxygen transfer during combustion, so the decrease in HRR is mostly the result of a decrease in oxygen transfer [30]. The addition of EG into PP and PP/wax blends therefore enhances the barrier properties of the char layer so that the heat transfer rate is reduced. It is interesting that the HRR of the PP/wax/EG composite is lower than that of PP/EG.

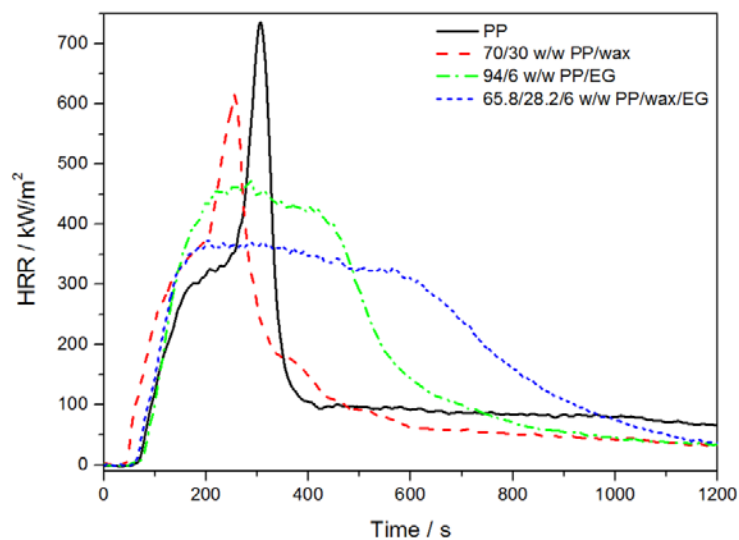


Figure 4.1 Heat release rate curves for PP, the PP/wax blend, and the PP/EG and PP/wax/EG composites

It seems as if the low molecular weight wax contributed to a better dispersion of EG in the PP matrix. This is probably because the wax penetrates in between the EG layers and separates the layers, giving rise to smaller and better dispersed EG particles. This enhanced the stability of the char layer formed, so that it was more difficult for the heat and oxygen to reach the PP matrix. The presence of wax accelerated the char layer formation and improved the compactness of the char layer. It has been reported that the rate of char layer formation and the compactness

of a char layer have a strong influence on the reduction of the heat release rate and improvement in the flame retardancy [16], and that low PHRR values correlate with well dispersed systems [31-32]. It is further clear from Figure 4.1 that the HRR peak of the PP/wax blend is less intense than that of the neat PP, which means that the presence of wax in some way reduces the flammability of PP. However, the time to ignition (TTI) values in Table 4.2 show that ignition starts earlier for the PP/wax blend and the PP/wax/EG composite than for the neat PP and the PP/EG composites. This is probably because of the lower pyrolysis temperature of the wax compared to PP and PP/EG. Because of its lower PHRR, the PP/wax/EG composite also shows a better fire performance index (FPI) value. FPI is considered to be the best individual indicator of overall fire hazard, and therefore smaller FPI values are an indication of a smaller fire hazard. The two composites further show better fire growth index (FIGRA) values (an index for estimating fire growth, thus a lower FIGRA value may indicate a better flame retardancy) than PP and the PP/wax blend.

Figure 4.1 also shows that the PHRR values decrease in the order $PP > PP/wax > PP/EG > PP/wax/EG$. The reason for this is probably that heat and flammable volatiles penetrated the PP and PP/wax blend in the absence of a flame retardant material (in this case EG), and therefore no char residues were formed. The PP/EG and PP/wax/EG composites show lower PHRR values because of the formation of a char layer. The char layer prevented heat and oxygen from penetrating the PP and wax, and the flammable volatiles from entering the flame zone, leading to an improved flame resistance. The PP/EG composite shows a higher PHRR value than the PP/wax/EG composite. This is attributed to the more compact and dense char layer formed in the presence of wax in the case of the PP/wax/EG composites (see discussion further on). Because of this there was a much slower diffusion of decomposition products out of the system, and a slower penetration of heat and oxygen into the system.

Li *et al.* [33] reported that an IFR consisting of a char-foaming agent (CFA), APP and lanthanum oxide is very effective in improving the flame retardance of PP. They observed that the neat PP burned very fast after ignition, showing one sharp HRR peak with a maximum at 1025 kW m^{-2} , which indicates a higher flammability than what we observed. They further observed that the addition of lanthanum oxide (La_2O_3) and intumescent flame retardants (CFA-APP) into PP improved the flame resistance of PP by 76%, which is better than the about 50% improvement we observed when mixing PP with wax and EG. Xu *et al.* [16] observed

improvements smaller than or similar to ours with the addition of 25% APP, poly[N⁴-bis(ethylenediamine)-phenyl phosphonic-N², and N⁶-bis(ethylenediamine)-1,3,5-triazine-N-phenyl phosphate] (PTPA). However, when combining APP and PTPA, a much more significant improvement in flame retardancy of 85% was obtained.

Table 4.2 Flammability data of PP, the PP/wax blend, and the PP/EG and PP/wax/EG composites

Samples	PHRR / kW m ⁻²	TTI / s	t _{PHRR} / s	FPI / kW m ⁻² s ⁻¹	FIGRA / kW m ⁻² s ⁻¹
PP	741.8 ± 10.6	72 ± 2.1	295 ± 14.1	10.3	2.5
70/30 w/w PP/wax	627.1 ± 0.9	47 ± 1.4	255 ± 10.9	13.3	2.5
65.8/28.2/6 w/w PP/wax/EG	405.1 ± 38.4	69 ± 7.1	220 ± 21.2	5.9	1.8
94/6 w/w PP/EG	480.2 ± 9.1	78 ± 2.1	278 ± 17.7	6.1	1.7

PHRR, TTI, FPI and FIGRA are respectively the peak heat release rate, time to ignition, fire performance index, and fire growth index

The physical structure of the char layer plays a significant role in the performance of an intumescent flame retardant material. The charred residues were photographed at the end of the combustion process (Figure 4.2). The PP and PP/wax blend did not show any char residue, while intumescent char layers were formed in the case of the PP/EG and PP/wax/EG composites. Heat and flammable volatiles must have penetrated the charred PP/EG and PP/wax/EG composites less than the PP and the PP/wax blend. This is because of the continuous, compact and thick carbonaceous layer in presence of EG. This prevented the decomposition products from escaping out of the system, and the penetration of heat and oxygen into the system. A char layer will become fragmented when a lot of gaseous decomposition products escape, which will make it easier for heat and oxygen to enter the system. Careful inspection of these photos show a much more compact char layer in the case of PP/wax/EG, which explains the improved flame retardancy of this system.

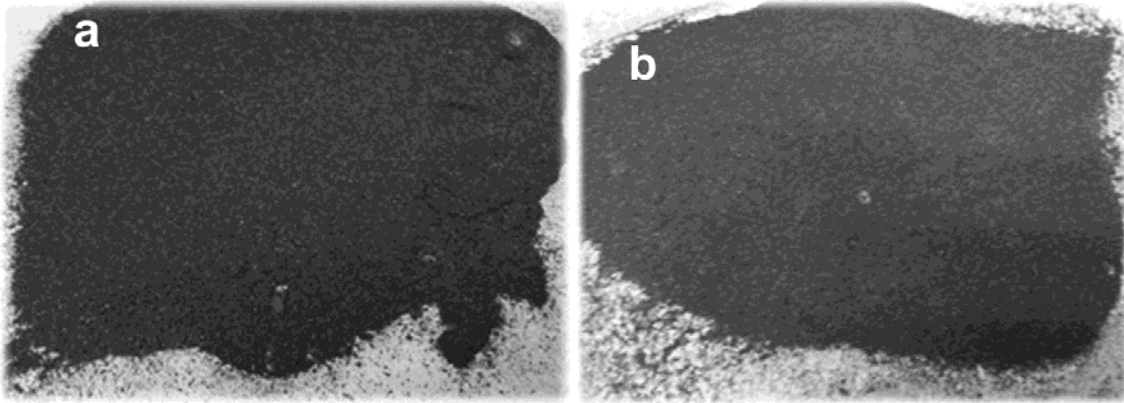


Figure 4.2 Photos of the (a) PP/EG and (b) PP/wax/EG charred residues obtained at the end of the combustion process

One important reaction to fire parameter is the formation of carbon monoxide and carbon dioxide. CO and CO₂ are present in large amounts in all fires. It is seen in Figure 4.3 that both CO and CO₂ production of PP increases and reaches a maximum around 300 s, after which it decreases until it reaches zero above 400 s. The CO and CO₂ production for the composites increases and reaches a much lower maximum around 200 s, but this value is maintained over a much longer period of time. This is probably because the insulating char layer trapped these gases, and they only gradually escape through micro-cracks over a longer period of time. The PP/wax blend and PP/EG composite also reach almost the same value for CO production, although the PP/wax blends releases the gases over a much shorter period of time. The reason for this is probably the presence of EG agglomerates which results in the formation of an ineffective char barrier which allows the slower release of CO over a longer period of time. The presence of wax in the PP/wax/EG composite results in a better dispersed system than PP/EG, and a more effective char is formed which allows the release of smaller amounts of CO and CO₂ over a longer period of time.

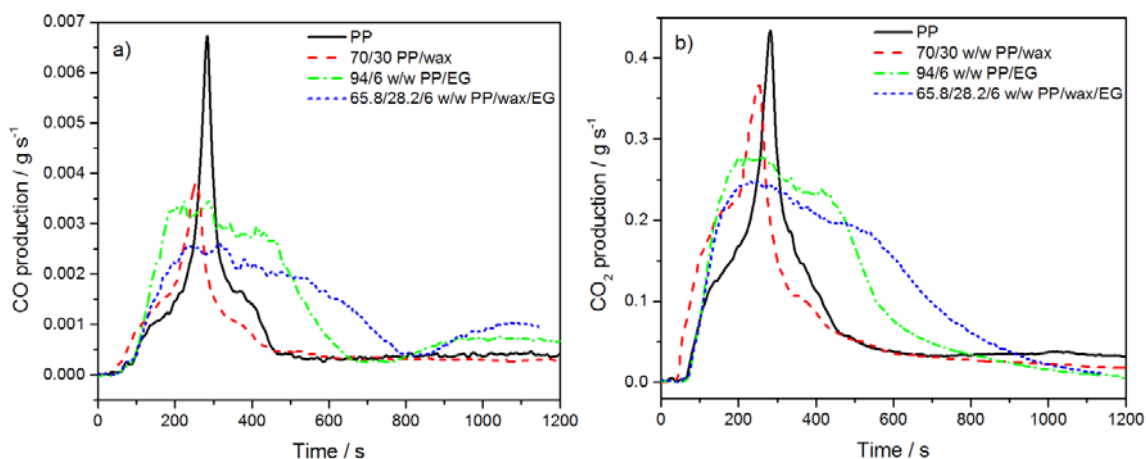


Figure 4.3 a) Carbon monoxide and b) carbon dioxide production plots of PP, PP/wax blend, as well as PP/EG and PP/wax/EG composites

4.3.2 Thermogravimetric analysis (TGA)

The TGA curves in Figure 4.4 show that EG is thermally stable up to temperatures higher than the decomposition temperatures of wax and PP. The wax decomposes at temperatures lower than that of PP. Scheme 4.1 shows the formation of the most general degradation products of PP [34]. Path A proceeds via a secondary radical and produces major products such as pentane (24.3%), 2-methyl-1-pentene (15.4%), and 2,4-dimethyl-1-heptene (18.9%). The primary radical of path B forms only minor products with propane being the most abundant. All these processes occur simultaneously as evident by a single TGA mass loss step in Figure 4.

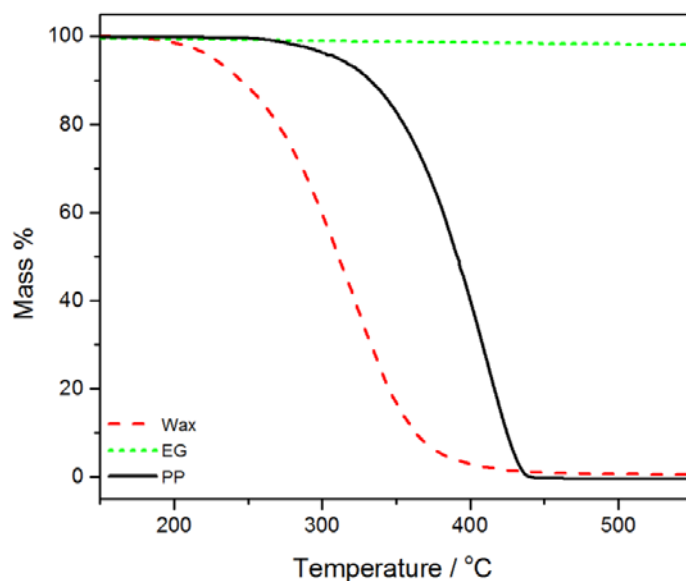
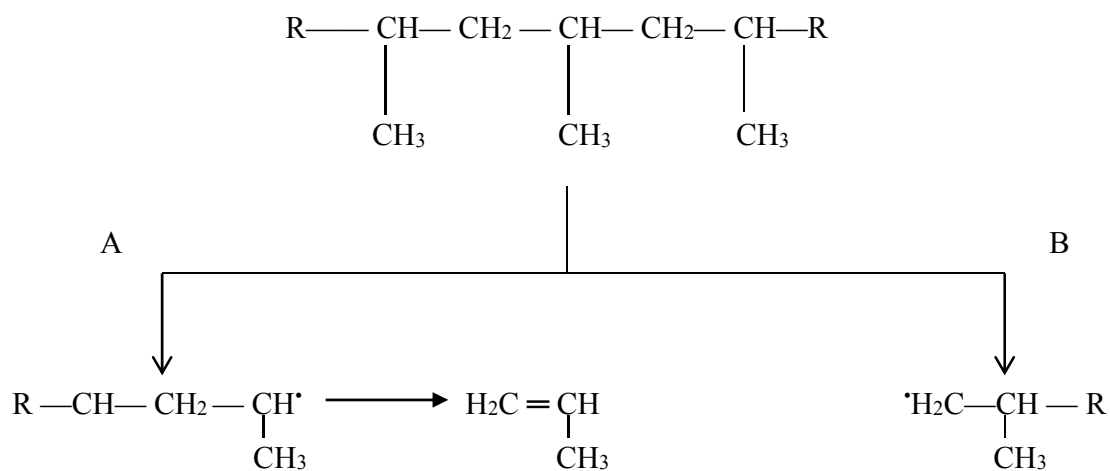


Figure 4.4 TGA curves of PP, wax and EG



Scheme 4.1 Degradation mechanism of polypropylene

The TGA curves of the PP/wax blend, and the PP/EG and PP/wax/EG composites, are shown in Figure 4.5 and 4.6. The thermal stability of PP increased significantly with the addition EG, irrespective of the filler content. This can be associated with the 2-dimensional planar structure of EG in the PP matrix, which served as a barrier preventing further degradation of the underlying PP matrix. It probably also trapped the volatile decomposition products, which could

only escape at much higher temperatures. However, Kim *et al.* [35] observed slightly lower mass loss temperatures for exfoliated graphite nanoplatelets/LLDPE nanocomposites compared to the neat LLDPE matrix. They attributed this to the physisorbed water evaporating at 450 °C.

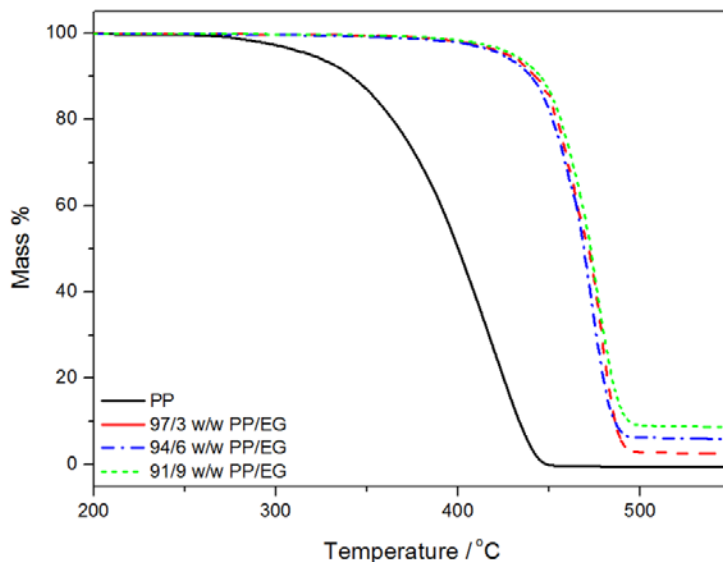


Figure 4.5 TGA curves of neat PP and the PP/EG composites

All the wax-containing samples degraded in two steps (Figure 4.6). The first step between 250 and 300 °C corresponds to the degradation of the wax, while the second step between 370 and 500 °C corresponds to the degradation of the PP. The 70/30 w/w PP/wax and 50/50 PP/wax blends and their EG containing composites (not shown) showed similar behaviour. The thermal stability of the blend improved in the presence of and with increasing graphite content. The interaction between the PP and wax in the PP/wax blend and the graphite particles probably reduced the free radical chain mobility and thus slowed down the degradation process. It is also possible that the volatile degradation products could have been trapped in the EG network (also because of a relatively strong interaction between these products and EG) and only started evaporating at higher temperatures. Our observations are most probably the result of a combination of these two effects.

For all composites there is a good correlation between the % residue at 550 °C and the amount of graphite originally mixed into the composite, which confirms that the graphite was generally well dispersed into the PP/wax blend.

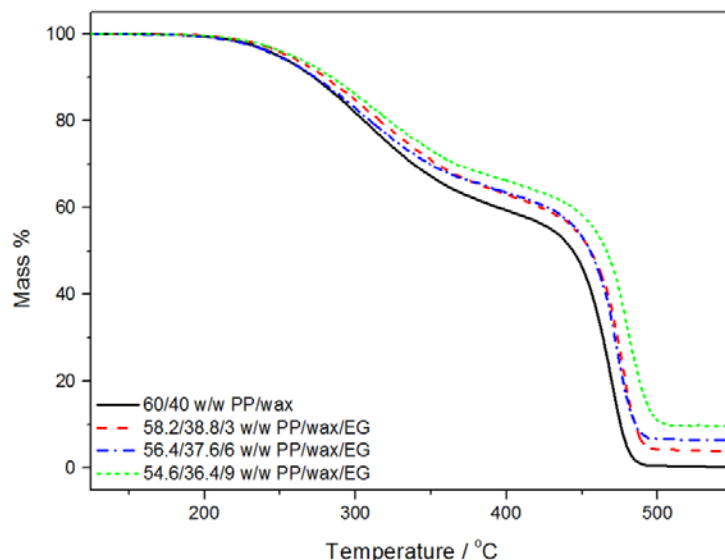


Figure 4.6 TGA curves of PP/wax blend and PP/wax/EG composites

4.3.3 Fourier-transform infrared (FTIR) analysis of volatiles from TGA analysis

TGA-FTIR analyses were done to establish the nature of the degradation products of PP and wax in the different samples. The degradation of PP normally occurs via a random chain scission mechanism; it does not involve crosslinking or chain branching. Because of the presence of tertiary carbons in PP, the bonds are ruptured through a β -scission mechanism followed by a radical transfer process which leads to the formation of the degradation products [36]. All these processes occur simultaneously as evident by a single TGA mass loss step (Figure 4.4). The degradation of PP occurs around 370 °C with the release of volatiles such as pentane, 2-methyl-1-pentene and 2,4-dimethyl-1-heptene. It has been reported that the degradation of PP occurs in a single degradation step that primarily occurs between 250 and 450 °C [34]. The paraffin wax releases volatiles at temperatures around 290 °C (Figure 4.4).

It can be seen that the main volatiles released are CO₂, which is more visible in the PP/EG composite, and aliphatic or unsaturated alkanes (C-H bending vibration, in plane rocking of CH₂ – Figures 4.7 to 4.10 and Table 4.3). It has been reported that during intercalation of natural graphite by strong acids some of the carbon double bonds are oxidized, which leads to the formation of oxygen containing functional groups like carboxylic (C=O), which will form CO₂ during decomposition [37]. There was no shift in the positions of the absorption peaks of all the

samples, which indicates that the presence of wax, EG and/or wax+EG did not change the decomposition mechanism of the blends and composites.

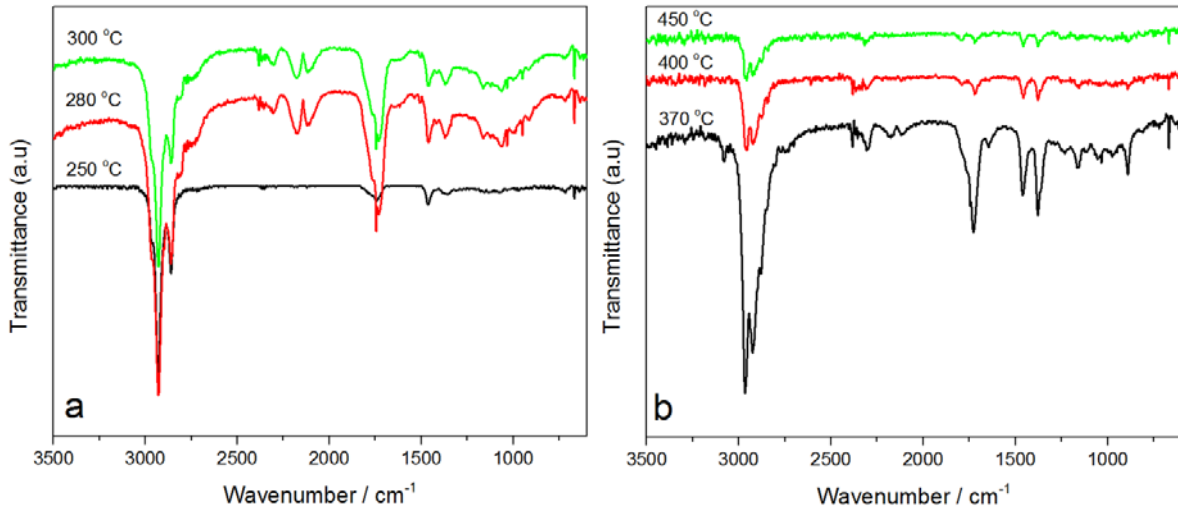


Figure 4.7 FTIR curves of a) wax and b) PP at different temperatures during the thermal degradation in a TGA at a heating rate of 10 °C min⁻¹

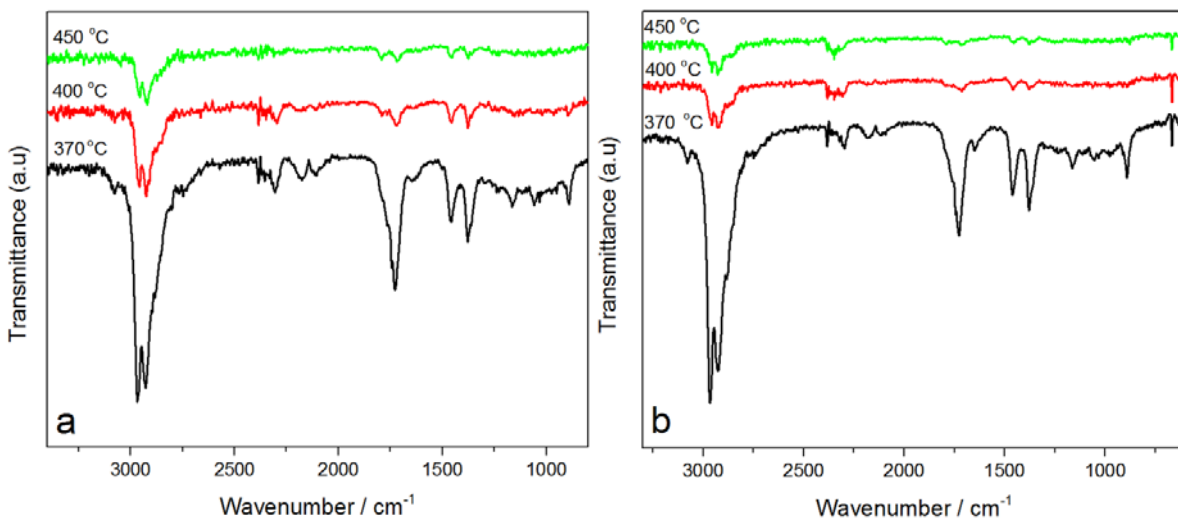


Figure 4.8 FTIR curves of a) 70/30 w/w PP/wax and b) 65.8/28.2/6 w/w PP/wax/EG at different temperatures during the thermal degradation in a TGA at a heating rate of 10 °C min⁻¹

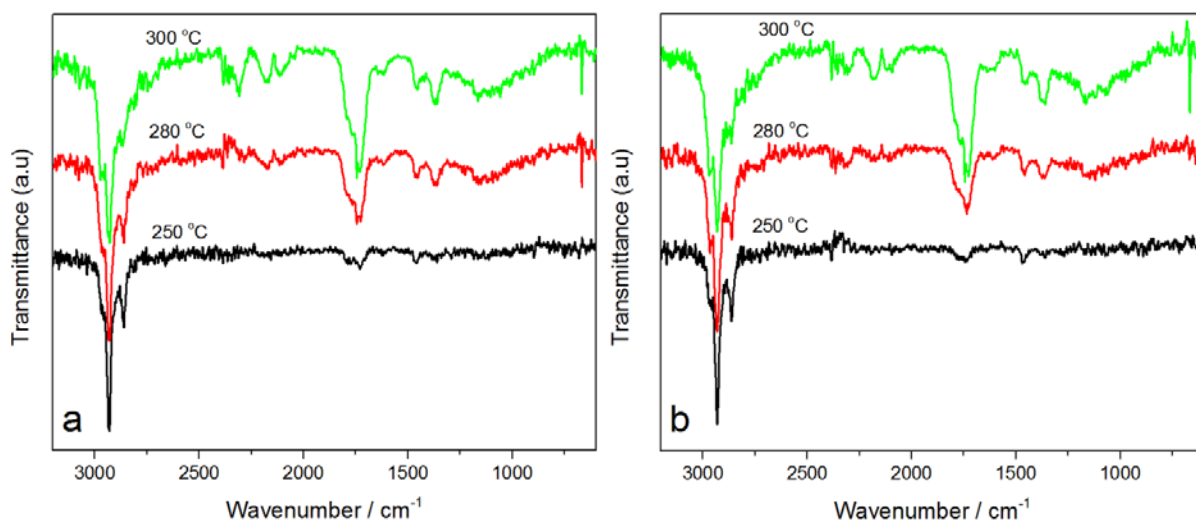


Figure 4.9 FTIR curves of a) 70/30 w/w PP/wax and b) 65.8/28.2/6 w/w PP/wax/EG during the thermal degradation in a TGA at a heating rate of $10\text{ }^{\circ}\text{C min}^{-1}$

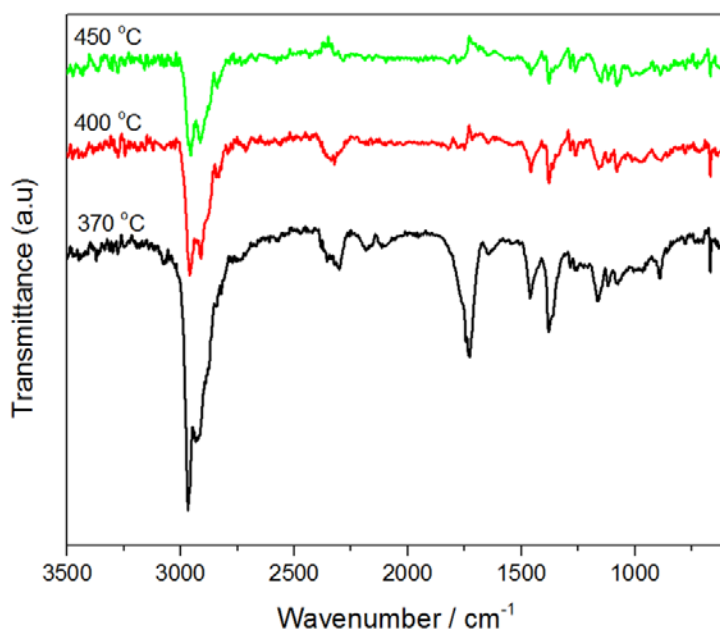


Figure 4.10 FTIR curves of 94/6 w/w PP/EG at different temperatures during the thermal degradation in a TGA at a heating rate of $10\text{ }^{\circ}\text{C min}^{-1}$

Table 4.3 Assignment of peaks for TGA-FTIR analysis results

Wavenumber / cm^{-1}	Assignment
2410-2305	CO_2
1459-1455	C-H bending vibration
1725-1740	in plane rocking of CH_2
2916-2848	Saturated and unsaturated C-H

4.3.4 Dynamic mechanical analysis (DMA)

The storage and loss modulus of the investigated samples are shown in Figures 4.11 and 4.12. It was not possible to analyse pure wax and the PP/wax blends, because they were too brittle to sustain the dynamic forces applied during the test. The storage modulus of neat PP and the PP/EG composite is higher than those of the PP/wax/EG composites, especially above 60 °C which is after the melting of the wax in the composites. This is because of the softening effect of the wax on the composite, especially when the wax is in the molten state when it acts as a typical plasticizer. A plasticizer typically creates more free volume, allowing the polymer chains a higher degree of mobility through Brownian movement. This lowers the temperature where segmental mobility can occur and makes the material more elastic.

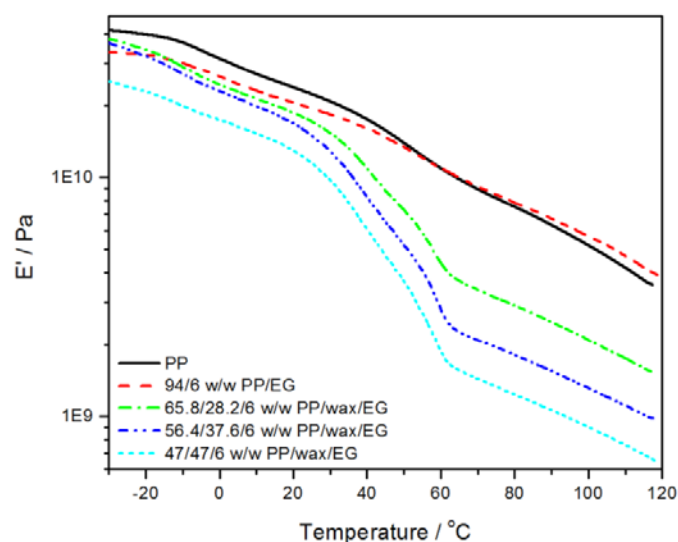


Figure 4.11 Storage modulus curves of PP, as well as the PP/EG and PP/wax/EG composites

Two transitions are observed in the loss modulus curves in Figure 4.12. The relaxation between -20 and 30 °C, which is the β -relaxation, is attributed to the glass transition of the amorphous phase of PP. The relaxation between 40 and 60 °C is because of the melting of wax, which is the reason why this transition is not observed for PP and PP/EG. The glass transition of PP in PP/EG is at the same temperature than that of PP, which confirms that there is a fairly weak interaction between the PP chains and the EG particles. The temperature of this transition decreased by about 15 °C in the PP/wax/EG composites. As mentioned above, the wax has a strong plasticizing effect on PP, and this is also the reason for this observed decrease in the glass transition temperature of the PP. The PP/wax blend samples are very brittle, despite the plasticizing effect of the wax, while the PP/wax/EG composites are not so brittle. This is because PP and wax are incompatible materials, and increasing the amount of the low molecular weight component reduces the number of tie chains that keep the structure together. In the case of the PP/wax/EG composites, the porous EG structure absorbs the wax resulting in fewer wax crystals in the PP matrix. The graphite therefore reinforced the samples and countered the brittle effect of the wax.

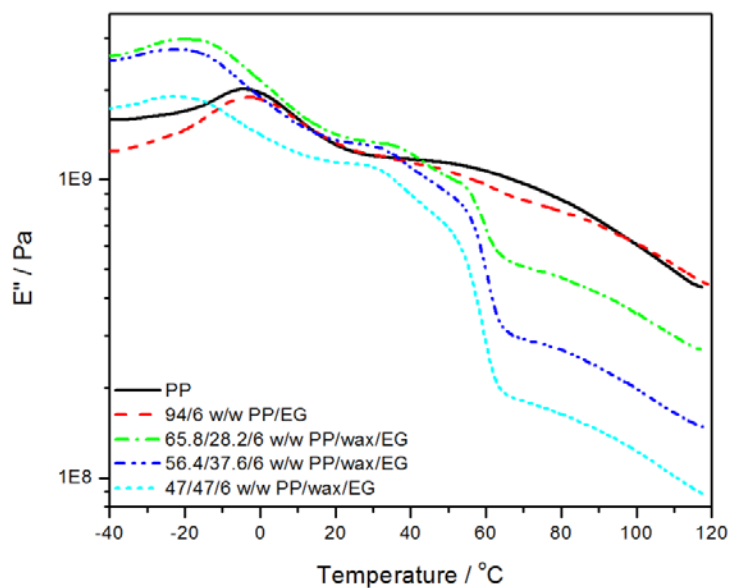


Figure 4.12 Loss modulus curves of PP, as well as the PP/EG and PP/wax/EG composites

4.3.5 Impact properties

The impact properties of a polymer may be modified by adding some fillers. Polymeric impact modifiers may be incorporated to act as barriers or crack blunting regions to the advancing crack. The impact strengths of the PP/wax blends and the PP/wax/EG composites are shown in Figures 4.13 and 4.14. The addition of wax decreased the impact strength of both PP and the PP/EG composites. The low molar mass wax crystals probably acted as internal flaws with high stress concentrations, and therefore as defects points for the initiation and propagation of stress cracking. It is known that the polymer matrix adds toughness to a composite, and therefore an increase in wax content will result in a decrease in the polymer content, resulting in a smaller amount of matrix to withstand the applied load. The impact strength of the PP/wax/EG composites increased in the presence of and with increasing expanded graphite content in all the investigated samples. One could expect a reduction in toughness with the addition of stiff graphite platelets due to the limited plastic flow of the PP matrix, because the more ductile matrix was replaced by the more rigid dispersed particles. Different factors, like filler particle size and interaction between the polymer and the other components, may have contributed to this improvement in the impact strength of the composites. In this case the wax on the EG surface improved the interaction between the EG and the PP, giving rise to a good dispersion and effective stress transfer. The particle dispersion is important in controlling the mechanical properties of composites; large particles act as crack nucleation sites [38] and if the agglomerated particles are far away from each other, it is easier for crazes to develop into cracks and for cracks to propagate. The smaller the size of the filler particles and the better they are dispersed, the easier it is for a craze to terminate at a neighboring particle without developing into a crack.

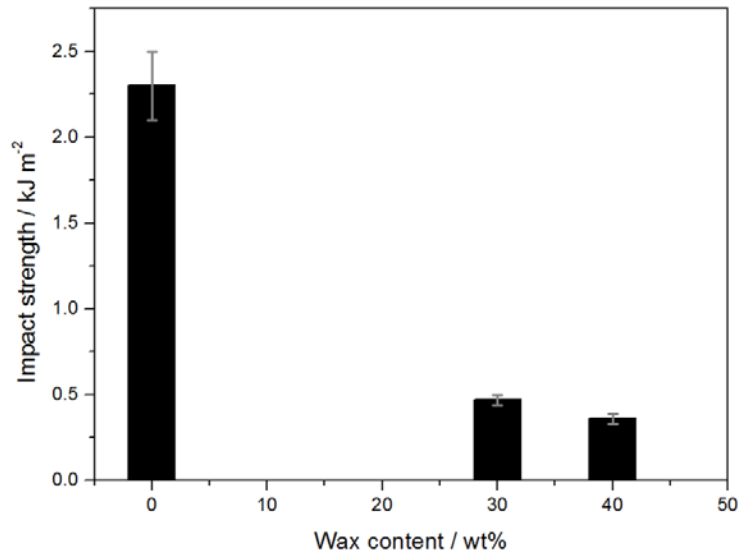


Figure 4.13 Impact strengths of PP and PP/wax blends

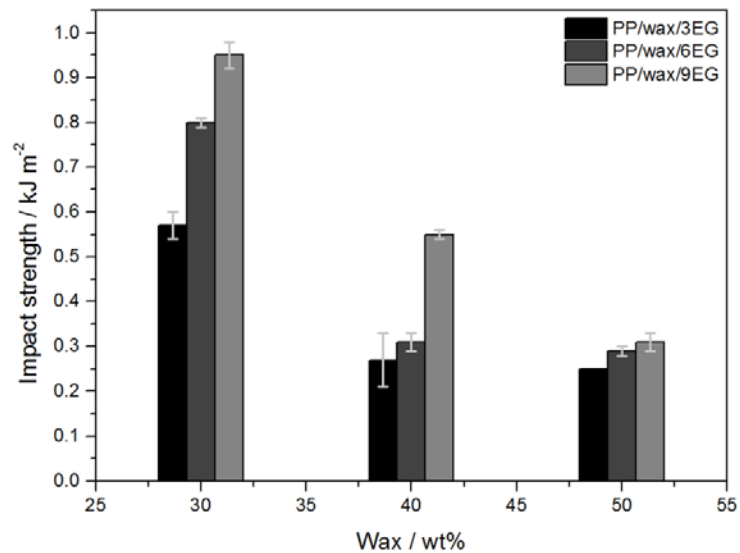


Figure 4.14 Impact strengths of PP/wax blends containing different contents of expanded graphite

4.3.6. Thermal conductivity

Phase change materials are used for the storage and release of thermal energy. One of the performance indicators is the rate of energy storage and release, which strongly depends on thermal conductivity of the PCMs. Since PP and wax both have very low thermal conductivities (Figure 4.15), it is important to investigate how the thermal conductivity of the PCM system can

be improved through the addition of conductive fillers. In our investigation the thermal conductivity of both PP and PP/wax blends increased with increasing graphite content (Figure 4.15). This can be attributed to high thermal conductivity of the EG [13]. However, it was observed that the thermal conductivities of the PP/wax/EG composites were higher than those of the PP/EG composites. It has been reported in the literature that the heat is conducted predominantly by phonons in the nanographite materials [39]. In order to improve the overall thermal transport in filled polymers, the acoustic impedance mismatch (a function of the acoustic speed and density of the medium) at the interface between the filler and the polymer has to be reduced. Because of the smaller and better dispersed EG particles in the PP/wax/EG composites, and their strong affinity for wax which sits at the interface between PP and the EG particles, the interfacial heat transfer between the graphite platelets and the PP matrix was obviously improved. For the PP/EG composites, the weak interaction between EG and PP increases the acoustic impedance which results in a large thermal contact resistance at the filler-PP interface and a reduction in the thermal conductivity of the overall system.

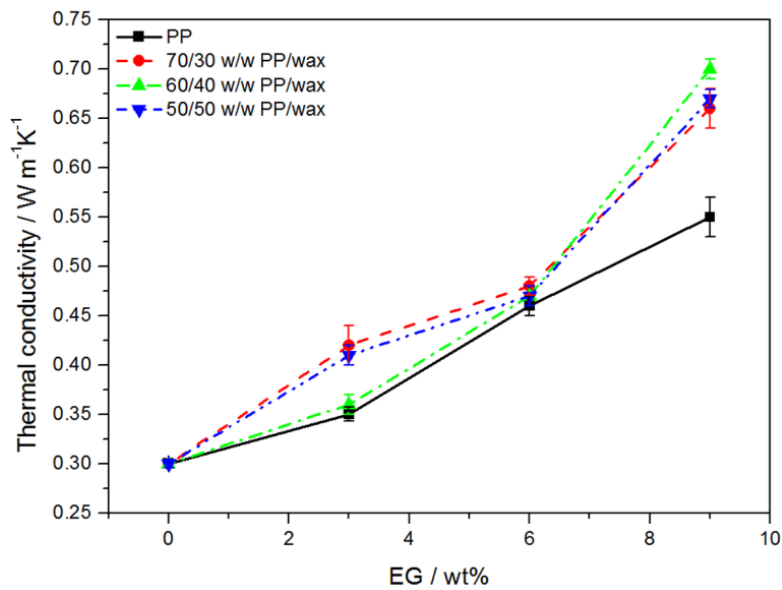


Figure 4.15 Thermal conductivities of PP and the PP/wax blends with different amounts of expanded graphite

4.4 Conclusions

The effect of expanded graphite on the flammability, thermal stability, thermomechanical behaviour and thermal conductivity of PP and PP/wax composites was investigated. Improvements in thermal stability, thermal conductivity and flame resistance were observed for the PP/EG, and these properties further improved for the PP/wax/EG composites. The improvement of the flame resistance in the presence of wax is especially interesting, and was attributed to the formation of a more compact char layer that more effectively prevented the penetration of heat and oxygen and the release of flammable volatiles. The thermomechanical results confirmed the plasticizing effect of the wax in the PP/wax/EG composites. It is interesting that the PP/wax blends could not be analysed because of their brittleness, but when the same blends contained EG, their brittleness significantly decreased because of the wax penetrating into the EG layered structure. The thermal conductivities of the PP/wax/EG composites were higher than those of the PP/EG composites, which was attributed to the smaller and better dispersed EG particles in the PP/wax/EG composites. TGA-FTIR analyses confirmed that the presence of wax, EG and/or wax+EG did not change the thermal decomposition mechanism of the blends and composites.

4.5 References

1. G. Song, S. Ma, G. Tang, Z. Yin, X. Wang. Preparation and characterization of flame retardant form-stable phase change materials composed by EPDM, paraffin and nano magnesium hydroxide. *Energy* 2010; 35:2179-2183.
DOI: 10.1016/j.energy.2010.02.002
2. B. Zalba, J.M. Marin, L.F. Cabeza, H. Mehling. Review on thermal energy storage with phase change materials, heat transfer analysis and applications. *Applied Thermal Engineering* 2003; 23:251-283.
DOI: 10.1016/S1359-4311(02)00192-8
3. M. Kenisarin, K. Mahkamov. Solar energy storage using phase change materials. *Renewable and Sustainable Energy Reviews* 2007; 11:1913-1965.
DOI: 10.1016/j.rser.2006.05.005

4. M.M. Farid, A.M. Khudhair, S.A.K. Razack, S. Al-Hallaj. A review on phase change energy storage: Materials and applications. *Energy Conversion and Management* 2004; 45:1597-1615.
DOI: 10.1016/j.enconman.2003.09.015
5. A. Sharma, V.V. Tyagi, C.R. Chen, D. Buddhi. Review on thermal energy storage with phase change materials and applications. *Renewable and Sustainable Energy Reviews* 2009; 13:318-345.
DOI: 10.1016/j.rser.2007.10.005
6. A.S. Luyt, I. Krupa. Phase change materials formed by UV curable epoxy matrix and Fischer-Tropsch paraffin wax. *Energy Conversion and Management* 2009; 50:57-61.
DOI: 10.1016/j.enconman.2008.08.026
7. M.E. Mngomezulu, A.S. Luyt, I. Krupa. Structure and properties of phase change materials based on high density polyethylene, hard Fischer-Tropsch paraffin wax, and wood flour. *Polymer Composites* 2011; 32:1155-1163.
DOI: 10.1002/pc.21134
8. M. Xiao, B. Feng, K. Gong. Preparation and performance of shape stabilized phase change thermal storage materials with high thermal conductivity. *Energy Conversion and Management* 2002; 43:103-1078.
DOI:10.1016/S0196-8904(01)00010-3
9. S. Shaikh, K. Lafdi, K. Hallinan. Carbon nano-additives to enhance latent energy storage of phase change materials. *Journal of Applied Physics* 2008; 103:094302.
DOI: 10.1063/1.2903538
10. A. Elgafy, K. Lafdi. Effect of carbon nanofiber additives on thermal behavior of phase change materials. *Carbon* 2005; 43:3067-3074.
DOI: 10.1016/j.carbon.2005.06.042
11. P. Bonnet, D. Siruede, B. Garrier, O. Chauvet. Thermal properties and percolation in carbon nanotubes-polymer composites. *Applied Physics Letters* 2007; 91:201910.
DOI: 10.1063/1.2813625
12. J.F. Wang, H.Q. Xie, X. Zhong. Thermal properties of heat storage composites containing multiwalled carbon nanotubes. *Journal of Applied Physics* 2008; 104:113537.
DOI: 10.1063/1.3041495

13. A. Sari, A. Karaipekli. Thermal conductivity and latent heat thermal energy storage characteristics of paraffin/expanded graphite composite as phase change material. *Applied Thermal Engineering* 2007; 27:1271-1277.
DOI: 10.1016/j.applthermaleng.2006.11.004
14. J. Fukai, Y. Morozumi, O. Miyatake. Improvement of thermal characteristics of latent heat thermal energy storage units using carbon-fiber brushes: experiment and modelling. *International Journal of Heat and Mass Transfer* 2003; 46:4513-4525.
DOI: 10.1016/S0017-9310(03)00290-4
15. Z.G. Zhang, X.M. Fang. Study on paraffin/expanded graphite composite phase change thermal energy storage material. *Energy Conversion and Management* 2006; 47:303-310.
DOI: 10.1016/j.enconman.2005.03.004
16. Z.Z. Xu, J.Q. Huang, M.J. Chen, Y. Tan, Y.Z. Wang. Flame retardant mechanism of an efficient flame-retardant polymeric synergist with ammonium polyphosphate for polypropylene. *Polymer Degradation and Stability* 2013; 98:2011-2020.
DOI: 10.1016/j.polymdegradstab.2013.07.010
17. Z.B. Shao, C. Deng, Y. Tan, M.J. Chen, L. Chen, Y.Z. Wang. Flame retardation of polypropylene via a novel intumescent flame retardant: Ethylenediamine-modified ammonium polyphosphate. *Polymer Degradation and Stability* 2014; 106:88-96.
DOI: 10.1016/j.polymdegrastab.2013.10.005
18. Z.Q. Lei, Y.M. Cao, F. Xie, H. Ren. Study on surface modification and flame retardants properties of ammonium polyphosphate for polypropylene. *Journal of Applied Polymer Science* 2012; 124:781-788.
DOI: 10.1002/app.35064
19. P. Zhang, Y. Hu, L. Song, J. Ni, W. Xing, J. Wang. Effect of expanded graphite on properties of high-density polyethylene/paraffin composite with intumescent flame retardant as a shape-stabilized phase change material. *Solar Energy Materials and Solar Cells* 2010; 94:360-365.
DOI: 10.1016/j.solmat.2009.10.014
20. B. Lecouvet, M. Sclavons, C. Bailly, S. Bourbigot. A comprehensive study of the synergistic flame retardant mechanisms of halloysite in intumescent polypropylene. *Polymer Degradation and Stability* 2013; 98:2268-2281.

- DOI: 10.1016/j.polymdegrastab.2013.08.024
21. X. Wu, L. Wang, C. Wu, J. Yu, L. Xie, G. Wang, P. Jiang. Influence of char residues on flammability of EVA/EG, EVA/NG and EVA/GO composites. *Polymer Degradation and Stability* 2012; 97:54-63.
DOI: 10.1016/j.polymdegrastab.2011.10.011
22. A. Ramani, A.E. Dahoe. On the performance and mechanism of brominated and halogen free flame retardants in formulations of glass fibre reinforced poly(butylene terephthalate). *Polymer Degradation and Stability* 2014; 104:71-86.
DOI: 10.1016/j.polymdegradstab.2014.03.021
23. Z. Li, B. Qu. Flammability characterization and synergistic effects of expandable graphite with magnesium hydroxide in halogen-free-retardant EVA blends. *Polymer Degradation and Stability* 2003; 81:401-408.
DOI: 10.1016/S014-3910(03)00123-X
24. G. Bai, C. Guo, L. Li. Synergistic effect of intumescent flame retardant and expandable graphite on mechanical and flame-retardant properties of wood flour-polypropylene composites. *Construction and Building Materials* 2014; 50:148-153.
DOI: 10.1016/j.conbuildmat.2013.09.028
25. X. Chen, C. Jiao. Synergistic effects of hydroxyl silicone oil on intumescent flame retardant polypropylene system. *Fire Safety Journal* 2009; 44:1010-1014.
DOI: 10.1016/j.firesaf.2009.06.008
26. Y. Xia, F. Jing, Z. Mao, Y. Guan, A. Zheng. Effects of ammonium polyphosphate to pentaerythritol ratio on composition and properties of carbonaceous foam deriving from intumescent flame-retardant polypropylene. *Polymer Degradation and Stability* 2014; 107:64-73.
DOI: 10.1016/j.polymdegradstab.2014.04.016
27. Y. Cai, L. Song, Q. He, D. Yang, Y. Hu. Preparation, thermal and flammability properties of a novel form-stable phase change materials based on high density polyethylene/poly(ethylene-co-vinylacetate)/organophilic montmorillonite nanocomposites/paraffin compounds. *Energy Conversion and Management* 2008; 49:2055-2062.
DOI: 10.1016/j.enconman.2008.02.013

28. Y. Cai, Q. Wei, F. Huang, W. Gao. Preparation and properties studies of halogen-free flame retardant form-stable phase change materials based on paraffin/high density polyethylene composites. *Applied Energy* 2008; 85:7654-775.
DOI: 10.1016/j.apenergy.2007.10.017
29. L. Ye, B. Qu. Flammability characteristics and flame retardant mechanism of phosphate-intercalated hydrotalcite in halogen-free flame retardant EVA blends. *Polymer Degradation and Stability* 2008; 93:918-924.
DOI: 10.1016/j.polymdegradstab.2008.02.002
30. P. Zhang, L. Song, H. Lu, J. Wang, Y. Hu. The influence of expanded graphite on thermal properties for paraffin/high density polyethylene/chlorinated paraffin/antimony trioxide as a flame retardant phase change material. *Energy Conversion and Management* 2010; 51:2733-2737.
DOI: 10.1016/j.enconman.2010.06.003
31. U.M. Fawn, Q. Yao, H. Nakajima, E. Manias, C.A. Wilkie. Expandable graphite/polyamide-6 nanocomposites. *Polymer Degradation and Stability* 2005; 89:70-84.
DOI: 10.1016/j.polymdegradstab.2005.01.004
32. X. Wang, R. Rathore, P. Songtipya, M.D.M.J. Gasco, E. Manias, C.A. Wilkie. EVA-layered double hydroxide (nano) composites: Mechanism of fire retardancy. *Polymer Degradation and Stability* 2011; 96:301-313.
DOI: 10.1016/j.polymdegradstab.2011.10.011
33. Y. Li, B. Li, J. Dai, H. Jia, S. Gao. Synergistic effects of lanthanum oxide on a novel intumescent flame retardant polypropylene system. *Polymer Degradation and Stability* 2008; 93:9-16.
DOI: 10.1016/j.polymdegradstab.2007.11.002
34. J.D. Peterson, S. Vyazovkin, C.A. Wight. Kinetics of the thermal and thermo-oxidative degradation of polystyrene, polyethylene and polypropylene. *Macromolecular Chemistry and Physics* 2001; 202:775-784.
DOI: 1022-1352/2001/0603-0775
35. S. Kim, I. Do, L.T. Drzal. Thermal stability and dynamic mechanical behavior of exfoliated graphite nanoplatelets-LLDPE nanocomposites. *Polymer Composites* 2010; 31:755-761.

- DOI: 10.1002/pc.20781
36. J. Palacios, R. Perera, C. Rosales, C. Albano, J.M. Pastor. Thermal degradation kinetics of PP/OMMT nanocomposites with mPE and EVA. *Polymer Degradation and Stability* 2012; 97:729-737.
DOI: 10.1016/j.polyimdegradstab.2012.02.009
37. P. Gogoi, M. Boruah, C. Bora, S.K. Dolui. Jatropha curcas oil alkyd/epoxy resin/expanded graphite (EG) reinforced bio-composite: Evaluation of the thermal, mechanical and flame retardancy properties. *Progress In Organic Coatings* 2014; 77:87-93.
DOI: 10.1016/j.porgcoat.2013.08.006
38. B. Chen, J.R.G. Evans. Impact strength of polymer-clay nanocomposites. *The Royal Society of Chemistry* 2009; 5:3572-3584.
DOI: 10.1039/b902073j
39. J.N. Shi, M.D. Ger, Y.M. Liu, Y.C. Fan, N.T. Wen, C.K. Lin, N.W. Pu. Improving the thermal conductivity and shape-stabilization of phase change materials using nanographite additives. *Carbon* 2013; 51:365-372.
DOI: 10.1016/j.carbon.2012.08.068

Chapter 5

Synergistic effect of expanded graphite, diammonium phosphate and Cloisite 15A on flame retardant properties of EVA and EVA/wax phase change blends

This chapter has been published:

Synergistic effect of expanded graphite, diammonium phosphate and Cloisite 15A on flame retardant properties of EVA and EVA/wax phase change blends. Journal of Materials Science 2015; 50:3485-3494.

Abstract

The influence of the introduction of expanded graphite (EG), as well as combinations of EG with Cloisite 15A clay and diammonium phosphate (DAP), into EVA and an EVA/wax blend on the thermal stability and flammability of the polymer and blend was investigated. In the presence of EG+Cloisite 15A the material formed a dense and stable char layer (carbonized ceramic) which significantly improved the flame resistance of the materials, while the presence of EG and EG+DAP much less uniform char layers were formed and the improvement in flame resistance was not so significant. X-ray diffractometry investigations showed intercalation of EVA into the organoclay, which became more effective in the presence of wax. It was, however, found that there was little separation of the EG platelets, although the presence of wax caused a decrease in the sizes of the EG agglomerates. The thermal stability of EVA and the EVA/wax blend improved in the presence of EG and its combination with Cloisite 15A and DAP.

Keywords: Ethylene vinyl acetate; wax; expanded graphite; flammability; thermal stability; organically modified clay

5.1 Introduction

Phase change materials (PCMs) have been considered for thermal storage in buildings since 1980 [1]. However, due to the chemical constitution of the paraffin and the polymer matrix, the shape-stabilized PCM is easily flammable. Little has been published on the flame retardance of ethylene vinyl acetate (EVA)/paraffin blends.

Halogen flame retardants, especially brominated flame retardants, are the most effective flame retardants materials and are widely used in most engineering plastics [2-4]. However, halogen flame retardants can release toxic gases during burning. To overcome the release of toxic gases by halogen flame retardants, brominated flame retardants started getting replaced by halogen-free flame retardants. Recent research work showed that the intumescent flame retardants, being less toxic and producing much less smoke, were so far amongst the best flame retardants to replace halogen flame retardants. Chemicals such as diammonium phosphate (DAP) [5,6], ammonium polyphosphate (APP) [7], ammonium polyphosphate with expandable graphite [8], and boric acid with magnesium hydroxide [9] have been used as halogen-free flame retardant materials.

Although the amount of fumes and the toxicity of the smoke generated when using halogen-free flame retardants are much lower during combustion, their flame retardant efficiency is very low and a large amount has to be added into the polymer to obtain acceptable flame retardant efficiency. This high filler loading causes processing difficulties and deterioration in the mechanical performance of the system. In order to obtain more effective flame retardancy, synergistic agents have been used in intumescent flame retardant (IFR) systems. These synergistic agents can effectively increase the strength and stability of the char layer [10-14]. Expanded graphite (EG) with high flame retardant efficiency and low cost is used as a new generation of intumescent efficient additives, in a growing number of fire retardant applications, as a blowing agent and carbonization compound [15-16].

A fair number of studies [10-11,14] investigated the flammability of shape-stabilized phase change materials based on the synergistic effect of EG with flame retardant materials such as chlorinated paraffin/antimony trioxide, and ammonium polyphosphate. Cai *et al.* [10] reported a reduction in peak heat release rate (PHRR) of PCM4 (21 wt% APP + 4 EG wt %) compared to PCM2 (25 wt% APP). The improvement in flame resistance of PCM4 was attributed to the

synergistic effect between EG and APP. The APP is used as an acid source and decomposes to yield polyphosphoric acid with strong dehydration during heating. The polyphosphoric acid takes part in the dehydration of the EG, which yields carbonaceous and phosphocarbonaceous residues that act as a physical protective barrier.

Recent studies [17-19] showed that the addition of nanoparticles such as nanoclay, carbon nanotubes, and POSS into polymers could reduce their flammability. Clay is a promising material for improving the performance of polymers against fire. Addition of clay alone in polymers mainly decreased the PHRR as one of the flame retardant properties in a cone calorimeter study [20]. It was further found that the presence of one kind of nanoparticle alone is not sufficient to achieve an acceptable level of flame retardancy [21-25].

We investigated the synergistic effect of EG and clay, as well as EG and diammonium phosphate (DAP), on the flammability of EVA/wax blends. DAP is safe, inexpensive and efficient in improving the flame resistance of polymers [5,6]. So far nobody else reported on the synergistic effect of these fillers in improving the flame retardance of wax-containing phase-change blends.

5.2 Materials and methods

5.2.1. Materials

Medium-soft Fischer-Tropsch paraffin wax (M3 wax) was supplied in powder form by Sasol Wax, Sasolburg, South Africa. It consists of approximately 99% straight chain hydrocarbons, and is primarily used in the candle-making industry. It has an average molar mass of 440 g mol^{-1} and a carbon distribution between C15 and C78. Its density is 0.90 g cm^{-3} and it has a melting point range of 40-60 °C. EVA-460 was manufactured and supplied in granule form by Du Pont Packaging & Industrial Polymers. EVA-460 contains 18% by weight of vinyl acetate (VA) with a BHT antioxidant thermal stabilizer. It has an MFI (190 °C / 2.16 kg) of 2.5 g/10 min (ASTM D1238-ISO 1133), a melting temperature of 88 °C, and a density of 0.941 g cm^{-3} . Expandable graphite ES 250 B5 was supplied by Qingdao Kropfmuehl Graphite (Hauzenberg, Germany). Diammonium phosphate (DAP, chemical formula $(\text{NH}_4)_2\text{HPO}_4$) was supplied by Sigma-Aldrich

(South Africa). Cloisite 15A (C15A) was supplied as a cream white powder by Southern Clay Products Inc. (Texas, USA).

5.2.2. Preparation of expanded graphite

The expandable graphite was first dried in an oven at 60 °C for 10 h, and then heated in a glass beaker in a furnace to 600 °C, and maintained at this temperature for 15 min to form expanded graphite.

5.2.3. Preparation of blend and composite samples

All the samples (Table 5.1) were prepared through melt mixing using a Brabender Plastograph 50 mL internal mixer at 130 °C and 60 rpm for 20 min. For the blends, the dry components were physically premixed and then fed into the heated mixer, whereas for the composites, the EG and flame retardant materials (diammonium phosphate and Cloisite 15A) were added into the Brabender mixing chamber within 5 minutes after adding the EVA or premixed EVA/wax blends. The samples were then melt-pressed at 130 °C for 5 min under 50 kPa pressure using a hydraulic melt press into 2 mm thick sheets.

Table 5.1 Sample compositions used in this study

Sample	wt.% composition
EVA	100
EVA/wax	60/40
EVA/wax/EG	56.4/37.6/6
EVA/wax/(EG+Cloisite 15A)	56.4/37.6/6
EVA/wax/(EG+DAP)	56.4/37.6/6
EVA/EG	94/6
EVA/(EG+Cloisite 15A)	94/6
EVA/(EG+DAP)	94/6

5.2.4. Sample analysis

To determine the morphology of the charred residues, a TESCAN VEGA 3 scanning electron microscope was used and the analysis was done at room temperature. The samples were gold coated by sputtering to produce conductive coatings onto the samples.

The crystalline structures of EG and Cloisite 15A were determined through X-ray diffraction (XRD). A D8 Advance diffractometer (BRUKER AXS, Germany) with PSD Vantec-1 detectors and Cu K α radiation ($\lambda = 1.5406$), a tube voltage of 40 kV, a current of 40 mA and a V20 slit were used. The samples were scanned in locked couple mode with 2θ increments in 0.5 s steps.

The TGA analyses were carried out in a Perkin Elmer Pyris-1 thermogravimetric analyzer. Samples ranging between 5 and 10 mg were heated from 30 to 650 °C at a heating rate of 10 °C min⁻¹ under nitrogen (flow rate 20 mL min⁻¹).

Cone calorimetry measurements were performed on a Dual Cone calorimeter using a cone shaped heater at an incident flux of 35 kW m⁻². The specimens, with dimensions of 6 mm x 100 mm x 100 mm, were prepared by compression molding. The following quantities were measured using the cone calorimeter: Peak heat release rate, time to ignition, mass loss rate, as well as carbon monoxide and carbon dioxide yields.

5.3 Results and discussion

5.3.1. X-ray diffraction (XRD)

When the crystal structure of a molecular compound is analysed, both the relative positions of the atoms on the molecular repeat units and the arrangement of these segments in the unit cell must be determined. This three-dimensional structure is normally determined using X-ray diffraction, involving the measurement of the positions and intensities of all the diffraction maxima from a single crystal or powder sample. Figure 5.1 shows the XRD patterns of EG and EVA. EG shows an intense peak at a 2θ value of 26.3°, which is attributed to the stacking of single graphene layers [26] at a distance of 0.35 nm (Table 5.1) – no other peak was observed. The EVA in Figure 5.1 shows three different diffraction peaks at $2\theta = 21.2, 23.5, \text{ and } 35.9^\circ$ that

respectively correspond to the (110), (200), and (020) crystallographic planes of an orthorhombic crystalline phase.

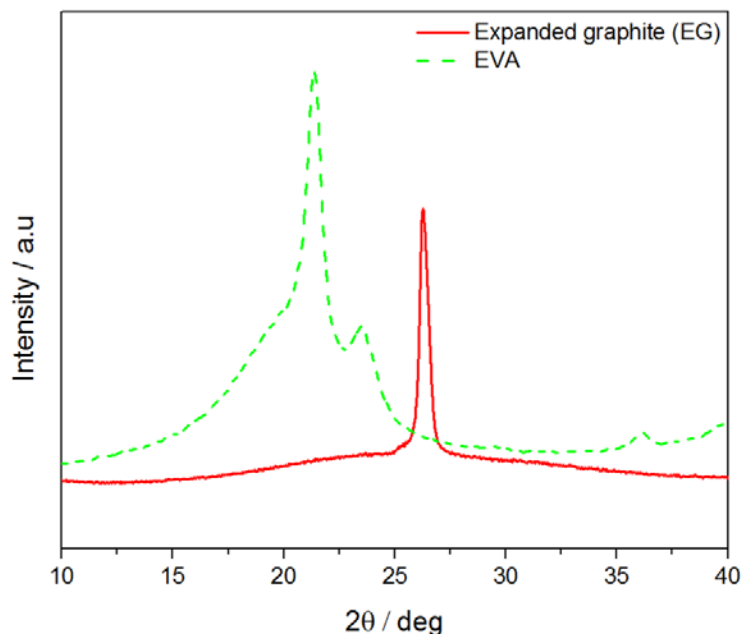


Figure 5.1 X-ray diffractograms of EG and EVA

Figure 5.2 shows the XRD spectra of Cloisite 15A, as well as the EVA/(EG+Cloisite 15A) and EVA/wax/(EG+Cloisite 15A) composites. The Cloisite 15A diffraction peaks in both composites shifted to lower angles compared to those of the original organoclay (Table 5.1 and Figure 5.2), indicating that intercalation of EVA chains into the organoclay layers occurred and separated them. This is because the polar vinyl acetate (VA) groups in the EVA chains interacted with the organic modifier in the clay and penetrated in between the clay platelets [27]. In the case of the wax-containing composites, the shorted wax chains could more easily penetrate in between the clay layers. This would have separated the layers enough to allow more easy penetration of the EVA chains into the layers, increasing the d-spacing of the clay. Similar results were reported for the investigation of clay-containing composites based on a blend of two polymers and a paraffin prepared through melt-mixing [27]. The second peak observed at 4.4 and 4.8° respectively in the EVA/(EG+Cloisite 15A) and EVA/wax/(EG + Cloisite 15A) composites, has been attributed to the presence of clay tactoids [28].

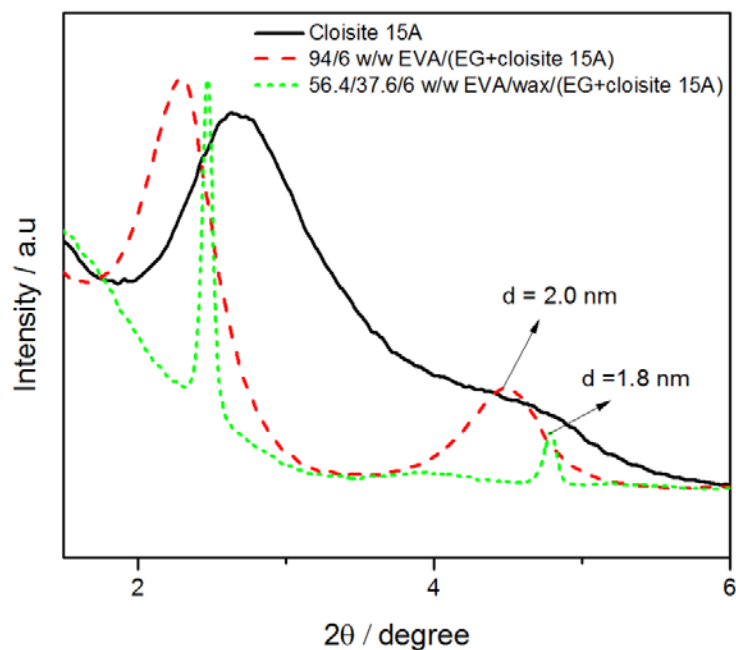


Figure 5.2 X-ray diffractograms of Cloisite 15A, EVA/(EG+Cloisite 15A) and EVA/wax/(EG+Cloisite 15A) at low diffraction angles

Table 5.2 Basal spacings of the clay and EG in the samples

Sample	2θ / deg	d ₀₀₁ / nm
Cloisite 15A	2.7	3.3
56.4/37.6/6 w/w EVA/wax(EG+Cloisite 15A)	2.4	3.6
94/6 w/w EVA/(EG+Cloisite 15A)	2.3	3.8
	2θ / deg	d ₀₀₂ / nm
EG	26.3	0.35
56.4/37.6/6 w/w EVA/wax/EG	26.5	0.35
56.4/37.6/6 w/w EVA/wax/(EG+DAP)	26.6	0.34
56.4/37.6/6 w/w EVA/wax/(EG+Cloisite 15A)	26.7	0.34
94/6 w/w EVA/EG	26.6	0.34
94/6 w/w EVA/(EG+DAP)	26.5	0.35
94/6 w/w EVA/(EG+Cloisite 15A)	26.7	0.34

The average size of the d - or basal spacing (d_{001}), which is the sum of the layer and interlayer distances between the clay platelets in clay powders and nanocomposites, was determined from the 2θ position of the (d_{001}) diffraction peak of each material using Bragg's law (Equation 1) and tabulated in Table 5.2.

$$n\lambda = 2d \sin \theta \quad \text{where } n = 1 \text{ and } \lambda = 1.54056\text{\AA} \quad (1)$$

Pure graphite and the graphite containing composites all show an intense peak at a 2θ values between 26.3 and 26.7° , corresponding to basal spacings around 0.34 - 0.35 nm. Although Figures 5.3 and 5.4 show an observable shift in this diffraction peak, depending on the investigated material, this shift does not translate into significant differences between the d -spacing values, because of the relatively high 2θ value at which the peak appears. There was therefore very little change in the gallery spaces between the EG layers after melt-mixing. This implies that the EVA chains could only enter the spaces between the EG stacks, but not into the graphite inter-planar space. The wax containing composites show a lower diffraction intensities than the non-wax containing samples (compare Figures 5.3 and 5.4), which is an indication that there are more EG aggregates in the composites without wax. It was suggested [29] that the stronger the intensity of the diffraction peak, the higher the degree of graphite stacking and the poorer its dispersion. The wax probably to some extent penetrated in between the EG layers and slightly separated them, giving rise to smaller and better dispersed EG particles. A similar investigation on latex composites [30] showed that the intensity of the diffraction peak at $2\theta = 26.6^\circ$ decreased significantly for composites prepared by latex compounding, which gave rise to better graphite dispersion and exfoliation with less re-stacking, than was the case for samples prepared through melt-mixing.

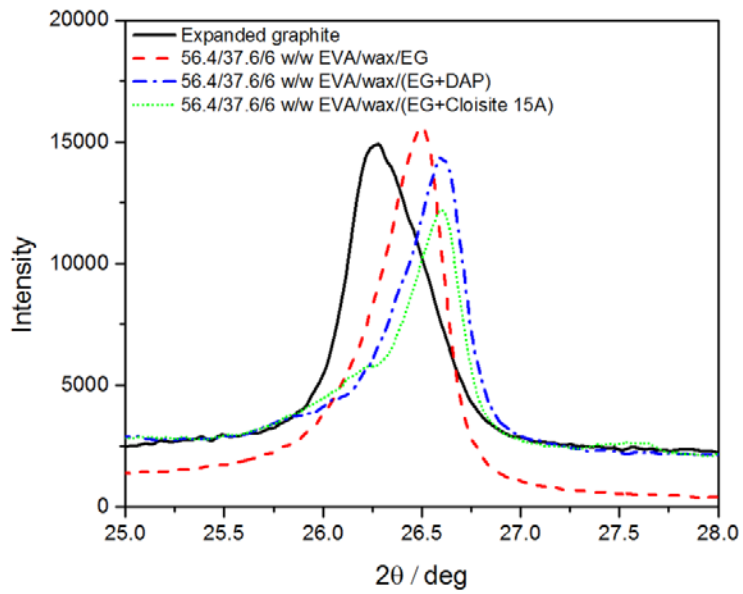


Figure 5.3 X-ray diffractograms showing the EG peak of EG and EG in the EVA/wax composites

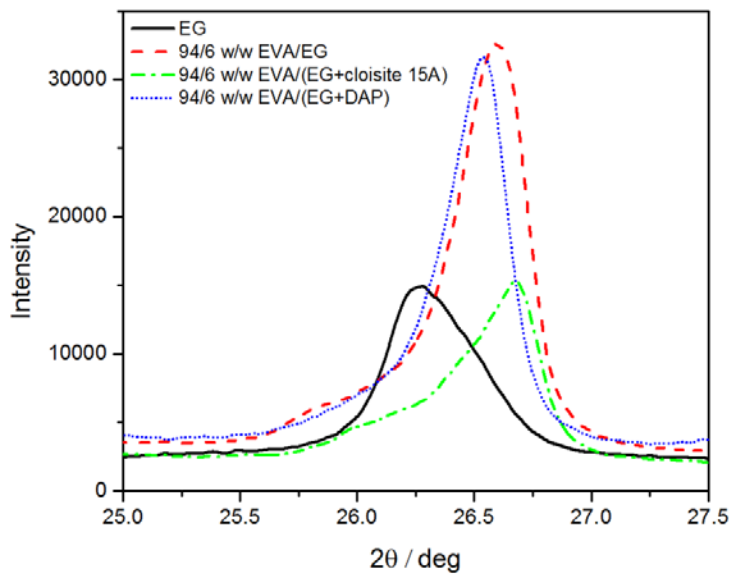


Figure 5.4 X-ray diffractograms showing the EG peak of EG and EG in the EVA composites

5.3.2. Thermal stability

The TGA curves in Figure 5.5 show that EG is thermally stable up to temperatures much higher than the decomposition temperature ranges for clay and DAP. Cloisite 15A shows a mass loss of almost 40% in the temperature range 200-400 °C. This is the result of the decomposition of the intercalated organic ammonium salts by a Hofmann elimination reaction [31]. Diammonium phosphate (DAP) decomposes to ammonia, water, mono-ammonium phosphate, and phosphoric acid in the temperature range 160-300 °C. In the same temperature range the formed phosphoric acid further decomposes to pyrophosphoric acid, which further forms phosphorus pentoxide [32].

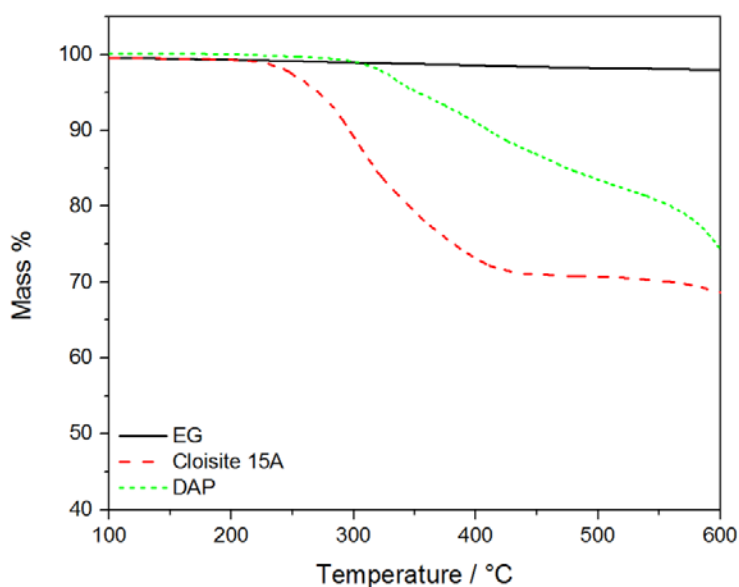


Figure 5.5 TGA curves of EG, DAP and Cloisite 15A

Figure 5.6 shows the TGA curves of EVA, EVA/EG, as well as the EVA/(EG+Cloisite 15A) and EVA/(EG+DAP) composites. All the samples showed a two-step thermal degradation process. The first step, occurring between 300 and 400 °C, corresponds to the loss of acetic acid as a result of the deacetylation of EVA, whilst the second step involves the thermal decomposition of the backbone by further radical scissions [33].

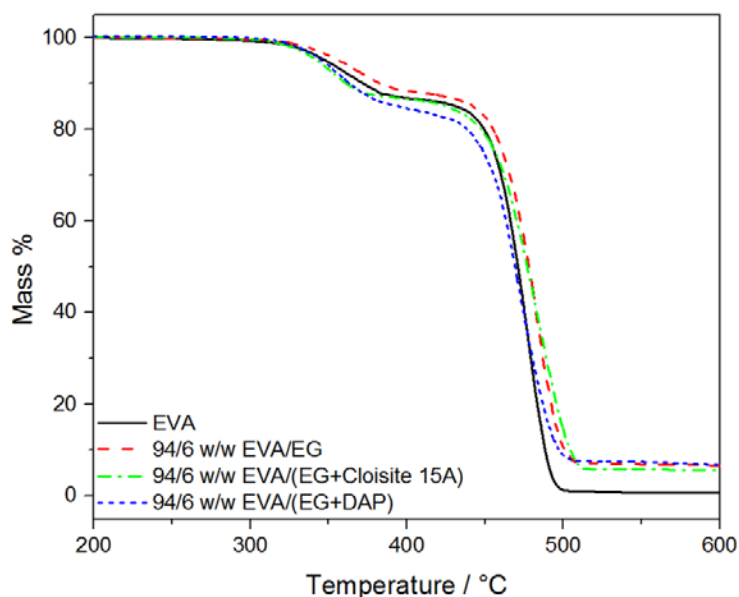


Figure 5.6 TGA curves of neat EVA, EVA/EG as well as EVA/ (EG+Cloisite 15A) and EVA/ (EG+DAP) composites

It is observed in Figure 5.6 and Table 5.3 that EVA/EG has a slightly better thermal stability than EVA/(EG+DAP) and EVA/(EG+Cloisite 15A), although it seems to degrade faster during the second degradation step. Previous investigations showed that the addition of a flame retardant (in this case DAP) reduced the degradation temperature due to the liberation of water in the flame retardant materials, and that the presence of nanoclay accelerated the deacetylation of EVA [23,35]. This was attributed to the products of the decomposition of the alkylammonium cations catalysing the degradation of the polymer matrices [31]. The elimination of the ammonium modifier apparently results in a substitution of the ammonium linkage on the clay with a hydrogen proton due to β -carbon fracture, which acts as a Brønsted acidic site to accelerate the polymer degradation. Ultimately, the α -olefins, by-products, or intermediates produced in this reaction could attack the polymer and promote polymer degradation.

Table 5.3 Degradation temperatures at 10 and 70% mass for all the investigated samples

Sample	T _{10%} (°C)	T _{70%} (°C)
EVA	371.9	478.9
EVA/wax	264.2	466.2
EVA/wax/EG	272.7	476.7
EVA/wax/(EG+Cloisite 15A)	312.2	476.2
EVA/wax/(EG+DAP)	308.2	475.2
EVA/EG	380.0	487.1
EVA/(EG+Cloisite 15A)	362.9	488.9
EVA/(EG+DAP)	362.1	477.0

The influence of EG, and its combination with respectively DAP and clay, on the thermal degradation of a 60/40 w/w EVA/wax blend are shown in Figure 5.7 and the results are tabulated in Table 5.3. All the samples show two degradation steps: the first is attributed to the evaporation of wax combined with the de-acetylation of EVA, and the second to the degradation of the EVA backbone. The degradation temperatures at 10% mass loss are higher for a combination of fillers compared to those for EVA/wax and EVA/wax/EG (Table 5.3), and this shift is also visible in the TGA curves in Figure 5.7. It is possible that the wax volatiles that evaporated before the onset of EVA degradation, interacted in some way with the combined fillers which reduced the rate of its diffusion from the molten sample. This is also clear from the observably smaller mass loss during the first degradation step, which hints at the wax being evaporated at much higher temperatures (in the range of the second degradation step) for the composites containing EG and combined fillers.

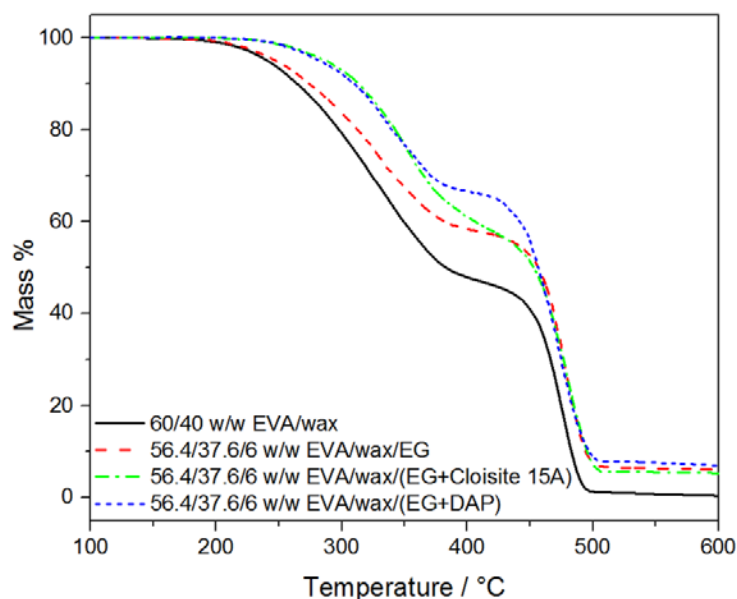


Figure 5.7 TGA curves of 60/40 w/w EVA/wax, EVA/wax/EG as well as EVA/wax/(EG+Cloisite 15A) and EVA/wax/(EG+DAP) composites

5.3.3 Flammability

The peak of heat release rate (PHRR) has been found to be one of the most important parameters to evaluate fire safety [10,14]. EVA/wax has a higher PHRR value than EVA (Table 5.4), which is probably because the highly flammable short wax chains evaporate at an early stage of the combustion and become additional fuel to the fire. The EVA/wax blend shows two HRR peaks (Figure 5.8). The first peak is attributed to the burning of the wax vapours, while the second, larger peak is caused by the heat released as a result of the burning of the polymer. The wax releases heat before the polymer because of a lower pyrolysis temperature. The presence of a combination of EG and Cloisite 15A in EVA/wax shows a considerable decrease in the heights of the heat release rate (HRR) peaks compared to the blends containing EG and its combination with DAP. EG+Cloisite 15A gave rise to a 53% improvement in the flame resistance of the EVA/wax blend, compared to respectively 35% and 25% enhancement in the case of EG and EG+DAP. This observation can be explained by comparing the SEM images of the char residues of the composites in Figure 5.9. The improvement in the flame resistance of the EVA/wax blend in the presence of EG+Cloisite 15A is attributed to the formation of a homogenous, compact, and stable char layer (carbonized ceramic char layer) (Figure 5.9(b)). Such a char layer improves the

flame resistance because it prevents oxygen and heat from entering the system, and flammable gases from diffusing out of the system. Stable and compact char also delays the accumulation of heat in the sample and prevents its further decomposition.

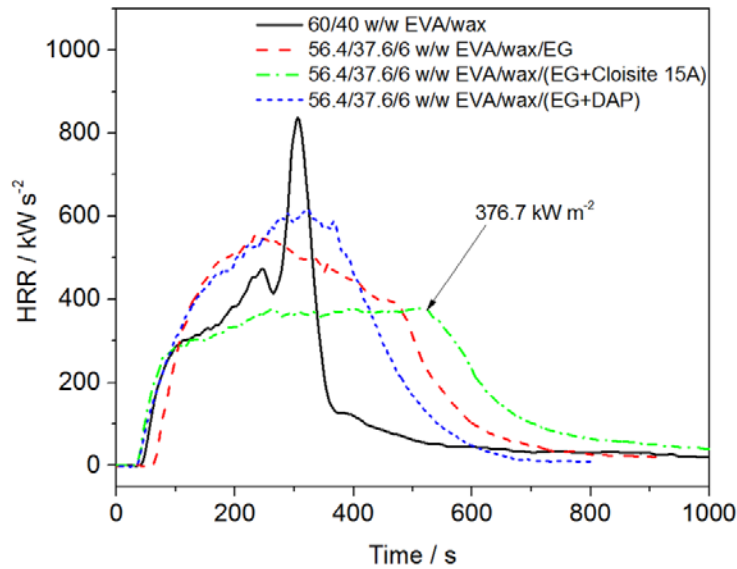


Figure 5.8 Heat release rate curves for the EVA/wax blend, as well as the EVA/wax/EG, EVA/wax/(EG+Cloisite 15A) and EVA/wax/(EG+DAP) composites

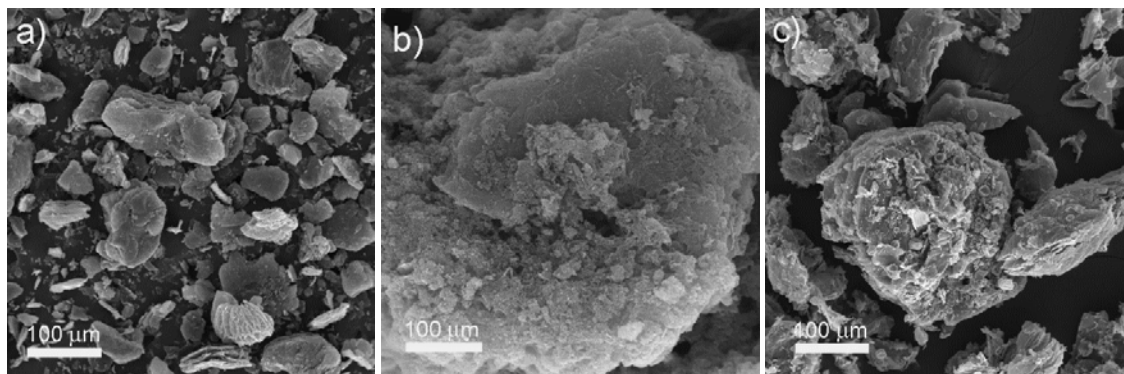


Figure 5.9 SEM images of the a) EVA/wax/EG, b) EVA/wax/(EG+Cloisite 15A), and c) EVA/wax/(EG+DAP) composites

However, in case of the EVA/wax/EG and EVA/wax/(EG+DAP) composites only a slight improvement in flammability is observed, which is attributed to the formation of an inhomogeneous char layer which is more discontinuous and brittle for the EG+DAP containing system (Figure 5.9(c)). Such a char layer would provide poor protection against the entering of

heat and the release of flammable volatiles, thereby leading to poor flame retardance. The EVA/wax/EG composite showed a more compact and stable char layer (Figure 5.9(a)) than the EVA/wax/(EG+DAP) composite, which is the reason why a lower PHRR value is observed for this system. This result suggests a possible anti-synergistic effect between EG and DAP. It seems as if the DAP content was not sufficient to provide a positive influence on the flame retardance. Other research [36] showed that inorganophosphorus flame retardant materials can only provide good flame retardance when their content reaches or exceeds 10 wt.%. Cai and co-workers [11] reported an anti-synergistic effect between EG and zinc borate (ZB) for the flame retardance of form-stable phase change materials based on paraffin/HDPE composites. This was attributed to the formation of a glassy B_2O_3 film coming from the thermal pyrolysis of ZB, which covered the material surface and prevented the expandables to swell into EG. However, EG+APP showed a 21% improvement in the flame retardance of HDPE/paraffin wax blends, which is less than the 34% improvement we observed for our EG+Cloisite 15A in the EVA/wax blends.

It is seen in Table 5.4 that the time to ignition (TTI) of the EVA/wax blend decreased after the addition of DAP and Cloisite 15A. TTI is attributed to a number of factors: homogeneity, chemical composition, rate of decomposition, and presence of impurities [37]. In this case the TTI is governed by the rate of decomposition of the polymer in the sample. DAP and the organic modifier in Cloisite 15A generally degrade at lower temperatures than EVA, which reduces the time to ignition. Because of its lower PHRR, the EVA/wax/(EG+Cloisite 15A) composite also shows a better fire performance index (FPI) value than EVA/wax, EVA/wax/EG and EVA/wax/(EG+DAP). FPI is considered to be the best individual indicator of overall fire hazard, and therefore smaller FPI values are an indication of a smaller fire hazard. The EVA/wax/(EG+Cloisite 15A) composite also shows better fire growth index (FIGRA) than EVA/wax, EVA/wax/EG and EVA/wax/(EG+DAP). FIGRA is calculated as the ratio of PHRR to the time-to-PHRR. EG+Cloisite 15A in the EVA/wax blend showed a 64% improvement in mass loss rate (MLR) compared to a 56% improvement when only EG and a 50% improvement when EG+DAP were added to the blend. The MLR data further support the flame retardant efficiency of EG+Cloisite 15A, which is very important for the practical use of EG+Cloisite 15A as a halogen-free flame retardants.

Table 5.4 Flammability data of the samples used in this study

Samples	PHRR / kW m ⁻²	TTI / S	t(PHRR) / s	FPI / kW m ⁻² s ⁻¹	MLR / g s ⁻¹	FIGRA / kW m ⁻² s ⁻¹
Neat EVA	768 ± 2	98 ± 2	345 ± 7	10.3	0.38 ± 0.06	2.7
60/40 w/w EVA/wax	836 ± 8	47 ± 5	300 ± 7	17.8	0.36 ± 0.07	2.8
56.4/37.6/6 w/w EVA/wax/EG	537 ± 2	68 ± 4	230 ± 7	7.9	0.16 ± 0.02	2.3
56.4/37.6/6 w/w EVA/wax/(EG+Cloisite 15A)	397 ± 2	39 ± 2	465 ± 14	10.2	0.13 ± 0.03	0.9
56.4/37.6/6 w/w EVA/wax/(EG+DAP)	630 ± 1	41 ± 0	320 ± 7	15.4	0.18 ± 0.02	2.0
94/6 w/w EVA/EG	615 ± 7	52 ± 3	275 ± 14	11.8	0.18 ± 1.4	2.2
94/6 w/w EVA/(EG+Cloisite 15A)	357 ± 6	85 ± 1	310 ± 14	4.2	0.12 ± 0.1	1.2
94/6 w/w EVA/(EG+DAP)	714 ± 8	71 ± 4	330 ± 7	10.1	0.19 ± 0.7	2.2

PHRR, TTI, FPI and FIGRA are respectively the peak heat release rate, time to ignition, fire performance index, and fire growth index

Figure 5.10 shows that the PHRR values for the non-wax containing samples decrease in order of EVA > EVA/(EG+DAP) > EVA/EG > EVA/(EG+Cloisite 15A). The reason for this is also that, because of the more stable and compact char layer formed in the case of EVA/(EG+Cloisite 15A) (Figure 5.11), there was less penetration of heat, oxygen and flammable volatiles, giving rise to a much better flame retardance effect. This stronger improvement in flame resistance is further supported by the decrease in mass loss rate (MLR), fire index properties (FPI), and fire growth index (FIGRA) values (Table 5.4). The presence of wax in EVA/EG and EVA/(EG+DAP) gave rise to lower PHRR values (Table 5.4). It seems as if the low molecular weight wax contributed to a better dispersion of EG in the EVA matrix, probably because the wax penetrated in between the EG layers and separated the layers, giving rise to smaller and better dispersed EG particles. The PHRR values for EVA/(EG+Cloisite 15A) and EVA/wax/(EG+Cloisite 15A) are very similar, probably because EG+Cloisite 15A is already a

very effective flame retardant, and therefore the presence of wax did not further improve its effect. Generally, the presence of wax in the composites reduced the time to ignition (TTI) (Table 5.4), probably because of the lower pyrolysis temperature of the wax compared to that of EVA. The HRR curves of EVA/wax/(EG+Cloisite 15A) and EVA/(EG+Cloisite 15A) also show a second peak with HRR values of 377 and 320 kW m⁻². This peak is due to the gradual degradation of the protective layer as the sample is continuously exposed to heat, and the formation of a new protective char [16].

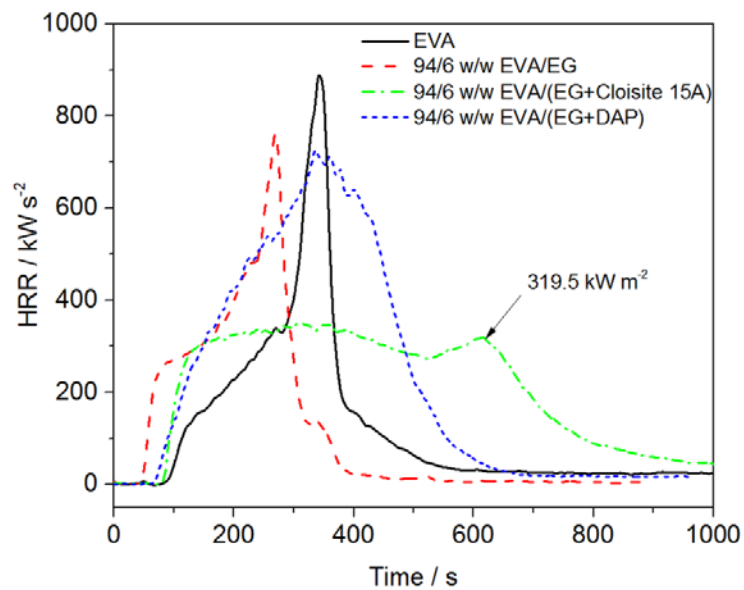


Figure 5.10 Heat release rate curves for EVA, as well as the EVA/EG, EVA/(EG+Cloisite 15A) and EVA/(EG+DAP) composites

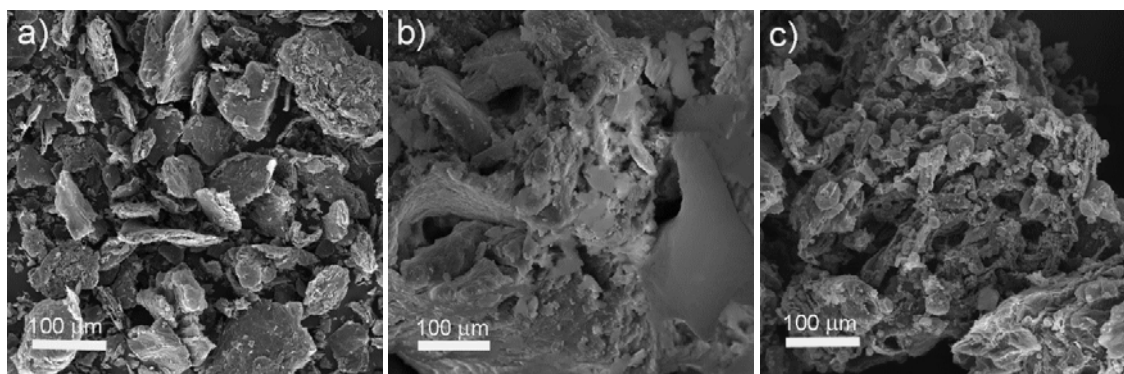


Figure 5.11 SEM images of the char layers of a) 94/6 w/w EVA/EG, b) 94/6 w/w EVA/(EG+Cloisite 15A), and c) 94/6 w/w EVA/(EG+DAP) composites

The emission of toxic gases is considered as an important parameter for the flame retardant materials. The production of carbon monoxide and carbon dioxide as function of burning time are shown in Figures 5.12 and 5.13. These results confirm that the synergistic effect of EG and Cloisite 15A significantly reduced the amounts of CO and CO₂ produced by both EVA and the EVA/wax blend, compared to EG and EG+DAP. This is attributed to the formation of a more effective carbonized ceramic protective surface layer, which will delay the penetration of heat and oxygen into the materials, and the release of flammable decomposition products from the materials. It was shown before that an effective char layer enhanced the strength of intumescent chars and prevented the collapse of the charred structure [38].

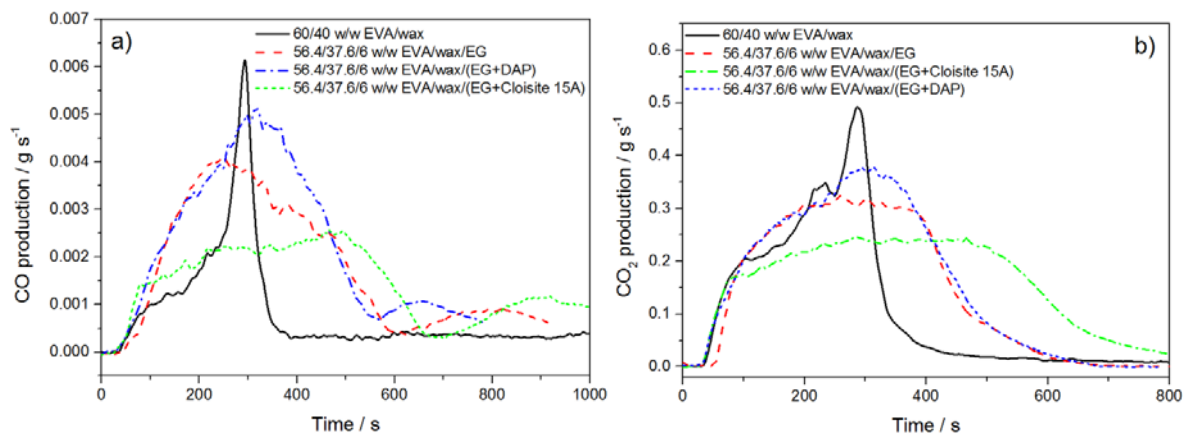


Figure 5.12 a) Carbon monoxide and b) carbon dioxide production plots of EVA/wax blend, EVA/wax/EG, EVA/wax/(EG+Cloisite 15A) and EVA/wax/(EG+DAP) composites

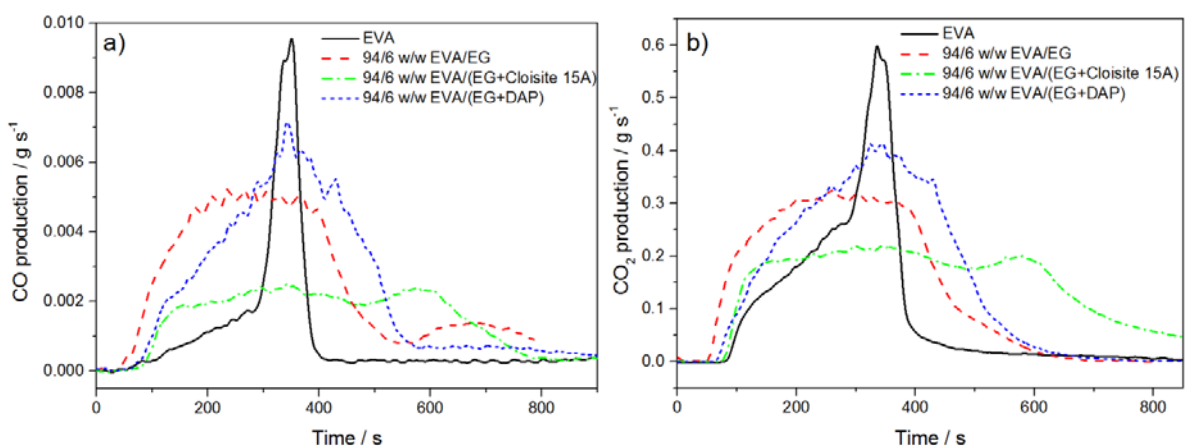


Figure 5.13 a) Carbon monoxide and b) carbon dioxide production plots of EVA, EVA/EG, EVA/(EG+Cloisite 15A) and EVA/(EG+DAP) composites

5.4 Conclusions

EVA and EVA/wax blends were melt-blended with EG, EG+Cloisite 15A and EG+DAP. Investigation of the char residues showed the formation of a more dense and stable char layer for the samples containing EG+Cloisite 15A after exposed to cone calorimetry analysis. The flammability results confirmed much better flame resistance of these composites, which was due to the dense char layer forming a more effective barrier against the penetration of oxygen and heat, and the release of flammable volatiles. The EG and EG+DAP were not so effective, and the reason for this was the formation of much more brittle and porous char layers. This is unexpected for an intumescent flame retardant like DAP, but the reason in this case could be that not enough DAP was mixed into EVA and the EVA/wax blend, which would reduce its effectiveness. An X-ray diffraction investigation of the composites showed a slight increase in d-spacing in the case of clay, but little change in the EG structure. EVA therefore penetrated the clay layers, and this became more efficient when wax was present in the composite. The thermal stability of EVA and EVA/wax generally improved in the presence of EG and its combination with Cloisite 15A and DAP.

5.5 References

1. A. Sharma, V.V. Tyagi, C.R. Chen, D. Buddhi. Review on thermal energy storage with phase change materials and applications. *Renewable and Sustainable Energy Reviews* 2009; 13:318-345.
DOI: 10.1016/rser.2007.10.005
2. G. Chigwada, P. Jash, D.D Jiang, C.A. Wilkie. Synergy between nanocomposite formation and low levels of bromine on fire retardancy in polystyrenes. *Polymer Degradation and Stability* 2005; 88:382-393.
DOI: 10.1016/polymdegradstab.2004.12.002
3. I. Finberg, Y.B. Yaakov, P. Georlette. New flame retardant systems for styrenic plastics and method of preparation. *Polymer Degradation and Stability* 1999; 64:465-470.
DOI: 10.1016/S0141-3910(98)00138-4

4. A.D.L. Risa, A. Recca, J.T. Carter, P.T. McGrail. An oxygen index evaluation of flammability on modified epoxy/polyester systems. *Polymer* 1999; 40:4093-4098.
DOI: 10.1016/S0032-3861(98)00646-6
5. G. Chen. In situ thermal condensation of glucose-diammonium phosphate in wood for fire and fungal decay protection. *Wood and Fiber Science* 2009; 41:105-116.
6. S. Gaan, G. Sun. Effect of phosphorus flame retardants on thermo-oxidative decomposition of cotton. *Polymer Degradation and Stability* 2007; 92:968-974.
DOI: 10.1016/polymdegradstab.2007.03.009
7. C. Reti, M. Casetta, S. Duquesne, S. Bourbigot, R. Delobel. Flammability properties of intumescent PLA including starch and lignin. *Polymers for Advanced Technologies* 2008; 19:628-635.
DOI: 10.1002/pat.1130
8. B. ScharTEL, U. Braun, U. Schwarz, S. Reinemann. Fire retardancy of polypropylene/flax blends. *Polymer* 2003; 44:6241-6250.
DOI: 10.1016/S0032-3861(03)00692-X
9. M. Sain, S.H. Park, F. Suhara, S. Law. Flame retardant and mechanical properties of natural fibre-PP composites containing magnesium hydroxide. *Polymer Degradation and Stability* 2004; 83:363-367.
DOI: 10.1016/S0141-3910(03)00280-5
10. Y. Cai, Q. Wei, F. Huang, S. Lin, F. Chen, W. Gao. Thermal stability, latent heat and flame retardant properties of the thermal energy storage phase change materials based on paraffin/high density polyethylene composites. *Renewable Energy* 2009; 34:2117-2123.
DOI: 10.1016/j.renene.2009.01.017
11. Y. Cai, Q. Wei, F. Huang, F. Chen, W. Gao. Preparation and properties studies of halogen-free flame retardant form-stable phase change materials based on paraffin/high density polyethylene composites. *Applied Energy* 2008; 85:765-775.
DOI: 10.1016/j.apenergy.2007.10.017
12. L. Gao, G. Zheng, Y. Zhou, L. Hu, G. Feng, M. Zhang. Synergistic effect of expandable graphite, diethyl ethylphosphonate and organically-modified layered double hydroxide on flame retardancy and fire behavior of polyisocyanurate-polyurethane foam nanocomposite. *Polymer Degradation and Stability* 2014; 101:92-101.

- DOI: 10.1016/j.polymdegradstab.2013.12.025
13. X. Su, Y. Yi, J. Tao, H. Qi. Synergistic effect of zinc hydroxystannate with intumescent flame-retardants on fire retardancy and thermal behavior of polypropylene. *Polymer Degradation and Stability* 2012; 97:2128-2135.
DOI: 10.1016/polymdegradstab.2012.08.017
 14. P. Zhang, L. Song, H. Lu, J. Wang, Y. Hu. The influence of expanded graphite on thermal properties for paraffin/high density polyethylene/chlorinated paraffin/antimony trioxide as a flame retardant phase change material. *Energy Conversion and Management* 2010; 51:2733-2737.
DOI: 10.1016/j.enconmann.2010.06.009
 15. G. Bai, C. Guo, L. Li. Synergistic effect of intumescent flame retardant and expandable graphite on mechanical and flame-retardant properties of wood flour-polypropylene composites. *Construction and Building Materials* 2014; 50:148-153.
DOI: 10.1016/conbuilmat.2013.09.028
 16. X.F. Wu, L.C. Wang, C. Wu, J.H. Yu, G.L. Wang. Influence of char residues on flammability of EVA/EG, EVA/NG, and EVA/GO composites. *Polymer Degradation and Stability* 2012; 97:54-63.
DOI: 10.1016/j.polymdegradstab.2011.10.011
 17. J.W. Gilman. Flammability and thermal stability studies of polymer layered-silicate (clay) nanocomposites. *Applied Clay Science* 1999; 15:31-49.
DOI: 10.1016/S0169-1317(99)00019-8
 18. A. Fina, H.C.L. Abbenhuis, D. Tabuani, A. Frache, G. Camino. Polypropylene metal functionalized POSS nanocomposites: A study by thermogravimetric analysis. *Polymer Degradation and Stability* 2006; 91:1064-1070.
DOI: 10.1016/j.polymdegradstab.2005.07.013
 19. T. Kashiwagi, E. Grulke, J. Hilding, K. Groth, R. Harris, K. Butler. Thermal and flammability properties of polypropylene/carbon nanotube nanocomposites. *Polymer* 2004; 45:4227-4239.
DOI: 10.1016/j.polymer.2004.03.088

20. J. Zhang, J. Hereid, M. Hagen, D. Bakirtzis, M.A. Delichatsios, A. Fina, A. Castrovinci, G. Camino, F. Samyn, S. Bourbigot. Effects of nanoclay and fire retardants on fire retardancy of polymer blend of EVA and LDPE. *Fire Safety Journal* 2009; 44:504-513.
DOI: 10.1016/j.firesaf.2008.10.005
21. C. Nyambo, E. Kanadare, D. Wang, C. Wilkie. Flame-retarded polystyrene: Investigating chemical interactions between ammonium polyphosphate and MgAl layered double hydroxide. *Polymer Degradation and Stability* 2008; 93:1656-1663.
DOI: 10.1016/j.polymdegradstab.2008.05.029
22. S. Pack, M. Si, J. Koo, J.C. Sokolov, T. Koga, T. Kashiwagi, M.H. Rafailovich. Mode-of-action of self-extinguishing polymer blends containing organoclays. *Polymer Degradation and Stability* 2009; 94:306-326.
DOI: 10.1016/j.polymdegradstab.2008.12.008
23. A.B. Morgan. Flame retarded polymer layered silicate nanocomposites: A review of commercial and open literature systems. *Polymers for Advanced Technologies* 2006; 17:206-217.
DOI: 10.1002/pat.685
24. R.L. Acosta, S.S. Valdes, E.R. Vargas, L.F.R. DeValle, A.B.E. Martinez, O.S.R. Fernandez, T.L. Ramirez, P.G. Lafleur. Effect of amino alcohol functionalized polyethylene as compatibilizer for LDPE/EVA/clay flame-retardant nanocomposites. *Materials Chemistry and Physics* 2014; 146:437-445.
DOI: 10.1016/j.matchemphys.2014.03.050
25. M. Liu, X. Zhang, M. Zammarano, J.W. Gilman, T. Kashiwagi. Flame retardancy of poly(styrene-co-acrylonitrile) by the synergistic interaction between clay and phosphomolybdate hydrates. *Polymer Degradation and Stability* 2011; 96:1000-1008.
DOI: 10.1016/j.polymdegradstab.2011.01.015
26. M. Murariu, A.L. Dechief, L. Bonnaud, Y. Paint, A. Gallos, G. Fontaine, S. Bourbigot, P. Dubois. The production and properties of polylactide composites filled with expanded graphite. *Polymer Degradation and Stability* 2010; 95:889-900.
DOI: 10.1016/j.polymdegrads.2009.12.019
27. Y. Cai, L. Song, Q. He, D. Yang, Y. Hu. Preparation, thermal and flammability properties of a novel form-stable phase change materials based on high density polyethylene/

- poly(ethylene-co-vinylacetate)/organophilic montmorillonite nanocomposites/paraffin compounds. *Energy Conversion and Management* 2008; 49:2055-2062.
DOI: 10.1016/j.enconman.2008.02.013
28. K. Fukushima, M. Murariu, G. Camino, P. Dubois. Effect of expanded graphite/layered-silicate clay on thermal, mechanical and fire retardant properties of poly(lactic acid). *Polymer Degradation and Stability* 2010; 95:1063-1076.
DOI: 10.1016/j.polymdegradstab.2010.02.029
29. L. Wang, L. Zhang, M. Tian. Improved polyvinylpyrrolidone (PVP)/graphite nanocomposites by solution compounding and spray drying. *Polymers for Advanced Technologies* 2011; 23:652-659.
DOI: 10.1002/pat.1940
30. L. Wang, L. Zhang, M. Tian. Effect of expanded graphite (EG) dispersion on the mechanical and tribological properties of nitrile rubber/EG composites. *Wear* 2012; 276-277:85-93.
DOI: 10.1010/j.wear.2011.12.009
31. X. Xu, Y. Ding, Z. Qian, F. Wang, B. Wen, H. Zhou, S. Zhang, M. Yang. Degradation of poly(ethylene terephthalate)/clay nanocomposites during melt extrusion: Effect of clay catalysis and chain extension. *Polymer Degradation and Stability* 2009; 94:113–123.
DOI: 10.1016/j.polymdegradstab.2008.09.009
32. C. Branca, C.D. Blasi. Semi-global mechanisms for the oxidation of diammonium phosphate impregnated wood. *Journal of Analytical and Applied Pyrolysis* 2011; 91:97-104.
DOI: 10.1016/j.jaap.2011.01.008
33. M.C. Costache, D.D. Jiang, C.A. Wilkie. Thermal degradation of ethylene-vinyl acetate copolymer nanocomposites. *Polymer* 2005; 46:6947-6958.
DOI: 10.1016/j.polymer.2005.05.084
34. C.L. Deng, S.L. Du, J. Zhao, Z.Q. Shen, C. Deng. An intumescent flame retardant polypropylene system with simultaneously improved flame retardancy and water resistance. *Polymer Degradation and Stability* 2014; 108:97-107.
DOI: 10.1016/j.polymdegradstab.2014.06.008

35. X. Chen, C. Jiao. Synergistic effects of hydroxy silicone oil on intumescent flame retardant polypropylene system. *Journal of Polymer Research* 2009; 16:537-543.
DOI: 10.1007/s10965-9257-4
36. W. Zhang, X. He, T. Song, Q. Jiao, R. Jang. The influence of the phosphorus-based flame retardant on the flame retardancy of the epoxy resins. *Polymer Degradation and Stability* 2014; 109:209-217.
DOI: 10.1016/j.polymdegradsta.2014.07.023
37. M. Lewin. Flame retarding polymer nanocomposites: Synergism, cooperation, antagonism. *Polymer Degradation and Stability* 2011; 96:256-269.
DOI: 10.1016/j.polymdegradstab.2010.12.006
38. Z.B. Shao, C. Deng, Y. Tan, M.J. Chen, L. Chen, Y.Z. Wang. Flame retardation of polypropylene via a novel intumescent flame retardant: Ethylenediamine-modified ammonium polyphosphate. *Polymer Degradation and Stability* 2014; 106:88-96.
DOI: 10.1016/j.polymdegradstab.2013.10.005

Chapter 6

Conclusions

The study investigated phase change materials based on polyolefins (EVA and PP) blended with wax and mixed with expanded graphite (EG) with the aim of enhancing both the thermal conductivity and flame resistance of the shape-stabilized PCMs.

The results showed that the addition of EG in the neat matrices and in the blends improved the flammability resistance and thermal conductivity, with these properties further improving in the presence of wax. The improvement in the presence of wax is especially interesting, and was attributed to the low molecular weight wax contributing to a better dispersion of EG in the PP and EVA matrices. The wax penetrates in between the EG layers and separates the layers, giving rise to smaller and better dispersed EG particles.

It was further found that the presence of EG alone was not sufficient to achieve an acceptable level of flame retardancy. We investigated the synergistic effect of EG and clay, as well as EG and diammonium phosphate (DAP), on the flammability of EVA/wax blends. The flammability results confirmed much better flammability resistance for EG +Cloisite 15A than EG alone and its combination with DAP, which was due to the dense char layers forming a more effective barrier against the penetration of oxygen and heat, and the release of flammable volatiles. The EG and EG+DAP were not so effective, and the reason for this was the formation of much more brittle and porous char layers.

The results further showed that the wax acted as a plasticizer in PP and EVA. This was evidenced by (a) a decrease in the melting point of EVA in the blends and composites with an increase in wax content, and b) higher storage moduli for neat PP and the PP/EG composite than for the PP/wax/EG composites. In the case of the EVA based samples the storage modulus results showed a reinforcing effect of the graphite and an immobilization of the EVA chains by the highly crystalline wax in the different investigated samples. This was evident in an increase in the storage modulus of the EVA/wax blend, as well as the EVA/EG and EVA/wax/EG composites, compared to that of pure EVA.

The impact strength of the EVA/wax/EG composites decreased with increasing wax and graphite contents because of the rigidity of EG and the brittleness of the wax. However, the impact strength of the PP/wax/EG composites increased in the presence of and with increasing expanded graphite content in all the investigated samples. In this case it was concluded that the wax on the EG surface improved the interaction between the EG and the PP, giving rise to a good dispersion and effective stress transfer. The tensile modulus and mechanical properties of the EVA/wax/EG composites were better than those of the EVA/EG composites because of the smaller and more well dispersed EG when wax was present in the blends, and because of the more rigid wax crystals.

Recommendations for future work:

- To investigate flammability properties of shape-stabilized phase change materials with a high content of DAP in combination with EG, in order to see if the unacceptable results observed in this study were the result of too low DAP contents.
- To investigate the degradation mechanism of the polymer/wax blends.
- To study the flammability properties of shape-stabilized phase change materials with other flame retardant materials such as zeolites, organo-boron siloxane, and some traditional metal oxides and metal compounds.

ACKNOWLEDGEMENTS

The preparation of this thesis would not have been possible without the will of the Almighty God and the support, hard work and endless efforts of a large number of individuals and institutions.

I would like to thank my supervisor, **Prof. Adriaan Stephanus Luyt**, for his great efforts to explain things clearly and simply, and his guidance during my research. I express my deep sense of gratitude for his guidance, cloudless source of inspiration and constant support all through the course of the study. Throughout my thesis-writing period, he provided encouragement, sound advice, good teaching, good company, and lots of good ideas. His overly enthusiasm and integral view on research and his mission for providing 'only high-quality work and not less', has made a deep impression on me. I owe him lots of gratitude for having shown me this way of research. He could not even realize how much I have learned from him.

I acknowledge the University of the Free State at large by providing me with an opportunity to study.

I am grateful to the Faculty programme secretary and programme officer, Mrs Marlize Jackson for her unself-centred service rendered.

The credit must be given to my **Parents** (The late Mr. Samuel Mochane and Mrs Elizabeth Mochane) for raising with their love, guidance, support, responsibility and a lot encouragement.

Sense of gratitude to all my fellow polymer science research group and former colleagues: Mr. Mfiso Mngomezulu, Dr. Duško Dudić, Dr. Tshwafo Motaung, Ms. Julia Puseletso Mofokeng, Dr. Thabang Hendrica Mokhothu, Ms. T.A. Makhetha, Mr. Teboho Motsoeneng. Mr. Teboho Mokhena, Ms. Motshabi Sibeko, Mr. Tladi Mofokeng, Ms. Zanele Clarke, Mr. Tsietsi Tsotetsi, Ms. Mamohano Molaba, Dr. Nomampondomise Molefe and Neo Moji, Mr. Shale Sefadi, Mr. Kgotso Mpitso, Mr. Tyson Mosoabisane for all their help, support, interest and valuable inputs. To Ms. T.P. Gumede thank you very much for your help throughout the whole research.

I would like to take this opportunity to thank **Ms. TP Molaba** for her patience and understanding during the demanding year of 2014.

All sense of gratitude to my siblings Elias Mochane, Monyatsi Mochane, Mokgethi Mochane, Ntswaki Mochane, and Nthloro Mochane.

I wish to thank greatly my best friends, Motsope Ben Mofokeng, Teboho Motsoeneng, Dr. Essa Ahmad, and Teboho Mokhena for helping me get through the tough times, and for all the good ideas shared.

Appendix A

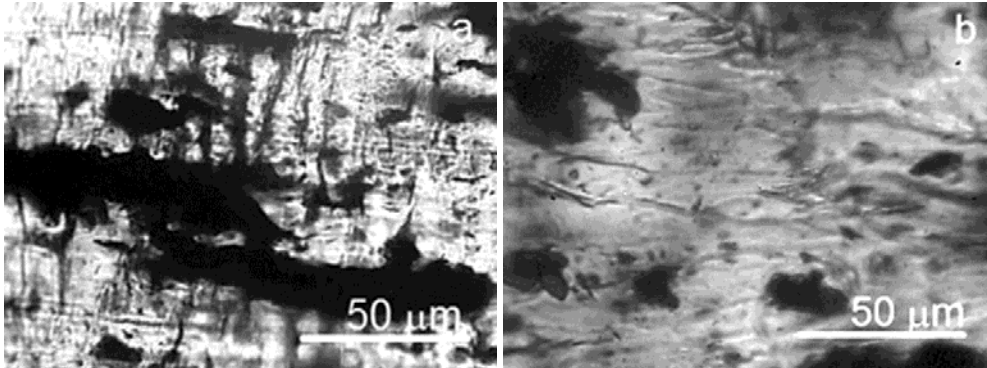


Figure A.1 Optical microscopy images of (a) 94/6 w/w PP/EG, and (b) 65.8/28.2/6 w/w PP/wax/EG

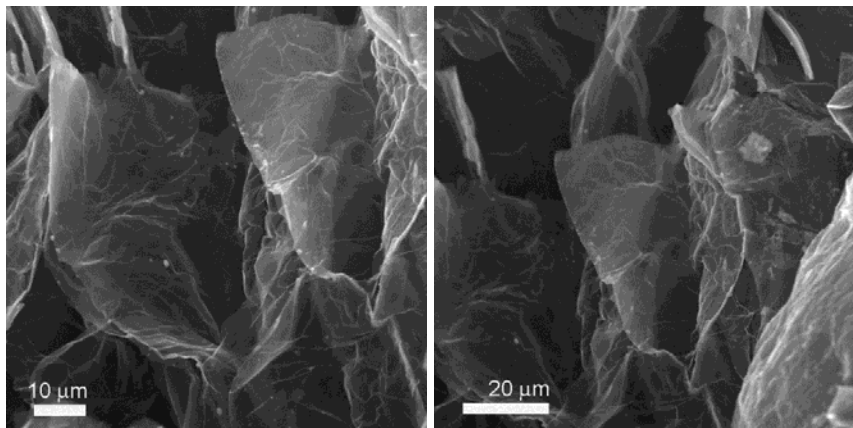


Figure A.2 SEM pictures of expanded graphite

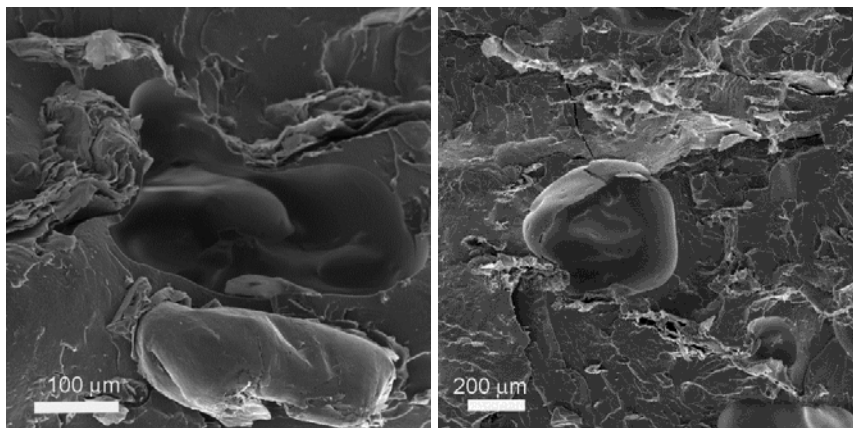


Figure A.3 SEM pictures of the 94/6 w/w EVA/EG composite

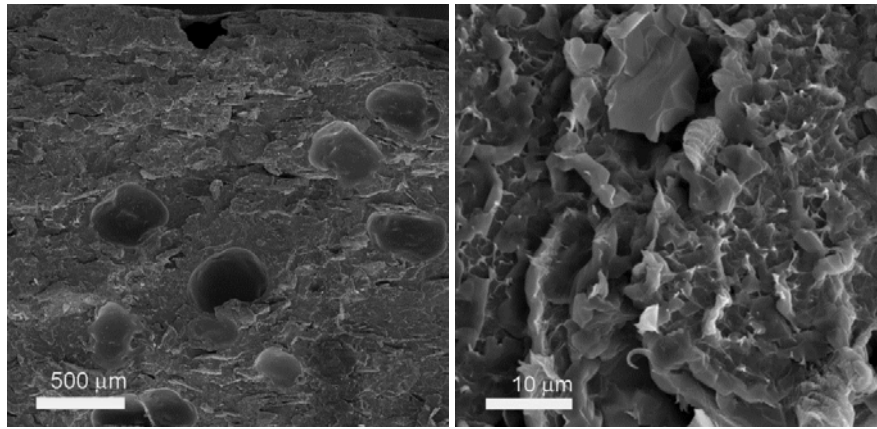


Figure A.4 SEM pictures of the 65.8/28.2/6 w/w EVA/wax/EG composite

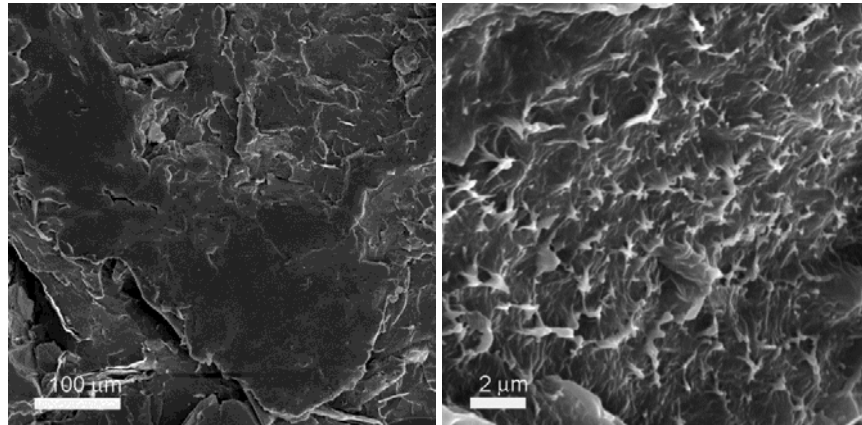


Figure A.5 SEM pictures of the 56.4/37.6/6 w/w EVA/wax/EG composite

Appendix B

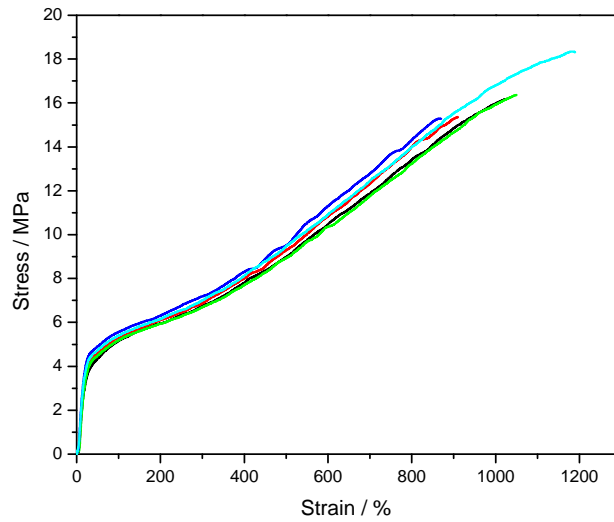


Figure B.1 Stress-strain curves of neat EVA

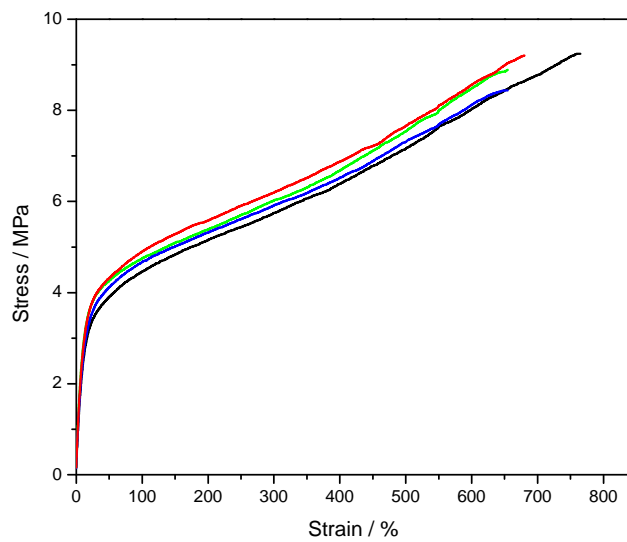


Figure B.2 Stress-strain curves of the 97/3 w/w EVA/EG composite

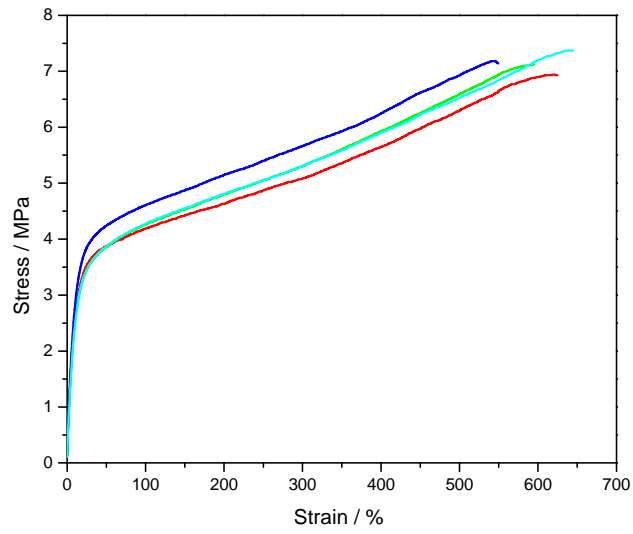


Figure B.3 Stress-strain curves of the 94/6 w/w EVA/EG composite

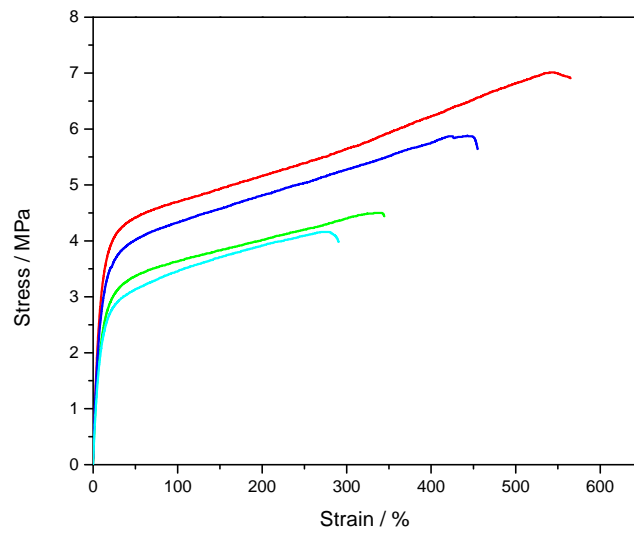


Figure B.4 Stress-strain curves of the 91/9 w/w EVA/EG composite

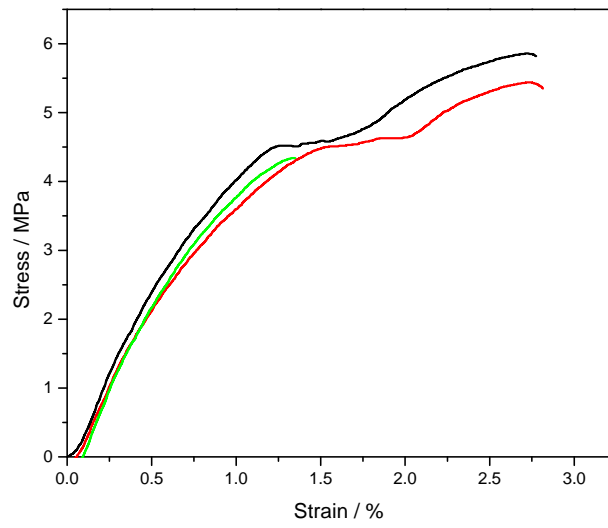


Figure B.5 Stress-strain curves of the 63.7/27.3/9 w/w EVA/wax/EG composite

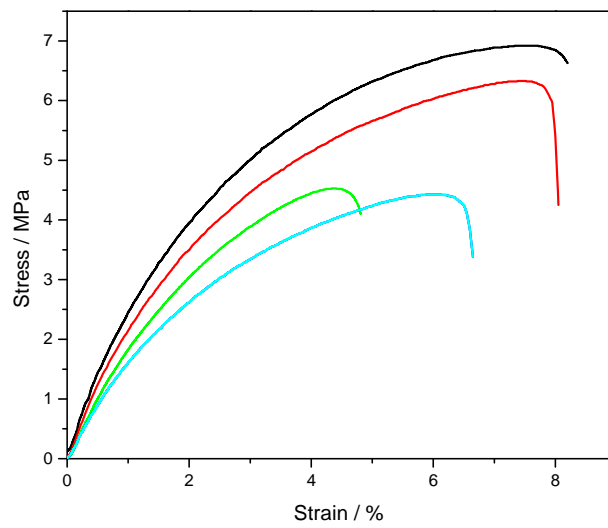


Figure B.6 Stress-strain curves of the the 58.2/38.8/3 w/w EVA/wax/EG composite

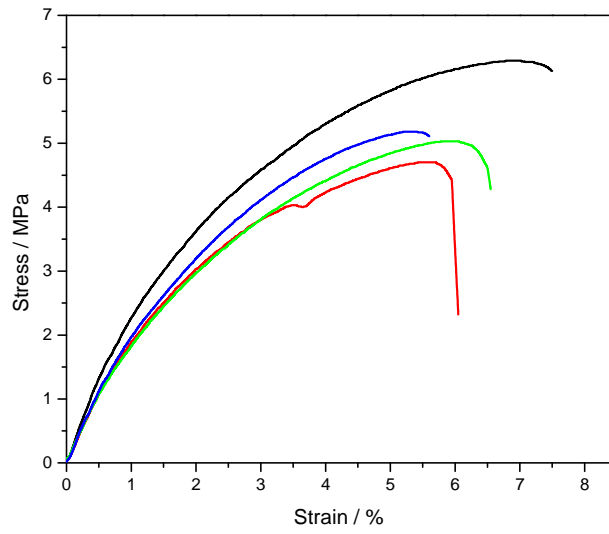


Figure B.7 Stress-strain curves of the 56.4/37.6/6 w/w EVA/wax/EG composite

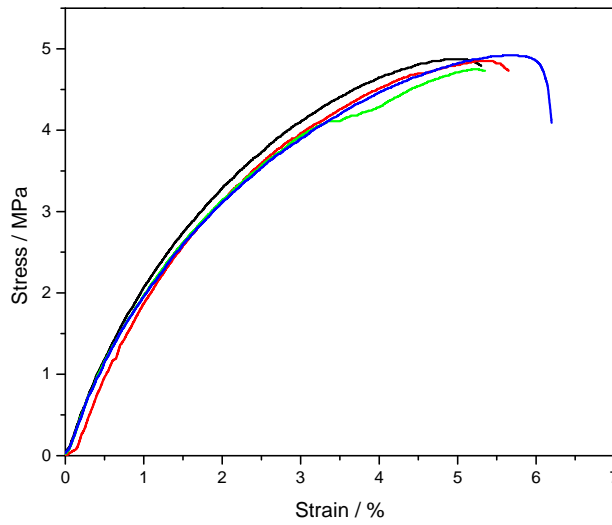


Figure B.8 Stress-strain curves of the 56.4/37.6/6 w/w EVA/wax/EG composite

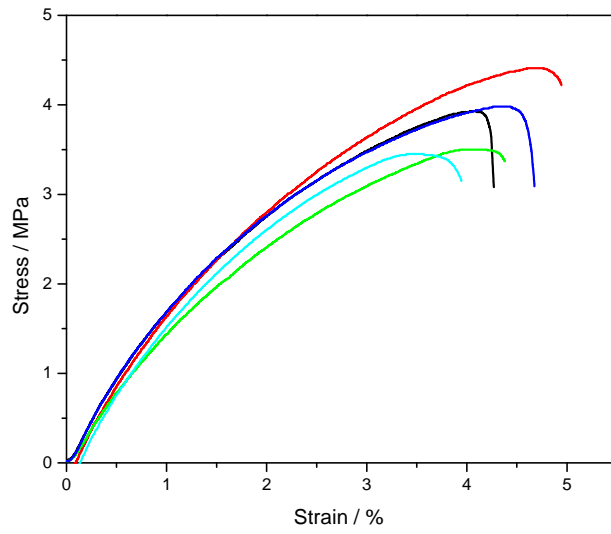


Figure B.8 Stress-strain curves of the 48.5/48.5/3 w/w EVA/wax/EG composite

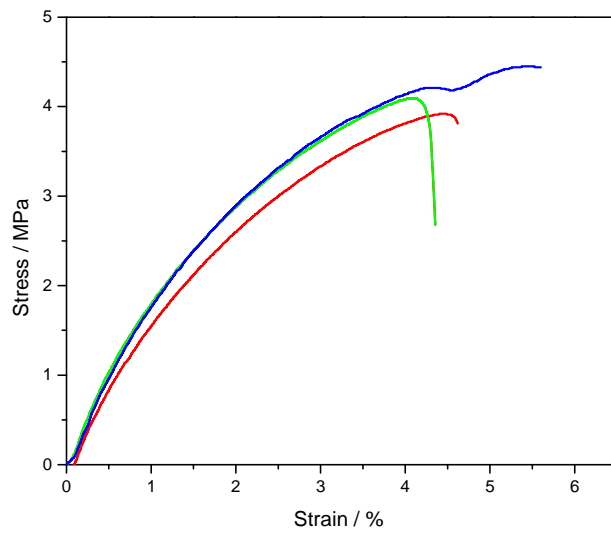


Figure B.8 Stress-strain curves of the 47/47/6 w/w EVA/wax/EG composite

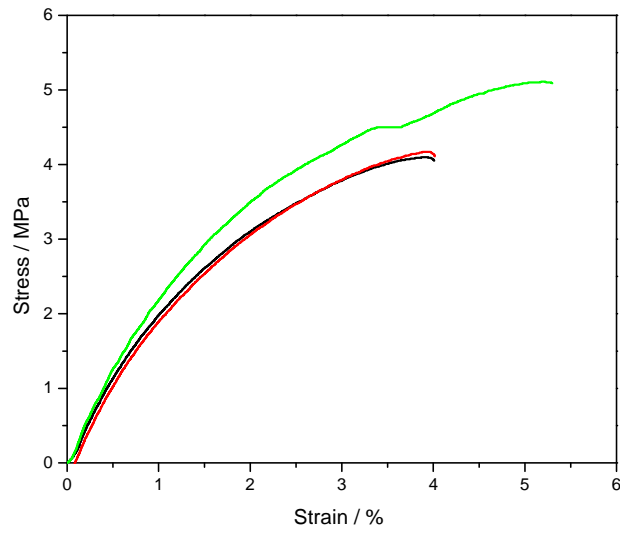


Figure B.9 Stress-strain curves of the 48.5/48.5/9 w/w EVA/wax/EG composite

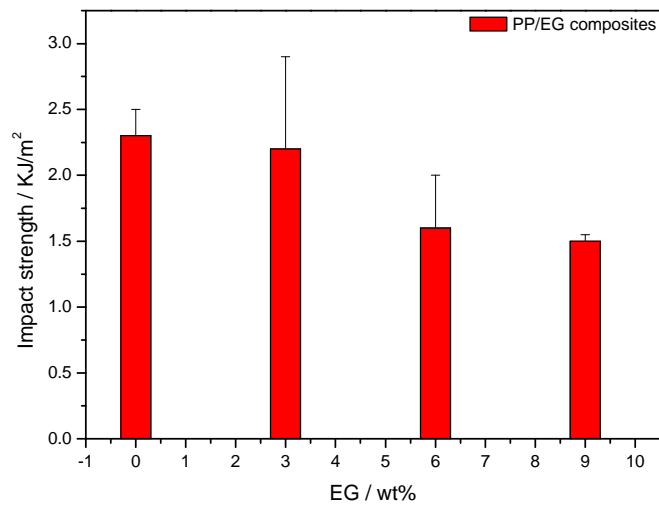


Figure B.10 Impact strengths of PP and its EG composites

Appendix C

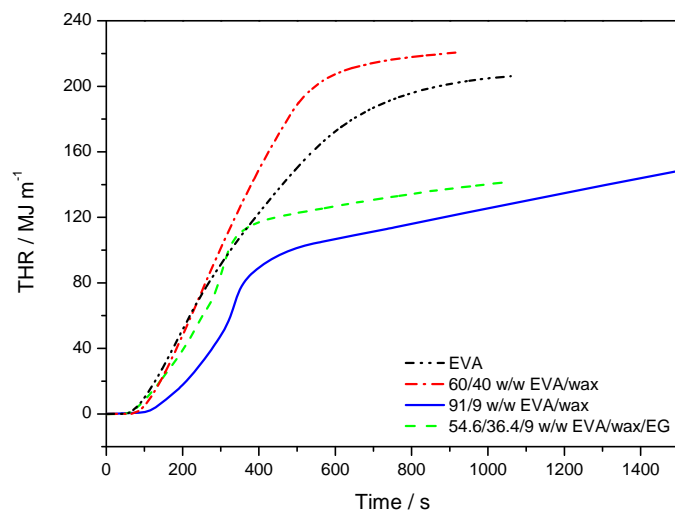


Figure C.1 THR curves of neat EVA, the EVA/wax blend, and the EVA/EG and EVA/wax/EG composites

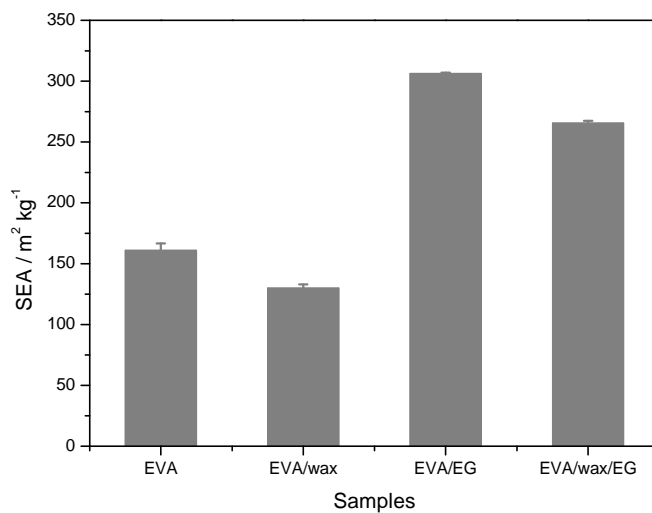


Figure C.2 SEA plots of neat EVA, the 60/40 w/w EVA/wax blend, and the 91/9 w/w EVA/EG and 54.6/36.4/9 w/w EVA/wax/EG composites

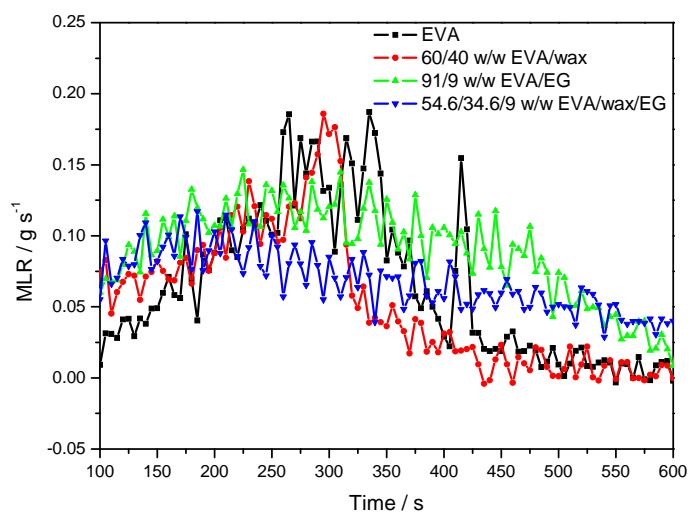


Figure C.3 MLR plots of neat EVA, the 60/40 w/w EVA/wax blend, and the 91/9 w/w EVA/EG and 54.6/36.4/9 w/w EVA/wax/EG composites

Appendix D

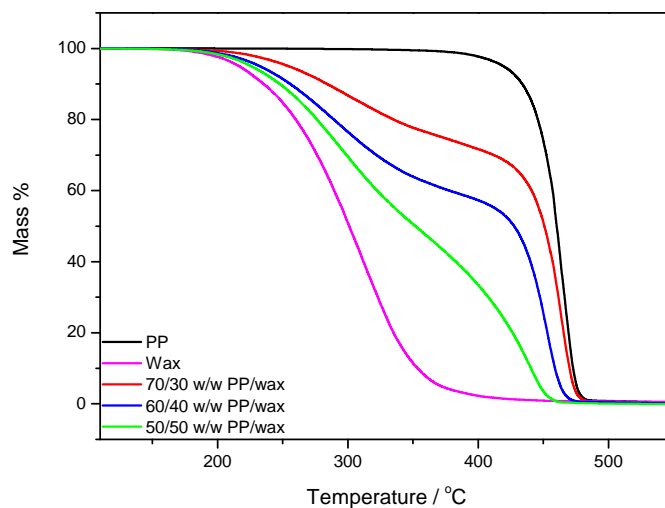


Figure D.1 TGA curves of the EVA/wax blends

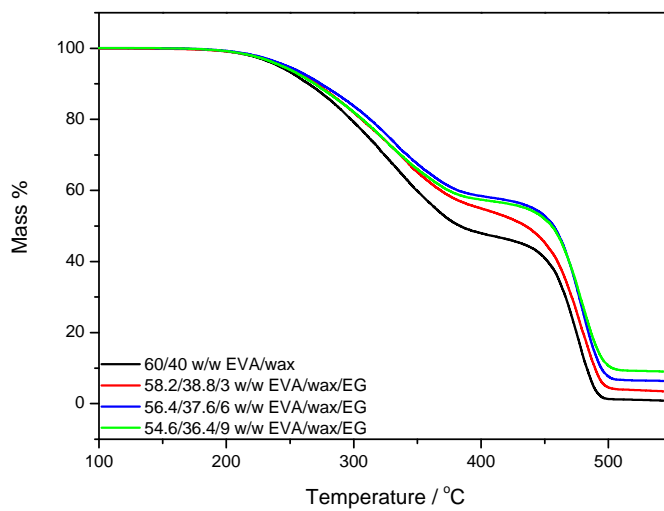


Figure D.2 TGA curves of the 60/40 w/w EVA/wax blend and the EVA/wax/EG composites

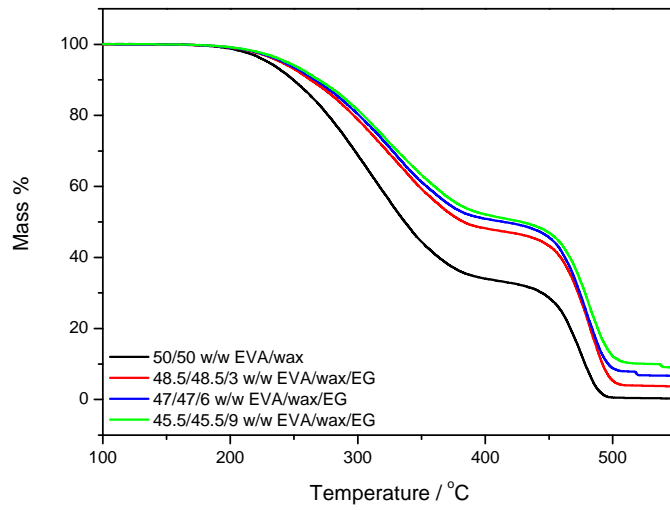


Figure D.3 TGA curves of the 50/50 w/w EVA/wax blend and the EVA/wax/EG composites

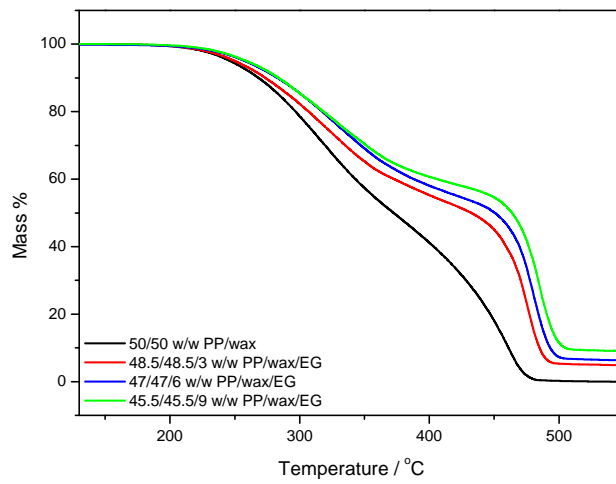


Figure D.4 TGA curves of the 50/50 w/w PP/wax blend and the PP/wax/EG composites